Advanced Protein Crystallization Facility (APCF)

Crystallization of EGFR-EGF

Principal Investigator:

Dr. Christian Betzel
European Molecular Biology Lab
Hamburg, Germany

subject: LMS One Year Science Review

protein crystal growth experiment / APCF

The EGF receptor is the prototype of a family of tyrosine kinase receptors involved in cell growth control. Many human malignancies are characterized by its overexpression. The solution of the EGF receptor structure would pave the way for drug design and novel concepts of therapeutical treatment of tumors. However, the crystal structure of none of the growth factor receptors has been solved so far. - The difficulty of crystallizing a membrane protein has been overcome by purifying only the hydrophilic external domain of the EGF receptor. Using this ectodomain the co-crystallization with the ligand EGF was achieved; diffraction of these crystals had been poor, probably due to the high amount (30% of molecular mass) of heterogenous carbohydrate. Microgravity conditions have been tested which seemed to favour crystal growth. However, results have been variable so far.

On LMS different batches of EGF receptor preparations were flown all of which have proved to crystallize in the laboratory, however after non-predictable time spans. Four hanging drop reactors and one dialysis reactor were used; comparable set-ups in APCF reactors served as laboratory controls.

Results:

Two hanging drop reactors yielded showers of non-usable micro-crystals (lab controls also). Crystals of 0.25 mm length grew in another hanging drop reactor (Fig. 1) whereas the corresponding lab control contained just amorphous precipitate. The fourth hanging drop reactor provided small lancet-like crystals (Fig. 2), with similar crystals in the lab controls. Fig. 3 shows the fragment of a larger crystal which grew in the dialysis reactor and broke during removal from the chamber; if in these reactors crystals grow sticking to the dialysis membrane, cracking during harvest is almost inevitable. The corresponding lab control did not yield crystals.
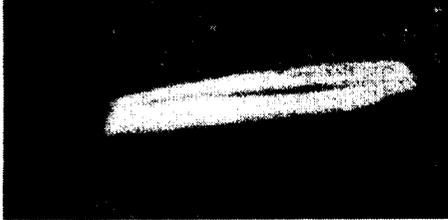

Fig. 1

Fig. 2

Fig. 3

Ten crystals from two reactors were analyzed using synchrotron radiation. However, the diffraction was poor, and collection of data was impossible. From previous experiments a high solvent content (65%) of EGF receptor crystals is known; therefore a larger crystal size is required for diffraction. This was e.g. achieved in a former microgravity experiment (STS-47) when a crystal of 0.5 x 0.3 mm was obtained.

Summarized, the growth of EGF receptor crystals seems to be favoured by microgravity conditions, since the results of 2 out of 5 set-ups were superiour to the corresponding lab controls, at least in terms of crystal growth. It emerges also that for a difficult protein like the EGF receptor the small number of 5 trials may be not sufficient to achieve satisfying results.

Dr. Wolfgang Weber

Institut für Physiologische Chemie

Universitätskrankenhaus Eppendorf, Hamburg

Advanced Protein Crystallization Facility (APCF)

Crystallization of Apocrustacyanin C1

Principal Investigator:

Dr. Naomi Chayen
Imperial College
London, England

Crystallization of Apocrustacyanin C1 on the LMS Mission

PI Naomi Chayen, Imperial College London

The results of the mission were obtained jointly with Prof Helliwell's group in Manchester University and P. Zagalsky of Royal Holloway College, U of London

Introduction

Apocrustacyanin C1 had previously been crystallised on the IML-2 and USML-2 and >Shuttle missions. On IML-2 the crystals grown in space were mostly better diffractors compared to the Earth grown crystals.CCD video was used to follow the crystallisation. The crystals, which grew in the vapour diffusion droplet moved in a circular way,consistent with that of Marangoni convection (Chayen et al. 1997). The images also display a ``halo" effect around the growing crystals which is attributed to the presence of a depletion zone (i.e., solution regions which are depleted of this coloured protein).

>The crystals from the USML-2 mission (which were not monitored by CCD video) >underwent an X-ray mosaicity analysis.The quality enhancement between earth grown and microgravity grown crystals was not as marked as for the lysozyme crystals grown in dialysis geometry nor was it consistent between the two populations, although the best crystal was microgravity grown (Snell et al. >1997).

Objectives of experiment

The crystallisations on LMS aimed to complement, and expand upon the X-ray analyses obtained from the USML-2 crystals (as CCD video was not available to >monitor the crystallisations on the LMS mission).

Experimental

>Apocrustacyanin C1 was crystallised on the LMS Shuttle mission. Four >crystallisations were carried out on the flight, and four identical experiments >were conducted as ground controls during the period of the mission. These >ground controls were set up at the same time, and used the same solutions as >those of the mission.

>Synchrotron X-ray analysis of the LMS apocrustacyanin crystals was carried out
>at two facilities. Firstly at the NSLS using beamline X26C. Here, protein crystal
mosaic spread measurements by use of rocking curves is an indicator of the internal
physical perfection present (Helliwell 1988). The addition of an analyser crystal
between the sample and detector enables reciprocal space mapping of omega, the
sample axis,and omega ', the analyser axis (Snell 1997). Reciprocal space maps, along
one axis provide a measure of pure mosaicity effects (volume and orientation), and
along the other axis strain effects.
>Combination of the use of this technique with X-ray topography (Stojanoff et
>al. 1996),can produce a finely detailed picture of a single reflection, and an in-depth
knowledge of the internal order of the crystal.The analysis of this data is still in
progress, however an example topograph,and reciprocal space map are shown in
figures 1 and 2.
>
>Secondly, at the bending magnet source beamline, BL19 at the ESRF, where two
>complete datasets,one of an LMS crystal, and one of an LMS ground control crystal
were obtained.
>The resolution limits of apocrustacyanin C1 crystals grown onboard the LMS
>missions in a vapour diffusion reactor and earth grown controls were
>determined from 1 degree oscillation images. Operating parameters during data
>collection were lambda = 0.7513 Angstroms ; CCD detector
> (image intensifier type), exposure times 30 secs, rotation angles 1 degree,
>delta lambda / lambda = 10-4. Overall I/Sigma I for LMS = 30.4,
>and for ground control = 9.5. LMS crystal volume = 0.0432 mm3, ground control
>crystal volume = 0.0034 mm3.
>The full data merge for both LMS and ground control is shown in table 1.
>Obviously the LMS crystal is diffracting
>off the edge of the detector, since the Rmerge at 2 A is 10.4%, by contrast,
>the earth control Rmerge at 2 A is 40 %. But the crystal volume for the earth
>is 12 times smaller, and for ground control = 9.5. LMS crystal volume = 0.0432
>mm3, ground control crystal volume = 0.0034 mm3.
>When compared to earlier data collections on earth and microgravity grown
>apocrustacyanin crystals, these results show that resolution limits are
>dependent on the data collection source and measuring conditions. The full
>exploitation of the crystal perfection
>available is very difficult if step widths of 10-4 degrees are required.
>Nevertheless, new area detectors like the pixel detector could exploit such
>quality (for a discussion see Helliwell (1992) and
>Chayen \et (1996)) when used in conjunction with X-ray undulator sources, which
>have extremely fine collimation inhorizontal and vertical directions.

>References
>
>Snell, E.H. 1997 Quality evaluation of macromolecular crystals using X-ray
>mosaicity measurements. Canadian Space Agency, in press
>
>Snell, E.H., Cassetta, A., Helliwell, J.R., Boggon, T.J., Chayen, N.E.,
>Weckert, E., H\"olzer, K., Schroer, K., Gordon, E.J. & Zagalsky, P.F. 1997
>Partial improvement of crystal quality for microgravity grown apocrustacyanin
>C1. Acta Cryst D 53 , 231-239.
>
>Chayen, N.E., Boggon, T.J., Cassetta, A., Deacon, A., Gleichmann, T., Habash,
>J., Harrop, S.J., Helliwell, J.R.,
>Neih, Y.P., Peterson, M.R., Raftery, J., Snell, E.H., H\"adener, A., Niemann,
>A.C., Siddons, D.P., Stojanoff, V.,
>Thompson, A.W., Ursby T. & Wulff, M. 1996
>Trends and challenges in experimental macromolecular crystallography.
> Quarterly Rev. Biophysics 29, 227-278.
>
>Chayen, N.E., Snell, E.H., Helliwell J.R. & Zagalsky, P.F. 1997 CCD video
>observation of
>microgravity: apocrustacyanin C1. J. Cryst. Growth, 171, 219-225.
>
>Stojanoff, V., Siddons, D.P., Snell E.H. & Helliwell, J.R., 1996 X-ray
>topography: An old technique with a new application. Synchrotron Radiation
>News, 9, 25-26.
>
>Helliwell, J.R. 1988 Protein crystal perfection and the nature of radiation
>damage. J. Cryst. Growth, 90, 259-272.
>
>Helliwell, J.R. 1992 Macromolecular Crystallography with Synchrotron Radiation.
>Cambridge University Press, UK
>
>Figure 1:
>Protein crystal quality assessment via topographic images of an LMS ground
>control apocrustacyanin C1 grown as an example.
>
>Figure 2:
>Protein crystal quality assessment via reciprocal space mapping of the same LMS
>ground control apocrustacyanin C1 crystal. The reciprocal space map shows omega
>verses omega ', with intensity on the z axis.

Table 1

| Resolution (Angstroms)	LMS				LMS Ground Control
	Rmerge	Completeness %	Rmerge	Completeness %	
25.00 -- 4.92	0.048	86.5	0.045		97.2
4.92 -- 3.91	0.048	91.0	0.047		99.0
3.91 -- 3.42	0.050	92.6	0.070		99.5
3.42 -- 3.11	0.051	94.2	0.089		99.8
3.11 -- 2.88	0.058	94.7	0.130		99.9
2.88 -- 2.71	0.064	95.0	0.172		99.7
2.71 -- 2.58	0.070	95.3	0.203		99.8
2.58 -- 2.47	0.074	96.6	0.230		99.6
2.47 -- 2.37	0.075	96.1	0.239		99.9
2.37 -- 2.29	0.084	95.2	0.266		99.5
2.29 -- 2.22	0.084	97.9	0.265		99.7
2.22 -- 2.15	0.085	95.7	0.275		99.1
2.15 -- 2.10	0.086	98.1	0.317		98.6
2.10 -- 2.05	0.094	95.3	0.358		98.9
2.05 -- 2.00	0.104	98.2	0.403		98.2
Overall	0.056	94.7	0.110		99.2
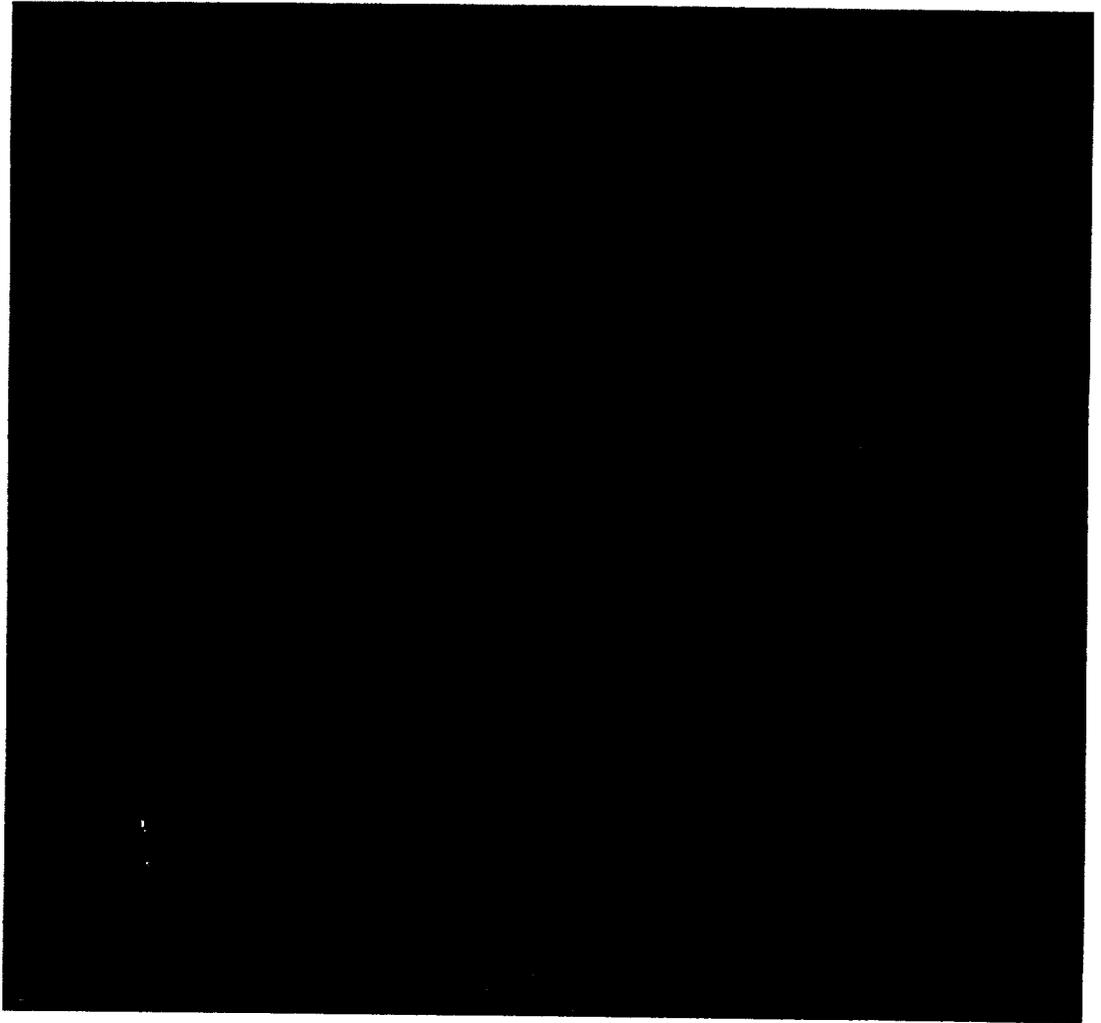
Figure 1
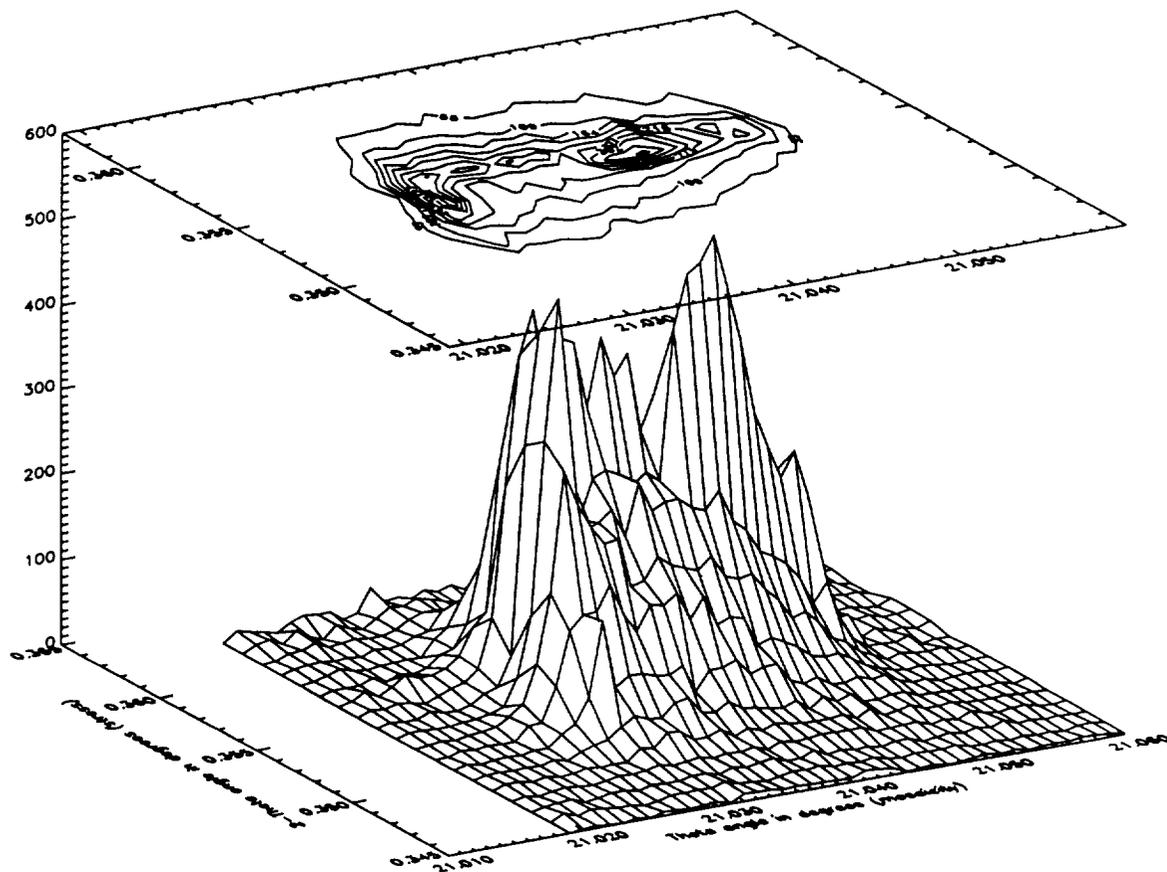
Figure 2

Advanced Protein Crystallization Facility (APCF)

Crystallization and X-ray Analysis of 5S rRNA and the 5S rRNA Domain A

Principal Investigator:

Dr. Volker Erdmann
Free University of Berlin
Berlin, Germany

Crystallization and x-ray analysis of 5S rRNA and the 5S rRNA domain A.

Prof. Dr. Volker A. Erdmann and Siegfried Lorenz

Freie Universität Berlin, Institut für Biochemie, Thielalle 63, D-14195 Berlin-Dahlem, Germany.

Introduction

The ribosomal 5S rRNA is an essential component of the ribosomes. Ribosomal particles lacking 5S rRNA have a greatly reduced peptidyltransferase activity. Because of its functional importance and the fact, that the 5S rRNA interacts specifically with several ribosomal proteins, it is of great interest to know its three dimensional structure at atomic resolution. Based upon chemical and enzymatic structural characterization and the comparison of more than 750 different 5S rRNA sequences a secondary structure for this class of RNA molecules has been derived, which is generally accepted. (**Figure 1**). The size of the 5S rRNA, 120 nucleotides in length, limits its structural determination to that by x-ray analysis. With this goal in mind we have tried for more than ten years the crystallization of about 20 different 5S rRNA species (**Figure 2**). The best results obtained so far are those for the 5S rRNA from *Thermus flavus*, whose crystals diffract up to a resolution of 8 Å (1).

Since crystal structure analysis of whole 5S rRNA molecules could provide so far only low resolution data at 8 Å, we turned to the chemical synthesis and structural determinations of the individual 5S rRNA domains.

Figure 3 shows as example the structure of the domain A from *Thermus flavus* 5S rRNA and the fact that a large number of solvent molecules are associated with this molecule. (2, 3).

Currently we are continueing our crystallization experiments with engineered *Thermus flavus* 5S rRNA molecules. Internal breathing of the structure on one hand and small differences in the primary structure of the 5S rRNA molecules on the other hand can significantly influence the ability to produce well ordered crystals. For example, crystals from the *Thermus aquatics* 5S rRNA gave a resolution up to 25 Å, while crystals from the *Thermus flavus* 5S rRNA gave a resolution up to 8 Å. The difference in the primary structure are only the exchange of 9 nucleotides. These nucleotides differing in the two structures are labeled by solid circles in **Figure 1**. With this observation in mind, we used engineered variants of *Thermus flavus* 5S RNA in such a fashion that an improved crystallization was anticipated. First results of the purified 5S rRNA variants show crystals in dimensions up to 0.6 mm. One of the engineered variants was used in the APCF (Advanced Protein Crystallography) microgravity experiment on the USML-2 space mission in November 1995 and one in the LMS space mission in June 1997.

Material and Methods

1. About 20 different 5S rRNAs were prepared from isolated ribosomes or ribosomal subunits by extraction with phenol and purified by two chromatographic procedures on Sephadex G 100 gelfiltration or by hydrophobic interaction chromatography with Phenylsuperose (1). Having tested various crystallization methods we found, that the best crystals were obtained by the microdialysis method.

2. The 5S rRNA domain A from *Thermus flavus* was prepared by solid phase chemical synthesis (3). Crystals of the dodecamer suitable for x-ray analysis were obtained by vapor diffusion in Linbro plates followed by repeated seeding of the crystals.

3. The engineered variants of *Thermus flavus* 5S rRNA were synthesized on the DNA level and then transcribed in large amounts *in vitro*. The chromatographically purified RNA was crystallized in Linbro plates by the hanging drop method and also in the APCF microdialysis reactors during the ESA and NASA USML 2 and LMS space mission. The crystals were analysed by using the

image plate detector at the EMBL Synchrotron beam line X 11 at DORIS / DESY, Hamburg, Germany and also at the ELETTRA Sincrotrone Trieste in Italy

Results and Discussion

The preliminary assignment of the wild type *Thermus flavus* 5S rRNA crystal lattice is monoclinic, space group C2, with units cell dimensions a = 190 Å, b = 110 Å, c = 138 Å and ß = 117 Å. The unit cell volume is 2.69×10^6 Å and the packing volume 4.3 Å / dalton. The solvent content for the crystals is about 70%. The resolution was up to 8 Å **(1)**. The reason for this low diffraction could be the internal breathing of the structure and the large size of the RNA molecule.

To overcome the problems associated with the crystallization of whole 5S rRNA molecules we tried to crystallize chemical synthesized structural domains of this RNA from *Thermus flavus* and *E.coli* **(Figure 1)**. It is anticipated that the knowledge of all domain structures of the 5S rRNA molecule will eventually permit the determination of the whole RNA structure. In this report we show for example the structure of the domain A from *Thermus flavus* 5S rRNA. Two crystals were used to collect data up to 2.3 Å resolution. The final structure of the dodecamer presented in **Figure 3** is a right handed A type double helix with two strands defined as A and B according to Figure 1. Strand A consists of 245 non-hydrogen atoms and strand B of 263. The structure includes a total of 159 solvent molecules. 49 water molecules were located (blue label) in the interior of the duplex and 68 externally involved in the first hydration shell around the surface of the duplex.

The remaining 42 represent crystal water filling the spaces between the domains. In conclusion it is quite apparent, that with the recent developments of the methodology to synthesize defined RNA molecules it will be possible to determine their atomic structures by x-ray analysis.

In addition to the crystallization experiments of the domain A from *Thermus flavus* 5S rRNA we crystallized the chemically synthesized domain E from the same RNA **(5)**. The crystals are trigonal with unit cell dimensions a = b = 42.8 Å, c = 162 Å. The resolution of the crystals reached a value of 2.8 Å. The chemically synthesized domain E from *E.coli* 5S rRNA was also crystallized. Data sets were collected (S. Klußmann et. al, unpublished results). In addition 11 other chemically synthesized RNA fragments have been crystallized (V.A. Erdmann et. al, unpublished results).

First results of the purified *Thermus flavus* 5S rRNA variants, isolated on the DNA level by *in vitro* transcription, in which the 3`and 5`ends were stabilized, yielded crystals up to 0.6 mm length. Although the crystals obtained so far did not show an improved resolution (10 Å), we are currently continuing these studies with different structural variants and by variations of crystallization conditions. The variations of crytallization conditions include also crystallization experiments under microgravity conditions. In November 1995 we initiated these studies with engineered *Thermus flavus* 5S rRNAs in the USML-2 Mission (ESA/NASA) in APCF (Advanced Crystallography Protein Facility) microdialysis reactors. Of five reactors three yielded crystals. The crystals obtained were larger in size than those obtained simultaneously from ground control experiments **(Figure 4)**. In the LMS mission in June 1996, we continued these experiments also in the APCF system. Of seven reactors all yielded crystals. The crystals obtained were larger in size than those obtained in silmultaneous ground control experiments. The largest space grown crystals in the LMS Mission exhibited a length of 0.45mm. In the ground-control experiment 5 chambers yielded crystals. These were smaller in size than those grown in space.**(Figure 5)**. The crystals were analyzed by synchrotron radiation at DESY in Hamburg, and at the ELETTRA Sincrotrone Trieste, Italy. In the LMS mission space crystals exhibited a resolution of about 8 Å. We were not able to determine the resolution of the simultaneously obtained ground crystals, because they were to small in size. The resolution of the best crystals of the engineered *Thermus flavus* 5S rRNA grown in the laboratory yielded until now a resolution of 8 Å.


Summary

1. 19 different 5S rRNAs were isolated from ribosomes and tested for their ability to crystallize. The best results gave the 5S rRNA from the thermophilic bacterial strain *Thermus flavus* AT62. The resolution of the crystals was up to 8 Å (1).

2. The chemical synthesized domain A from *Thermus flavus* 5S rRNA was crystallized. The diffractions of the crystals were 2.3 Å. The structure has been solved (2). Chemically synthesized domain A from *Thermus flavus* has been also crystallized (5). Data sets from domain E from *E. coli* are collected.

3. Engineered variants of 5S rRNA are produced on the DNA level by *in vitro* transcription. It is anticipated that stabilizing elements at the 3` and 5´ends in the primary structure will reduce the flexibilities of these RNA molecules in order to yield crystals for x-ray analysis.

4. The influence of microgravity on the crystal growth was tested with one engineered 5S rRNA variants in the ESA and NASA APCF/USML-2 and LMS space missions. The results obtained show clearly that the space grown crystals were larger in size than those in the ground controls.The diffraction of engineered *Thermus flavus* 5S rRNA crystals grown in space is nearly the same then the crystals in the best laboratory experiments. The crystals from the simultaneous ground control experiments were to small for diffraction studies.

References:

1) Lorenz, S., Betzel, Ch., Raderschall, E., Dauter, Z., Wilson, K.S. and Erdmann, V.A. (1991) J. Mol. Biol. 219, 399-402.

2) Lorenz, S. Betzel, Ch., Fürste, J.P., Bald, R., Zhang, M., Raderschall, E., Dauter, Z.,Wilson, K.S. and Erdmann, V.A. (1993) Acta Crystallogr. D 49, 418-420.

3) Betzel, Ch., Lorenz, S., Fürste, J.P., Bald, R., Zhang,M., Schneider, T.R., Wilson, K.S. and Erdmann, V.A. (1994) FEBS Letters 351, 159-164.

4) Bald, R., Brumm, K., Buchholz, B., Fürste, J.P., Hartmann, R.K., Jäschke, A., Kretschmer-Kazemi, R., Lorenz, S., Raderschall, E., Schlegl, J., Specht, T., Zhang, M., Cech, D. and Erdmann, V.A. (1992) in: (Lilley, D.J. Heumann, H. and Suck, D., eds.) pp. 449-466, Basel-Birkhäuser-Verlag.

5) Nolte, A., Klußmmann, S., Lorenz, S., Bald, R., Betzel, Ch., Dauter, Z., Wilson, K.S., Fürste, J.P. and Erdmann, V.A. (1995) FEBS Letters 374, 292-294.
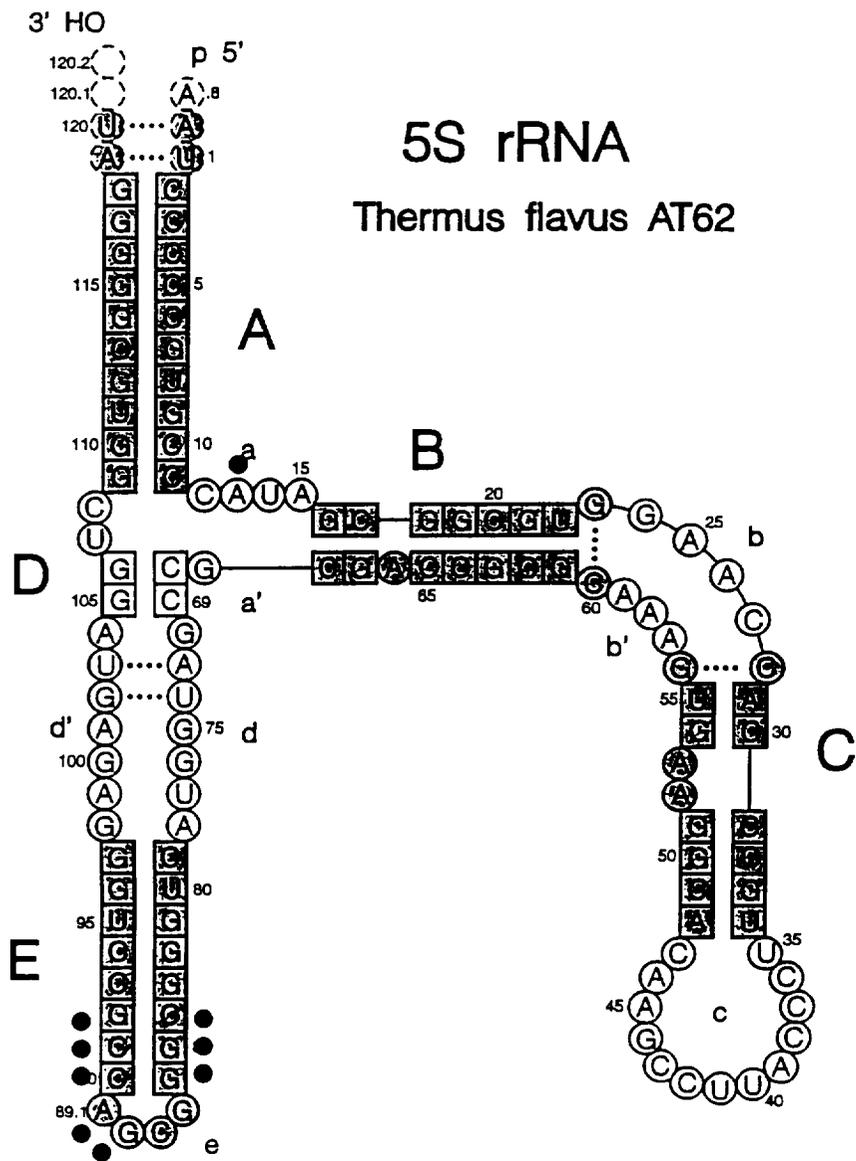
Figure 1
Secundary structure model of 5S rRNA.

5S rRNA Species:

Azobacter vinelandii
Bacillus lichiformis
Bacillus stearothermophilus
Bacillus subtilis
Caulobacter
Echerichia coli
Halobacter cutirubum
Lupinus luteus
Mung bean
Micrococcus luteus
Proteus vulgaris
Pseudomonas fluorescens
Rat (liver)
Staphylococcus aureus
Thermotoga
Thermus aquaticus
Thermus flavus
Wheat germ
Yeast

5S rRNA Protein-complexes:

Bacillus stearothermophilus
Echerichia coli
Thermus thermophilus
Thermus flavus

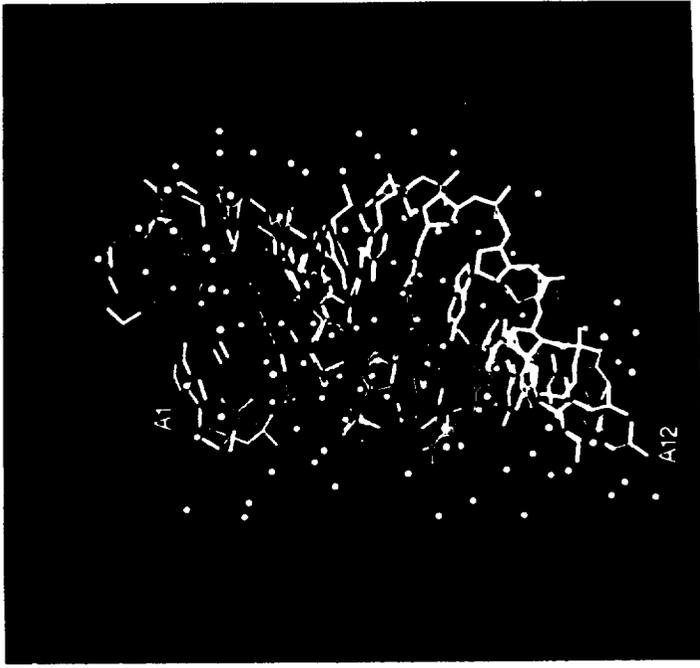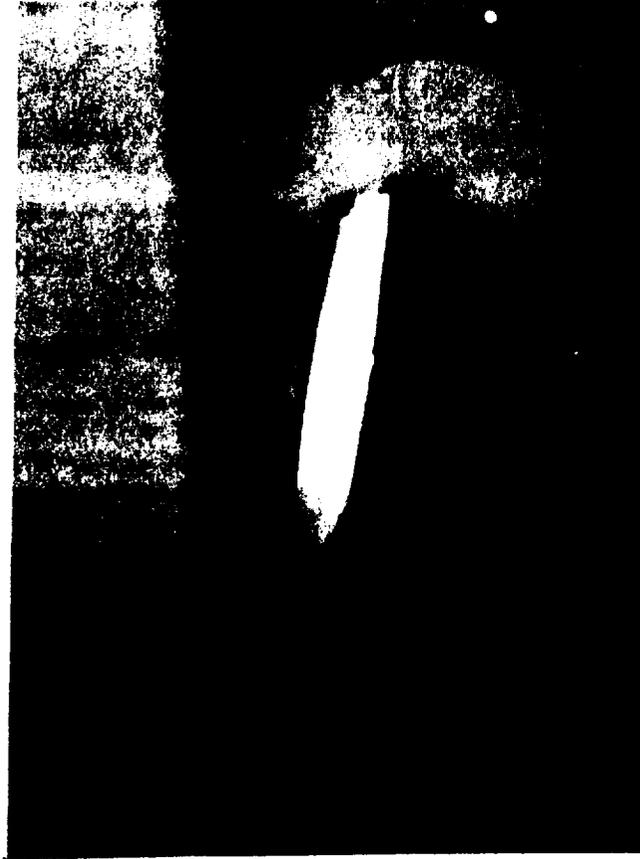# Figure 2

5S rRNA species for crystallization experiments.
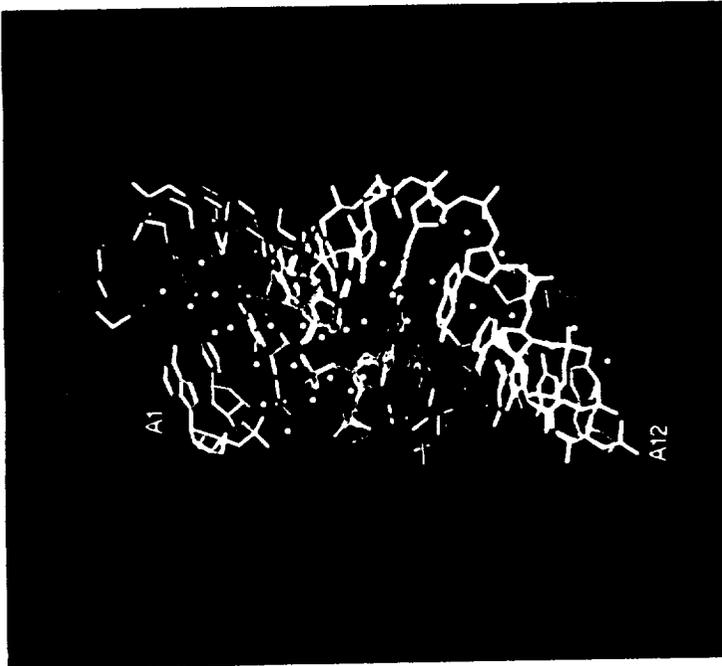
Figure 3

Crystal structure
of the dodecamer
5S rRNA domain Helix A
with 117 water
molecules.

(Left side: 49 water
molecules in the
interior of the duplex).

(Right side: 49 internal
plus 68 external water
molecules).

Figure 4

Crystals of engineered *Thermus flavus* 5S rRNA

a) grown on earth, (0.4 mm length),

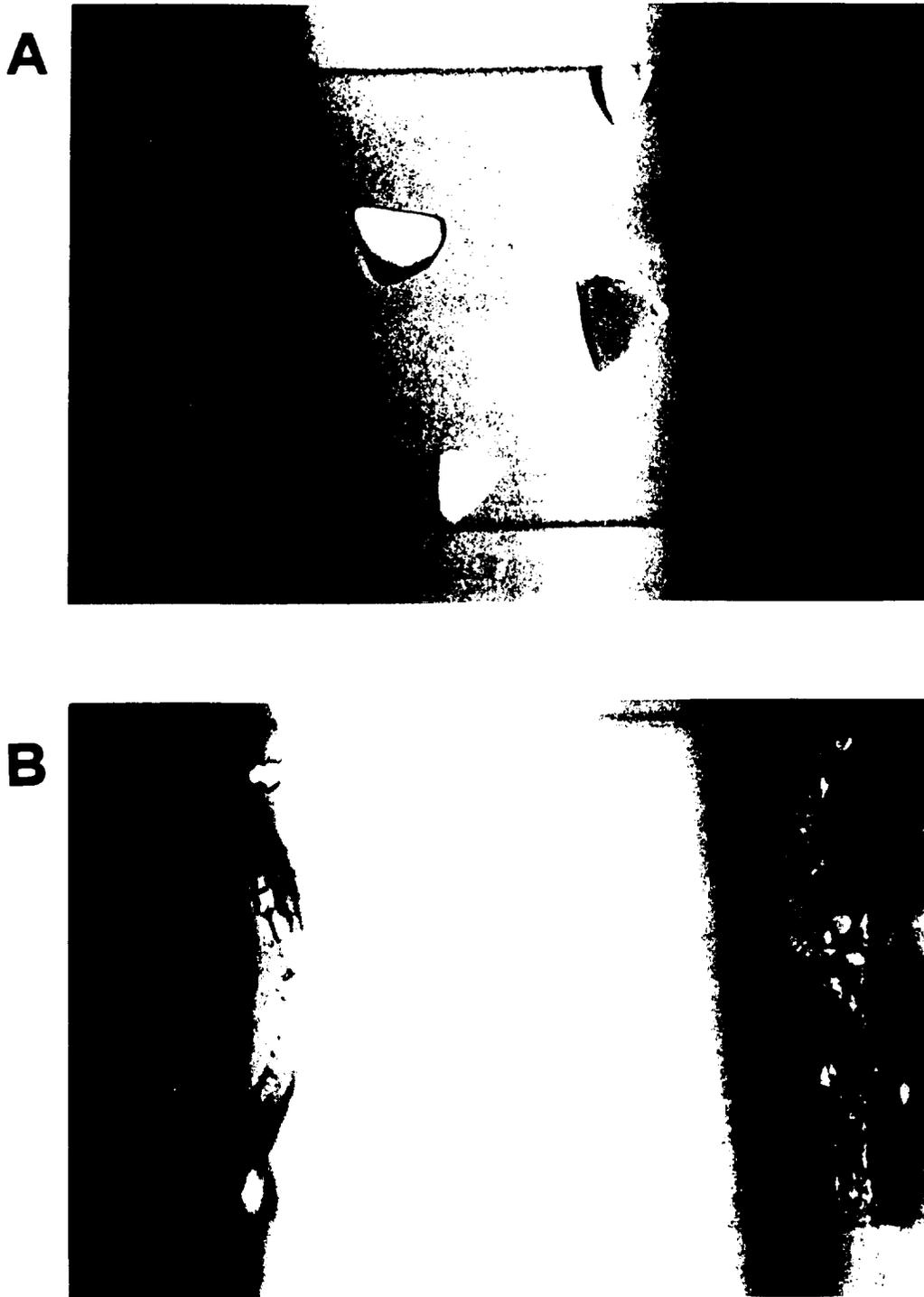b) grown in APCF reactor under microgravity, (0.7 mm length).

Figure 5

Crystals of the bacterial 5S rRNA *Thermus flavus* under microgravity conditions crystallize better in size, shape and quality (A) than the ground control crystals (B). The crystals were obtained in the ESA / NASA mission LMS, 1996
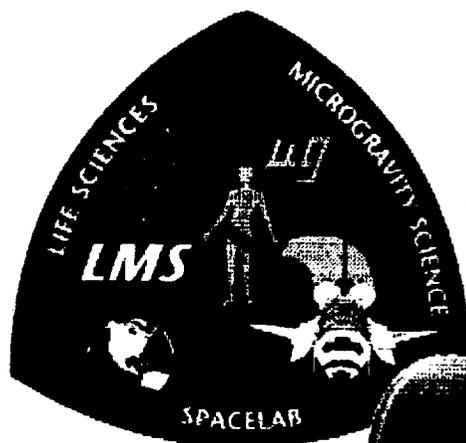
111

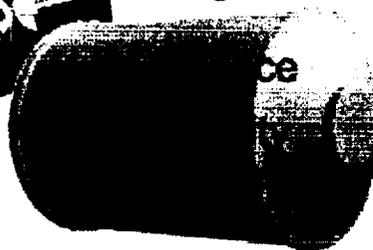Advanced Protein Crystallization Facility (APCF)

Growth of Lysozyme Crystals at Low Nucleation Density

Principal Investigator:

Dr. Juan Garcia-Ruiz
University of Granada
Granada, Spain

Life and Microgravity Spacelab

LMS

SPACELAB

Growth of Lysozyme Crystals at Low Nucleation Density. Experimental Report.

Mission Data	
Facility	APCF
Mission Number	STS-78
Shuttle	Columbia
Launch Date	10:49 am EDT on June 20, 1996 at KSC
Landing Date	08:37 am EDT on July 7, 1996 at KSC
Activation of APCF	05:19 pm EDT on June 20, 1996
Deactivation of APCF	03:49 am EDT on July 6, 1996
Process Phase Duration	15 days, 10 hours, 30 min.

Research Team	
Principal Investigator	Juan Manuel García Ruiz
Participants	Fermín Otálora
	Deyanira Rondón
	M. Luisa Novella
Report Prepared by	F. Otálora & J.M. Garcia-Ruiz

Laboratorio de Estudios Cristalográficos
IACT, Campus Fuentenueva (Fac. Ciencias)
18002, Granada Spain

Tel: +34-58-243360   Fax: +34-58-243384   Email: otalora@goliat.ugr.es   jmgruiz@goliat.ugr.es

This Report is available on-line at http://gazpacho.ugr.es/wwwbook/apcf_rep.htm

1. Objectives

Five experiments were prepared for this flight in the same reactor type (FID200) and with the same initial concentrations (10% Sodium Chloride and 100 mg/ml Lysozyme). The experiments were prepared with the following objectives:

- **Test of the new Mach-Zehnder interferometer installed in the APCF facility.** During mission STS-78, the APCF has flown equipped for the first time with a Mach-Zehnder interferometer to study the concentration of reactants inside the protein chamber. The experiment at position 1L3 was designed to test this feature.

- **Crystal growth rate and movement studies.** Three of the five reactors were accessible by the APCF video camera. Time series of images during crystal growth can be used to study growth rate and crystal movement due to residual acceleration in the microgravity environment.

- **Precipitation of Lysozyme at high concentration.** Non equilibrium one-dimensional techniques for crystal growth has shown their potential for crystal growth. The space-time self organisation of supersaturation provokes inhomogeneous distributions of nucleation density, growth rate and crystal size[1]. Our experience from on-ground experiments shows that long growth chambers and high protein concentration are the optimum conditions to explore the properties of these systems. This is the reason to use 100 mg/ml lysozyme solutions and to fill with this solution the plug channel in experiments (1R2 and 2R2).

- **Testing the use of capillaries inside the protein chamber.** In soft materials like proteins, handling of crystals is supposed to create defects that can potentially lower the crystal quality. Very good quality crystals are obtained routinely on ground by growing the crystals inside X-ray capillaries, which allows its use in diffraction experiments without further handling of crystals and mother liquor. Shocks during manoeuvres of the spaceship (specilly during landing) are also avoided. A pack of flat capillaries is introducing filling the protein chamber in two of the experiments (1R1 and 1R2) to check the usefulness of this technique in the APCF.

The following table summarises the configuration and initial conditions of the five experiments:

Flight Configuration					Initial Conditions		
Stack	Type	Pos.	S/N	Video	Interf.	Salt Res.	Rot. Plug	Prot. Ch.
1	FID200	1L3	324/B	5	5	10 % ClNa	Agarose 0.5%	100 mg/ml Lysozyme
1	FID200	1R2	316/B	-	-	10 % ClNa	100 mg/ml Lysozyme	100 mg/ml Lys. Cap.
1	FID200	1R1	207/B	-	-	10 % ClNa	Acetate buffer	100 mg/ml Lys. Cap.
2	FID200	2R3	208/B	6	-	10 % ClNa	Acetate buffer	100 mg/ml Lysozyme
2	FID200	2R2	322/B	4	-	10 % ClNa	100 mg/ml Lysozyme	100 mg/ml Lysozyme

Initial conditions for the experiments were selected based on our experience in protein crystal growth into capillaries[2] after test experiments performed on ground using APCF reactors with the protein chamber filled with a gelled protein solution to mimic microgravity conditions.

[1] J.M. Garcia-Ruiz, F. Otálora (1997) ESTEC contract 11629/95/NL//JS final report. J.M. Garcia-Ruiz, A. Moreno, F. Otálora, C. Viedma, D. Rondón and F. Zautscher (1997) *J. Chem. Education.* In Press. F. Otálora & J.M. Garcia-Ruiz. *J. Crystal Growth* 169 (1996) 361-367. F.Otálora and J.M. Garcia-Ruiz *J. Crystal Growth* 169 (1997) In Press.

[2] J.M. Garcia-Ruiz, A. Moreno, C. Viedma & M. Coll. *Res. Bull.* 28 (1993) 541-546. J.M. Garcia-Ruiz and A. Moreno. *Acta Crystal. D50 (1994) 483-490.* J.M. Garcia-Ruiz, A. Moreno, A. Parraga & M. Coll. *Acta Crystal. D* 51 (1995) 278-281. J.M. Garcia-Ruiz, A. Moreno, F. Otálora. C. Viedma, D. Rondón and F. Zautscher, *J. Chem. Education.* (1997) (In press). J.M. Garcia-Ruiz and A. Moreno, *J. Crystal Growth. 169 (1996) 361-367.* A. Moreno, D. Rondón & J.M. Garcia-Ruiz. *J. Crystal Growth* 166 (1996) 919-924. F. Otálora & J.M. Garcia-Ruiz. *J. Crystal Growth* 169 (1996) 361-367. F. Otálora, J.M. Garcia-Ruiz y A. Moreno, *J. Crystal Growth* 168 (1996) 93-98.

2. Results

2.1. Nucleation

Experiments in which the plug channel contains lysozyme solution produced a larger number of smaller crystals than experiments in which buffer solution is used inside the plug. In the first case, nucleation flux is very large at the plug channel, where concentrated salt and protein solutions meet. In general, even for the experiments containing buffer solution in the plug channel, nucleation flux was higher than expected. This fact is due to the short length of the protein chamber in the APCF. In counterdiffusion experiments in which long enough growth chambers are used (as in the Gel Acupuncture method[2]), the incoming of one reactant is expected to produce a supersaturation gradient along the growth chamber resulting in a spatio-temporal structuration of the supersaturation field. As a result, crystals nucleate at different supersaturation in different parts of the systems and growth at different rates to different final sizes. If the growth chamber is too short for a given waiting time for nucleation, precipitation takes place after the homogenisation of the system that, therefore, loss its spatio-temporal structuration. Although FID200 reactors are the APCF reactors with longer protein chambers (this was the reason for selecting these reactors), they proven to be short for the kind of experiment proposed. Induction times for lysozyme (figure 1) are long enough to provoke nucleation after the almost complete homogenisation of the salt concentration
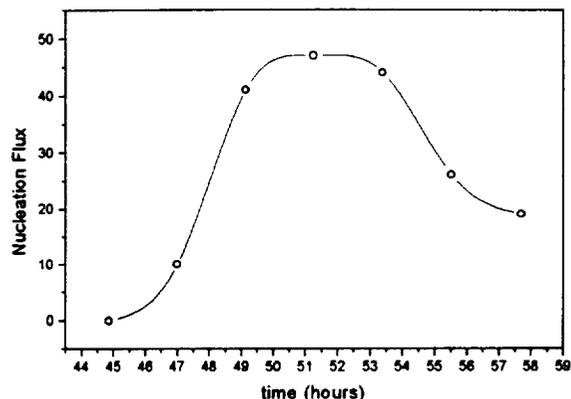

Figure 1. Nucleation flux versus time plot for Experiment 1L3. The number of new crystals observed in each image acquired at the given time is plotted versus the acquisition time. Maximum nucleation flux is observed after 51'5 hours, The shape of the peak is asymmetric. The tail of the peak cannot be explored to later times due to the large number of crystals already in the field of view that avoids clear recognition of new nucleation events.

inside the protein chamber, giving rise to a large number of crystals evenly distributed over the chamber (figure 2). The expected spatial structuration of the nucleation flux is therefore masked by the apparently homogeneous precipitation over the protein chamber due to salt homogeneisation. Even in this case, the effect is still observable, specially when only the early formed nucleus (after 47 hours) are taken into account. Figure 3 shows the spatial distribution of these first nucleation events into the protein chamber.

Nucleation flux in the direction of the salt gradient is structured, displaying a maximum approximately at the centre of the chamber. Some structure is also shown in the perpendicular (y) direction, but this is probably due to the presence of bubbles at the entry of the protein chamber close to the corners (see figure 2).

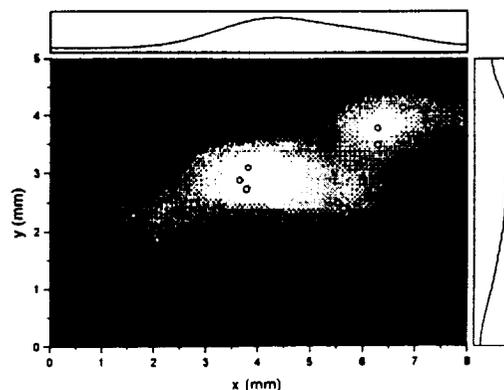Figure 2: View of the experiment 1L3 57 hours after activation.

Figure 3: Spatial distribution of the first nucleated crystals (circles) inside the protein chamber. Cumulative nucleatio probability curves are projected in the direction of both axis.

116

2.2 Growth Rate

Image analysis methods has been used to study the growth rate of crystals. These methods has been discussed in detail elsewhere[3], therefore only a brief description of the methodology is included here. Six crystals has been selected from reactor 1L3. Crystals in reactors 2R2 and 2R3 cannot be used for this study because the first image is acquired after 91 hours, late after the nucleation in these reactors. Time series for the growth history of the crystals selected are automatically cut and pasted to have a single image displaying their growth history. From this image, shown in figure 4, the projected area after form factor correction is obtained at each step. The square root of this projected area is used as a representative lengthscale to be used in the absence of the crystal length perpendicular to a crystal face, a figure not directly obtainable from the APCF image recording system.
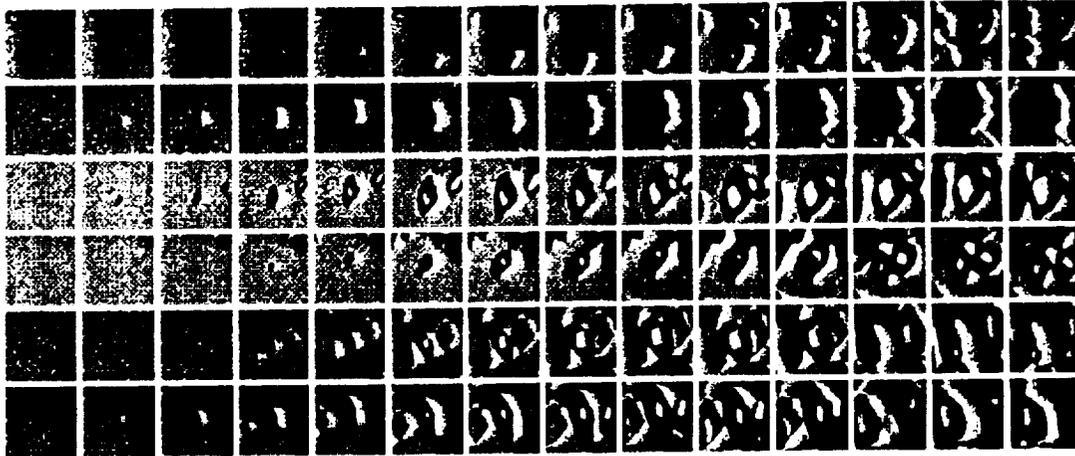

Figure 4: Collage of subimages displaying the growth history of the six crystals analysed. Frames are time aligned and start at the image where the first nucleation is detected. Time series ends at a time where the number and size of crystals makes unreliable the detecion of projected areas.

Figure 5 shows the square root of projected area (length) of the crystals versus the square root of time plots for these crystals. These plots display large linear areas consistent with the dynamics of diffusive transport. These linear regions are limited by an initial non-linear region in which growth rate is controlled by the nucleation kinetics and a second non-linear region at late times due to the exhaustion of protein concentration by the coalescence of the protein depletion zones around the growing crystals.
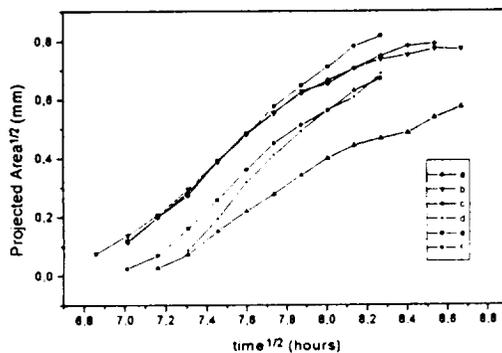

Figure 5: Time evolution of the crystal size for the six crystals analysed. The central part of most of the curves are clearly straight.
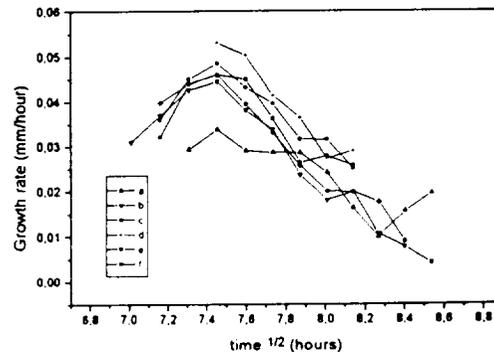
Figure 6: Growth rate of the crystals analysed. A maximum growth rate exists at the end of the kinetics regime.

[3] J.M. Garcia-Ruiz, F. Otálora (1997) ESTEC contract 11629/95/NL/JS final report. F.Otálora and J.M. Garcia-Ruiz J. Crystal Growth 169 (1997) In Press.

Figure 6 shows the growth rate of the six crystals analysed. Maximum growth rates up to 140 Å/sec are observed slightly after nucleation. These growth rates then slowly decrease towards zero. The measured maximum growth rates, the initial regime of increasing growth rate and the time lapse between maximum and close to zero growth rate are consistent with previous observation of flight experiments[3] as well as with on-ground observations.

2.3. Crystal movement

Crystals move during their growth. This movement has been studied by computing the centre of mass of the projected area computed for growth rate measurements. Figure 7 shows the position of each of the six crystals at equivalent times and a path interpolated between these positions. Average displacement during the 28 hours period represented is 0.1 mm although displacements as large as 0.6 mm are observed.
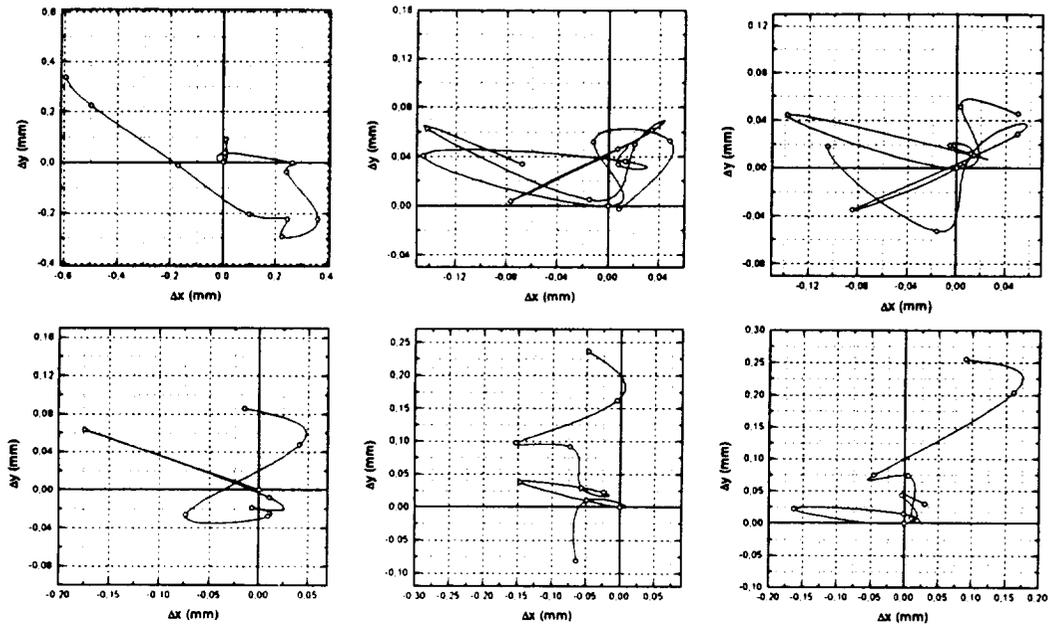

Figure 7: Crystal movements during the first 28 hours of crystal growth. The paths has been represented in such a way that they are comparable: all plots contains a data point at x=y=0. This point corresponds to the same time in all paths.

To understand the origin of these displacements, the first important question is: Do all crystals move in the same direction at the same time? This question addresses the lengthscale of the mechanism giving rise to the crystal movement. If this mechanism is at the sub-reactor lengthscale (for example some kind of convection), the direction of movement of different crystals is expected to be uncorrelated. On the other hand, if the motion is related to mechanisms working at a suprareactor lengthscale (for example residual accelerations of the spaceship) crystals would move in the same direction. Although from figure 7 the movement of crystals seems uncorrelated, a more systematic study undercover the correlation of crystal movements. Taking the position of crystals in two consecutive images and subtracting their x and y co-ordinates in each image, we get a displacement representing the direction and velocity of movement during the period between images. Representing these vectors in a polar plot, the head of the vectors corresponding to different crystals during the same time period must be grouped if the movement of crystals is correlated, else they must be scattered. Such a plot is shown in figure 8, each symbol represents a different time period. This plot shows a collective movement of the crystals, the heads of the displacement vectors are close to each other, and this clustering of the data points seems proportional to the net displacement: data points are more grouped for larger displacements (distance from origin) than for smaller ones. This can be due to random errors during the measurement of the crystal position or to the coexistence of two processes producing crystal movements, one at a subreactor lengthscale and of roughly constant strength and other of suprareactor lengthscale and of varying strength.
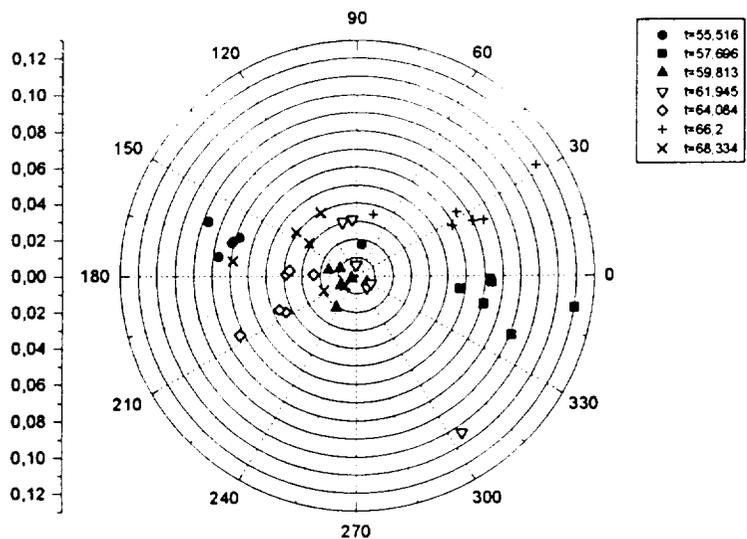
118

Figure 8: Movement of crystals inside the 1L3 reactor. Data points represented in the polar plot indicate the head of the displacement vectors. Each symbol correspond to a different time period starting at the time indicated in the symbol caption. Radial axis is net displacement in millimetres.

We have tried to correlate these movements with acceleration data. To this aim, we contacted colleges managing the ASTRE accelerometer measurements who kindly supplied us their data. Unfortunately, when we start processing these records, no information was found for the time period we were interested in. Later, it was confirmed that, from 174/16:00 to 175/00 the ASTRE data have been lost. We are contacting now teams managing other accelerometers onboard STS-78 to get new acceleration data.

2.4 Interferometry

Experiment 1L3 was selected to test the new Mach-Zehnder interferometer installed in the APCF and flown for the first time during the STS-78 mission. During the first 15 hours, the average grey intensity inside five image windows was recorded at a rate of 12 samples per hour (The position of these windows is shown in figure 9). Then the whole interference pattern is recorded at a rate starting at 5 samples per hour and decreasing until the end of the experiment.
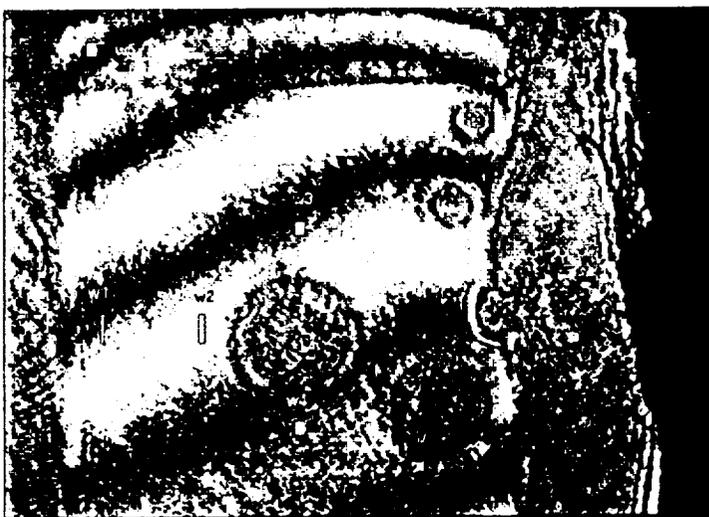
Figure 9: Reference fringe pattern and position of grey value measurement windows in experiment 1L3.

Each interferogram carries only information on relative phase along the image. This phase must be corrected subtracting an initial phase (derived from the pattern in figure 9) and followed during time to record phase increments of 2π each time a new fringe crosses over a given pixel or window. This phase is

$$\varphi(x,y,t) = \varphi_0(x,y) + 2\pi F(x,y,t)$$

119

where φ_0 is the initial phase difference (mostly due to slightly non-parallel reactor walls) and F is the number of fringes that crossed over the pixel at (x,y) since the beginning of the experiment until time t. This phase can be finally converted to salt concentration values multiplying it by a factor that linearly relates the change in refraction index produced by a given change of concentration with this change in concentration.

It is clear that, to evaluate concentrations using this technique, a spatial reference (initial status of the system before inhomogeneisation) is needed to compute φ_0 and a time reference (time series of grey values at each pixel sampled at a frequency large enough to detect all the travelling fringes) is needed to compute F. To have this time reference, laser illumination must be very stable because laser instabilities produce random displacements of the fringe pattern that make impossible to evaluate F. Unfortunately, during the LMS mission, the laser of the interferometer installed in the APCF was unstable, producing frequent jumps of the fringe pattern. This fact was confirmed by people managing the APCF project. This erratic jumps can be seen in figure 10 where the time history of the grey value inside three different windows (see figure 9) is plotted.
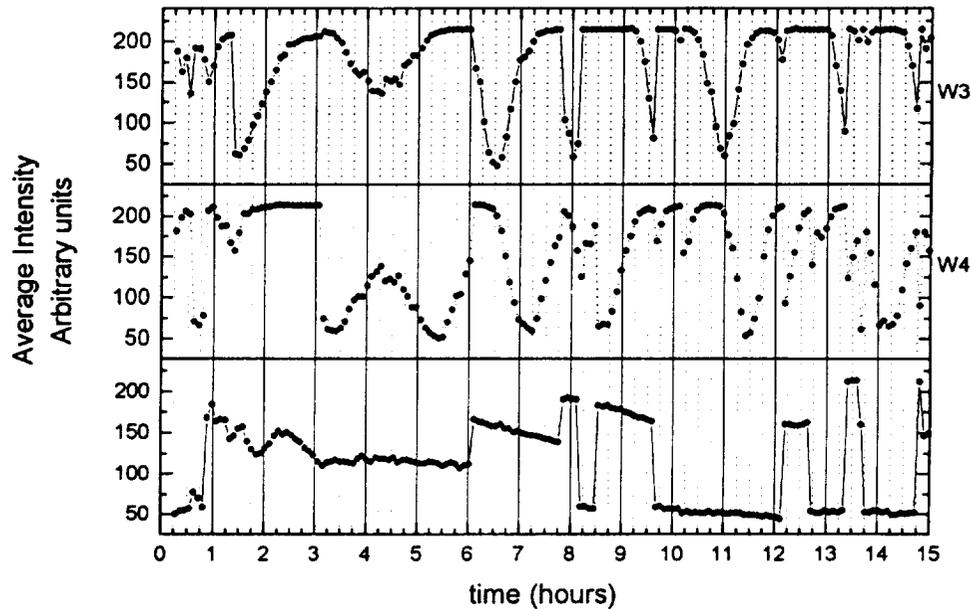

Figure 10: Time evolution for the first 15 hours of the average grey value inside three of the windows defined in figure 9.

The bottom plot show the grey value time evolution for the w5 window. This window is located on the quartz glass of the reactor body. Therefore no change in grey value is expected in this window during the experiment because the optical path at this position is constant. It can be clearly seen that this grey value, related with the local phase, randomly jumps with time in an unpredictable way. This instability destroys the information on the number of fringes that travels over a given window. The two top plots show the grey value evolution in windows w3 and w4, inside the protein chamber. This curves should be sinusoidal-like waves (as can be seen in w3 and w4 from 3 to 6 hours) of variable frequency related to the time derivative of salt concentration allowing the evaluation of the F function. This lack of stability continues during the whole experiment as can be seen in figure 11, where the grey value at a window on the glass body (obtained from the full interferograms recorded after 15 hours) is plotted from t=15 hours to the end of the mission.
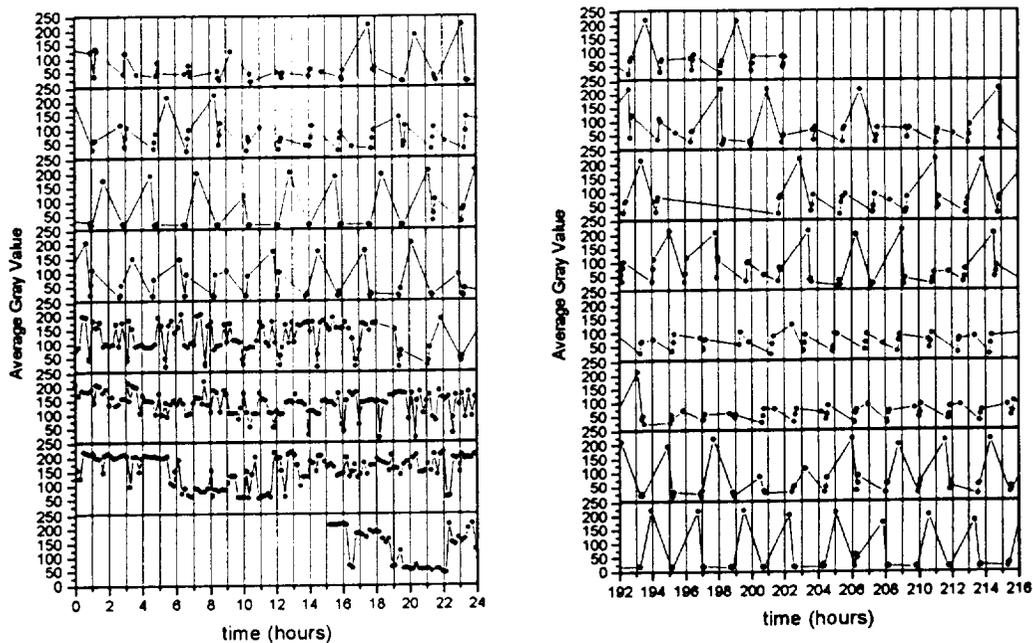
120

Figure 11: Average grey value inside a window positioned on the glass body of the reactor for times covering the whole experiment. First day is at left bottom and last day at right top.

With these data, only relative information is available, that is: we only know the spatial concentration gradient for each image without any knowledge of the time gradient (the concentration change at a given point between two consecutive images). Therefore, we cannot reconstruct absolute concentration maps inside the protein chamber. Only relative concentration maps, i.e. maps of concentration where an unknown offset is uniformly added to all concentration values can be computed. Two of such maps for the experiment 1L3 are shown in figure 12 for one time before nucleation and a time after nucleation of crystals in the protein chamber.

t = 47:04:58

t = 57:49:29
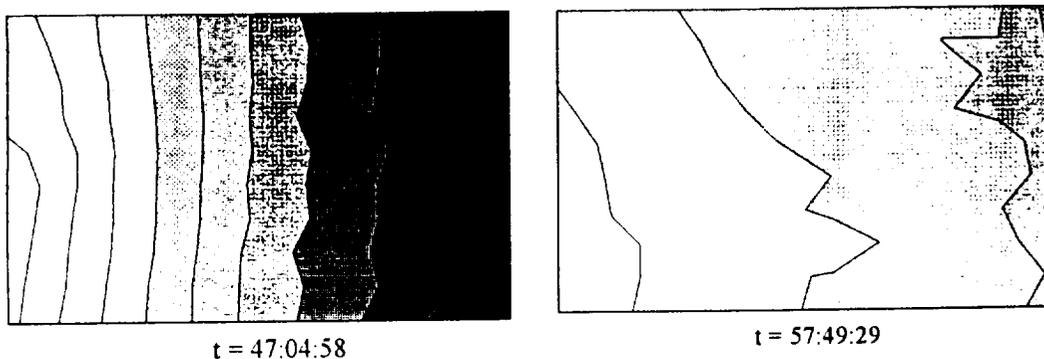
Figure 12: Relative concentration maps inside the protein chamber. Concentration difference between consecutive lines is 0.2 % w/v.

To improve the usefulness of these data we are currently trying to use external extra information in order to recovery the lost time derivative information. Our approach consist in using simulation data for this task. Simulations of diffusion-reactions systems have been developed in our laboratory during

121

the last years[4]. These simulations include one and three dimensional simulations of the APCF. Fitting the experimental gradients to the simulated profiles for the same time, an estimation of the unknown offset can be calculated. Figure 13 shows our preliminary data fitting for the interferometric data obtained from an on-ground preliminary interferometry study performed inside the APCF flight model[5] to the salt diffusion profiles computed using a three dimensional simulation of the APCF. Although the fit is very good, the use of this technique deserve further discussion in our laboratory.

Figure 13: Experimental (from interferometry) and simulated salt concentration profiles inside the FID200 APCF reactor for two different times.
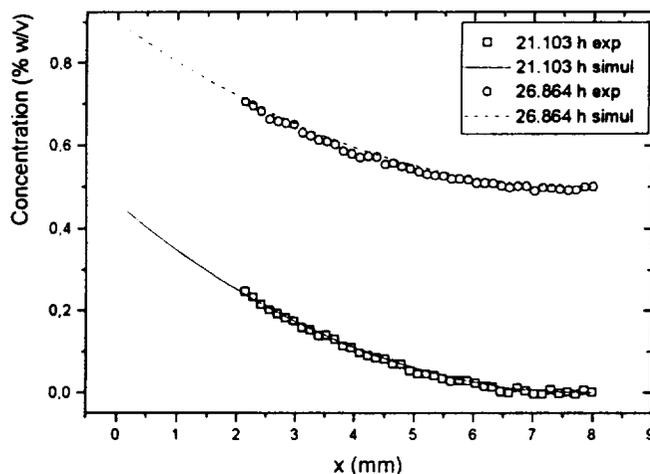
2.5. X Ray studies

Limit of resolution for these crystals has been measured at station W32 at LURE (Orsay, France), the average resolution limit for the crystals analysed being about 1.25Å. The use of flat capillaries inside the protein chamber simplify the handling of crystals although some problems related to the sealing of capillaries must be solved. One crystal grown inside them produced a diffraction pattern of higher resolution than those grown without capillaries (1.15 Å), but this result was not reproducible, therefore there is no clear evidence of limit of resolution improvement using these capillaries.

Line profiles for diffraction spots at 3Å resolution were measured in station D25b installed at the positron storage ring DCI at LURE. This station is optimised for mosaicity measurement using extremely low vertical divergence and bandwidth as well as a very high resolution goniometer. During the experiments reported here, we used a four reflections (three of them symmetric) Si 111 monochromator (d=3.1353 Å) oriented to reflect in the vertical plane. The wavelength was adjusted to 1.2 Å (11.033°). The NaI scintillation detector was set at 2θ=22.07° (symmetrical setting) to record diffraction spots having the same spacing than the monochromator. Using this combination of monochromator and recording geometry, a total experimental width of only 0.8'' is superimposed to the measured peaks. All widths in this work are reported without correction for this experimental width. Line profiles acquired were fitted as the addition of several (from 2 to 4) gaussian functions

$$y = y_0 + \frac{A}{w\sqrt{\pi/2}} Exp\left(-2\left(\frac{(x-x_c)}{w}\right)^2\right)$$

[4] F. Otálora (1995) PhD Thesis, Univ. Granada. F. Otálora & J.M. Garcia-Ruiz. J. Crystal Growth 169 (1996) 361-367. F. Otálora and J.M. Garcia-Ruiz. (1997) J. Crystal Growth. In Press. J.M. Garcia-Ruiz, F. Otálora (1997) ESTEC contract 11629/95/NL/JS final report

where y_0 is an offset (background noise level), A is the area (integrated intensity) of the peak, w is its width and x_c is the co-ordinate of the maximum. Lorentzian functions has been also tested, but they produce fits of lower quality.

Very small mosaicity values has been found. All peaks show non-corrected FWHM ranging from 10'' to 20''. All these peaks are fitted to the addition of 2 to 4 domain peaks. The width of these components ranges from 4.5 to 15 arc seconds. Figure 14a shows a very narrow peak (FWHM = 10.5''). This crystal peak is composed of only two domain peaks, having widths of 6.1'' and 12.3''. The integrated intensity of these domain peaks is 17165 for the narrow peak and 26311 for the wide one (a ratio of 0.65). Figure 14b shows the profile of the same peak after closing the beam by adjusting the slits while controlling the beam size and position using an X-ray camera in the path of the direct beam
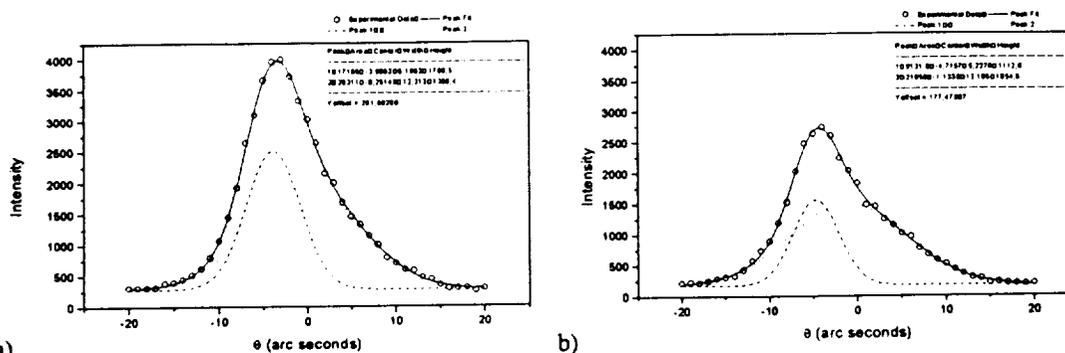

Figure 14:. Line profile of a diffraction peak from a space-grown lysozyme crystal. a) profile recorded when the whole crystal is exposed. B) profile recorded exposing only the central part of the crystal.

through the crystal. This peak, records the contribution of the central part of the crystal. The position and width of the two domain peaks is very similar (5.2'' and 13.2''), but their relative intensity has changed to 9131 for the narrow peak and 21858 for the wide one (a ratio of 0.42).
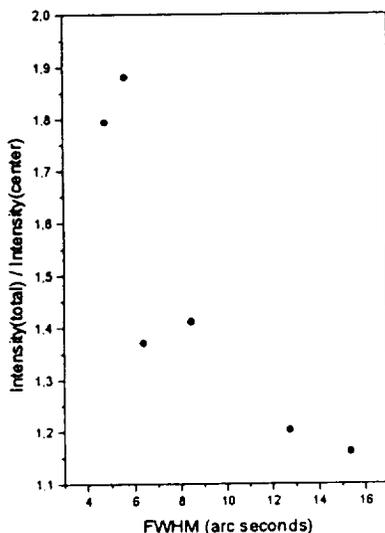

Figure 15: Ratio of the integrated intensity recorded exposing the whole crystal and only the central part versus the width of the corresponding domain peak.

The volume of the crystal is composed of two mosaic blocks although no conclusions can be derived in terms on their nature and defect structure except that they are not perfect mosaic domains and they are not homogeneously distributed over the crystal, the parts of lower quality being concentrated at the centre of the crystal. This is reasonable since the growth rate of these crystals changes with time as shown in chapter 2.2, being faster at the beginning of the experiment (while the centre of the crystal is growing). It has been previously shown that the domains of different quality making up a lysozyme single crystal are not homogeneously distributed and that this inhomogenity can be caused by differences in growth rates[6]. Figure 15 shows the ratio between the intensity of different domain peaks when exposing the whole crystal and the intensity when only the centre of the crystal is exposed versus the width of the domain peak. This figure clearly shows that the intensity reduction is larger for narrow peaks than for wider ones and therefore that the average quality of he central zones of the crystals is lower that that of peripheral zones.

Different crystals in the same experiment show different number of domain peaks although the average width of these components is in the same range. Figure 16a shows the line profile of a crystal from the

[6] F. Otálora, J.M. Garcia-Ruiz and A. Moreno. J. Crystal Growth 168 (1996) 93-98.

same experiment as that illustrated in figure 14. This profile has a FWHM of 13.8" and is composed of four gaussians of widths 14.5", 8.13", 6.4" and 4.6". After acquiring this profile we rotated the crystal by 80 degrees (the limit of the goniometer) and recorded another spot at the same resolution (3 Å). This peak is illustrated in figure 16b. Large differences are observed between both crystal peaks. At first sight, it is clear than the peak illustrated in figure 16b is wider (27.0"). This means that the mosaicity (mean misalignment between mosaic blocks) and probably also the internal defect structure of each block are anisotropic properties. The same domain peak, seen from different directions can show different widths and therefore different heights (though the same amplitude) and the relative position of these domain peaks change depending on the crystallographic directions, producing crystal peaks of different width. Anisotropy in the width of domain peaks can be due to the accumulation of one of two-dimensional crystal defects in a given direction, or by differences in the mechanic properties of the crystal lattice giving rise to microbending (at the scale of several unit cells) of different amplitudes depending on the orientation.

a)   b)
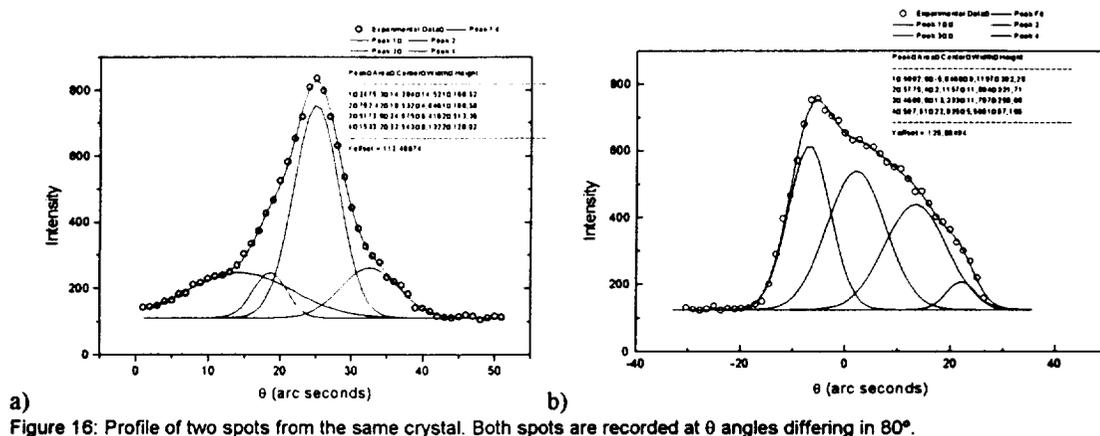
Figure 16: Profile of two spots from the same crystal. Both spots are recorded at θ angles differing in 80°.
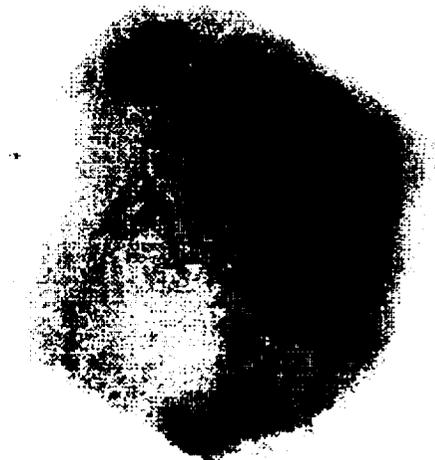
Figure 17. Topography recorder from the spot whose profile is ilustrated in figure 14. As faces and edges are observed, this spot is a very clear projection of the crystal.

Taking into account that the intrinsic width of a perfect lysozyme crystal can be estimated[7] to be less than 1" and that the experimental width with the set-up used is about 0.8", a width of, at most, 1.8" can be attributed to factors other than the real mosaic spread of the samples. The best domain peaks found (having a width of about 5") must, therefore, contain some kind of further defect structure such as a given concentration of discrete crystalline defects or a continuous bending of the crystal structure at the scale of a few arc seconds. This second possibility seems to be coherent with the mechanical properties of protein crystals and with the absence of sharp domain boundaries in topography (figure 17).

[7] J.R. Helliwell. J. Crystal Growth 90 (1988) 259

Conclusions

Nucleation in the experiments was higher than expected. Studies performed after the flight and the results presented here on time and space distribution of the nucleation flux support indicate that this fact is due to a early homogenization of the salt concentration inside the protein chamber because of the shortness of that chamber. Although the final result is an almost equal probability of nucleation over the whole chamber, taking into account only the first nucleation events, a spatial structure similar to that observed in one dimensional counterdiffusion experiments is observed. This control on the spatio-temporal distribution of non-constant nucleation flux inside APCF reactors has never been attempted before this experiment Further experiments with lower protein concentration and, if possible, longer protein chambers are necessary to continue advancing in this direction.

Crystal size (length) versus square root of time for the crystals studied show linear zones during most of the experimental time with two crossovers, the first one at the beginning of the experiment and another close to he homogenization. This behaviour is interpreted as a result of the diffusion control of the growth rate during the experiment after a first short stage controlled by nucleation kinetics. This trend is broken when the protein exhaustion zones around growing crystals display important overlapping. Maximum growth rates up to 0.05 mm/hour are observed slightly after nucleation.

Crystal movement has been observed at average rates of 3.6 μ/h (maximum rate of 20 μ/h). The movements of different crystals are correlated, for a given time all crystals move in the same direction, suggesting that they are produced by a mechanism operating at a lengthscale larger than the growth cell such as residual accelerations of the spaceship. Another mechanism producing uncorrelated movements of crystals at lower rates seems to be superimposed to the previous one. These random displacements can be due to random errors in the determination of the crystal position or to a short lengthscale mechanism (such as some kind of convection) operating inside the protein chamber. More measurements of crystal movements are being performed to confirm the existence of this second mechanism.

Progresses with interferometric data have been difficult (and continue to be) because of technical problems. The laser installed in the Mach-Zehnder interferometer was unstable during the mission, cluttering the interferograms with random phase jumps. These data, as supplied, are unsuitable for absolute concentration calculations inside the reactor, and our work is being concentrated in recovering this reference information by using simulation of transport dynamics inside APCF reactors. Our first results seems promising, with a good agreement between simulation and experiments, but they are still under active development and discussion.

X-ray diffraction showed the very good quality of crystals, an average limit of resolution of 1.25 Å has been observed. The use of flat capillaries reduces the crystal handling by getting rid of the mounting step. Most of our work using X-rays has been devoted to an exhaustive study of mosaicity.

At a larger scale, very good lysozyme crystals seem to be composed of several slightly defective mosaic domains, in a number ranging from two to four for the samples examined. Very small mosaicity values has been found. All peaks show FWHM ranging from 10'' to 20'' and are composed by at least two domains having FWHM as low as 5'' (without correction). These values are comparable with those found for crystals grown on-ground by the gel acupuncture method. Therefore, in this case no advantages seem to be derived from the microgravity growth of lysozyme in terms of mosaicity. Since mosaicity is mainly controlled by the density and nature of crystalline defects in the crystal and this concentration is mainly a function of the growth rate, this result is consistent with the large initial growth rates measured in crystal lysozyme crystal growth experiments in the APCF and with the mixed regime for lysozyme growth kinetics[8] that provokes large fluctuations in growth rate. This conclusion cannot be interpreted, as a claim against microgravity experiments because no relation has yet been demonstrated between mosaicity and limit of resolution and, from our results, it may even not exist. More experimentation in microgravity crystal growth is needed to complete our present knowledge on this problem, including the systematic determination of accurate limit of resolution and mosaicity values for different macromolecules growing under different kinetic regimes.

---

[8] P.G. Vekilov, J.I.D. Alexander, F. Rosenberger. Phys. Rev. E 54 (1996) 6650-6660.

Mosaicity is an inhomogeneous and anisotropic property. Domains of different quality are not homogeneously distributed. The central part of crystals analysed, that has grown at a faster rate, accumulates the domains having higher mosaicity. We found large FWHM differences for peaks at the same resolution in the same crystal observed from different orientations. This proves that mosaicity can be anisotropic. This anisotropy must be due to differences in the width of domain peaks contributing to the shape of the whole peak or to differences in the relative position of these domain peaks. Further enhancement in the mosaicity values is expected by using protein of very high purity. Our experiments in microgravity (as well as those on-ground) has been performed using lysozyme from Sigma without further purification. The influence of impurities will be tested and compared with that of other physicochemical parameters.

Articles/presentations resulting from the flight

Our results on X-ray studies have been presented at the Spacebound 97 held in Montreal (May 1997) and will be published in the conference proceedings. Nucleation, growth rate and crystal movements will be presented at the ECM-17 to be held in Lisbon (August, 1997) and are the subject of an article in preparation to be submitted to Journal of Crystal Growth. Crystal movement result are being used as part of an article on this topic to be submitted to Microgravity Sci.Technol. References are collected in the following list:

- F. Otálora, B. Capelle, A. Ducruix and J.M. García-Ruiz (1997) "Characterisation of tetragonal lysozyme single crystals grown in the sts-78 mission" oral communication presented in the Spacebound97 Montreal, Mayo 1997.

- F. Otálora, B. Capelle, A. Ducruix and J.M. García-Ruiz (1997) "The mosaicity of protein crystals grown in normal and reduced gravity environments". Accepted for publication into the conference Proceedings.

- Otálora, F., Rondón, D., Novella, M.L. and García-Ruiz, J.M. (1997) "Lysozyme crystal growth in microgravity. X-ray, image analysis and interferometric results from the APCF during LMS mission." oral communication presented in the ECM-17 to be held in Lisbon, August 1997.

- Otálora, F., Rondón, D., Novella, M.L. and García-Ruiz, J.M. (1997) "Lysozyme crystal growth in microgravity. X-ray, image analysis and interferometric results from the apcf during lms mission." In preparation, to be submitted to Journal of Crystal Growth.

- J.M. García-Ruiz and F. Otálora (1997) "Crystal movements during microgravity crystal growth experiments" In preparation, to be submitted to Microgravity Sci.Technol.

Summary of the experiment and the accomplishments

The objectives of this set of experiments were concentrated on the technical and phenomenological aspects of protein crystal growth in the APCF. Therefore, a well known protein, lysozyme, was selected. Technical topics investigated were the new APCF Mach-Zehnder interferometer available for the first time during this mission and new experimental settings for APCF reactors such as the use of gelled solutions, the filling of the rotatory plug with protein solution and the use of a pack of flat capillaries filling the protein chamber. Phenomenological studies include investigations on the growth kinetics of lysozyme under counterdiffusion conditions in microgravity and the movement of crystals during growth. Additionally, an in-depth study on the mosaicity of these microgravity crystals has been performed including the comparison of these results with on-ground observations.

The underlying idea of this set of experiments was to get information on how the APCF performs as a device for purely diffusive counterdiffusion experiments. In this framework, interferometry is useful to control the dynamics of diffusive transport, gelled solutions can be used to control the time and space gradients of supersaturation and the use of the rotatory plug as part of the growth chamber makes it longer reinforcing the one-dimensional nature of the experiment. Nucleation flux and growth rate are a function of the rich spatio-temporal behaviour of the system due to its out of equilibrium nature. The movement of crystals during growth acts, in principle, as a limiting factor for the ideal diffusive experiment and, therefore, must be studied and understood, but it can be used even as a beneficial feature for crystal growth if it its predictable and manageable. The final output of the whole process are the, hopefully, good protein crystals for structural analysis; here we tried the use of flat capillaries to have pre-mounted crystals free of further mounting and handling and performed a exhaustive study on the mosaicity of the crystals obtained, comparing the results from this mission with that from on-ground experiments using one-dimensional counterdiffusion techniques and assessing the usefulness of this value in terms of crystal quality meassure.

Lysozyme crystals grown in a diffusive regime, although the out of equilibrium counterdiffusive nature of the experiments was not fully exploited due to the shortness of the reactors that causes the almost complete homogenisation of the protein chamber before nucleation. Crystals move during crystal growth due mainly to small residual accelerations of the spaceship. The use of capillaries inside the protein chamber is a beneficial feature that eliminates the need of further crystal handling. The usefulness of interferometric data was compromised by laser instabilities. Mosaicity of the crystals obtained is very good, although no significantly better than that of crystals grown on-ground by the Gel Acupuncture method. In any case, mosaicity seems not to be directly correlated with the resolution limit in diffraction studies.

127

Advanced Protein Crystallization Facility (APCF)

Comparative Analysis of Aspartyl tRNA-synthetase and Thaumatin Crystals Grown on Earth and In Microgravity

Principal Investigator:

Dr. Richard Giegé
CNRS
Strasbourg, France

Comparative analysis of Aspartyl tRNA-synthetase and Thaumatin crystals grown on earth and in microgravity

LMS (STS-78) L+1 Report

by

Joseph D. Ng, Bernard Lorber, and [‡]Richard Giegé

UPR 'Structure des Macromolécules Biologiques et Mécanismes de Reconnaissance ' Institut de Biologie Moléculaire et Cellulaire du CNRS, 15 rue René Descartes, F-67084 Strasbourg Cedex, France

[‡]Corresponding Author

Introduction

Evidence has accumulated in the past years from a variety of experiments performed in microgravity, that suggest reduced gravity conditions can diminish the deleterious factors and consequently improve the quality and increase order for protein crystals (DeLucas *et al.*, 1986; 1989; 1991; DeLucas & Bugg, 1987; Erdmann *et al.*, 1989; McPherson *et al.*, 1991). Macromolecular crystal growth experiments, using the *T. thermophilus* AspRS expressed in *E. coli* (ttAspRS) and the plant sweetening protein, Thaumatin, were conducted on a US Space Shuttle mission designated Life Microgravity Spacelab (LMS) mission STS-78, flown June 20-July 7, 1996. The studies were carried out using dialysis reactors of the Advanced Protein Crystallization Facility (APCF) provided by Dornier Deustche Aerospace. The experiments in each device were performed at a constant temperature during a complete mission elapsed time of 16 days. The fundamental objectives of this study was to obtain crystals of protein in microgravity, to determine if the influence of microgravity affects crystal growth and to observe any anomalies or enhancement in growth that may implicate a gravity effect.

Model Proteins

Thaumatin

Thaumatin is a monomeric protein from the African Serendipity Berry *(Thaumatococcus daniellii)* valued for its intensely sweet taste and its use as a non caloric sweetener. It has a molecular weight of 21,500, contains four disulfide bridges, and possesses a high degree of stability. It consists primarily of beta structure organized in two associated domains. The structure was first determined in an orthorhombic crystal at 1.7 Å resolution (Ogata *et al.* , 1992), and later in a second orthorhombic, a monoclinic, and a tetragonal crystal form (Ko *et al.*, 1994). The tetragonal crystal form, grown from tartrate, and refined to 1.7 Å resolution (Ko *et al.*, 1994) was that studied in these experiments. The mechanisms and kinetics of growth at the molecular level for thaumatin crystals are among the most thoroughly characterized of any protein crystal (Malkin *et al.*, 1996a; Malkin *et al.*, 1996b). Crystals can be grown in a conventional laboratory in 12 to 48 hours at room temperature by a variety of methods. The crystals are of space group $P4_12_12$ with a = b= 59 Å and c = 158 Å having a single molecule as the asymmetric unit. The habit is that of a tetragonal bipyramid, often reaching linear dimensions in the conventional laboratory greater than 1 mm. The crystals, which contain about 45% solvent, are mechanically robust. Their growth has been studied by a variety of physical techniques including interferometry (Kuznetsov *et al.*, 1995) and atomic force microscopy (Malkin *et al.*, 1996a; Malkin *et al.*, 1996b).

Aspartyl-tRNA synthetase

The vital and key step in the process of translating genetic information is the aminoacylation of tRNA (Giegé *et al*, 1993). The enzymes that mediate this action are the aminoacyl-tRNA synthetases which catalyze the addition of an amino acid to their cognate tRNAs (*e.g.* Schimmel & Söll, 1979; Schimmel, 1987; Giegé *et al*, 1993). Structurally, aaRS's exhibit a wide divergence shown by differences in their molecular size, oligomeric state, modular and three-dimensional structures (Moras, 1992). Sequence analyses of all known aaRS's have led to the categorization of these enzymes into two classes having each ten members (Eriani *et al*, 1990). The class distribution is correlated to the functional property of aaRS's and to their capacity to charge the amino acid at either the 2'- or the 3'-hydroxyl group of the 3' end ribose (Fraser *et al*, 1975; Sprinzl & Cramer, 1975).

Two of the most well characterized class II synthetases are the aspartyl-tRNA synthetases from yeast and *Thermus theromophilus*. Structural information have been obtained for both of these enzymes and have found to share common structural motifs (Ruff *et al,* 1991; Delarue *et al,* 1994). In particular, the aspartyl-tRNA synthetase from *T. thermophilus* (ttAspRS) has been cloned, overexpressed in *Escherichia coli,* crystallized and its structure determined to 2.5 Å resolution (Poterszman *et al,* 1993; Delarue *et al,* 1994). Orthorhombic crystals of the ttAspRS can be grown out of precipitation with the space group $P2_12_12_1$ with cell dimensions a = 61.4Å, b = 156.1 Å and c = 177.3 Å (Ng, *et al.,* 1996) . ttAspRS is a homodimer with each subunit having a molecular weight of 66 kD and a polypeptide composed of 580 amino acids (Poterszman *et al,* 1993). This enzyme has sequence and structural features that can be related to other AspRS's and class II aaRS's. A comparison among seven known sequences of AspRS's has revealed a clear partition between eucaryotes and prokaryotes having molecular features that are uniquely exhibited in the thermophilic enzyme which are not found in any of the other known AspRS's (Poterszman *et al.,* 1993). The crystallographic structure of ttAspRS revealed the first atomic description of a prokaryotic AspRS and showed structural motifs that are specific to prokaryotes (Delarue *et al.,* 1994).

The most striking biochemical property of ttAspRS, as with most other thermophilic enzymes, is its resistance to denaturation under high temperatures. It is relatively very stable in that it can sustain biological activity at temperatures up to 80°C and is able to charge aspartate to its cognate tRNA at a wide range of temperatures. This property makes ttAspRS a favorable model protein for crystal growth studies, in particular for explaining effects of temperature. This is most interesting for studies on synthetases which are relatively unstable molecules in contrast to other proteins like lysozyme that are often studied under microgravity.

Materials and Methods

Proteins and chemicals

Preparation of Thaumatin

Thaumatin was purchased from Sigma (St Louis, MO). A single batch (Cat. N° T-7638, lot 108F0299) of dry protein powder was used. The protein was dissolved either in a buffer prepared with 0.1 M N-[2-acetamido]-2 iminodiacetic acid (ADA) (Cat. N° A-9883, lot 92H5635, Sigma) adjusted at pH 6.5 with NaOH or in water (see Table 1). For crystallization, the precipitant stock solution was 1.6 M sodium DL-tartaric acid (Cat. N°T-5259, lot 101H0695, Sigma) in 0.1 M ADA titrated with NaOH to pH 6.5. All solutions were prepared with ultrapure sterile water (Fresenius, Louviers, France) and sterilized by filtration through 0.22 μm pore size membranes (Millex, Millipore).

A concentrated stock solution of thaumatin was freshly prepared by adding 1 ml of ADA buffer pH 6.5 to 100 mg protein powder. After dissolution, the solution was centrifuged for 20 min at 15,000 g. The supernatant was filtered through 0.22 μm Ultrafree low binding membranes (Cat. N°UFC3 0GV 00, Millipore). The protein concentration was calculated from the UV absorbance of a 1/250 dilution using a molar extinction coefficient of 28,270 (based on the tryptophan and tyrosine content).

Isolation and purification of ttAspRS

The ttAspRS expressed in *E. coli* was purified with two chromatographic steps as described by Poterszman *et al* (1993) with slight modifications. An attractive property of recombinant ttAspRS is that it is heat tolerant. Crude bacterial cell extract can be exposed to elevated temperature, thus denaturing contaminant proteins. The ttAspRS thus can be found exclusively in the soluble portion of the cell extract and use of denaturants is not required for recovery at any stage. The ttAspRS enzyme can essentially be purified to more than 90% homogeneity.

Crystallization apparatus and conditions used

We have utilized dialysis liquid diffusion reactors (DIA) for crystallization within the Advanced Protein Crystallization Facility (APCF) developed by Dornier Deutsch Aerospace (Snyder *et al*, 1991; Bosch *et al.*, 1992) aboard the NASA Space Shuttle, Columbia (STS-78, mission LMS). The dialysis reactor consists of two quartz glass blocks separated by a dialysis membrane. The upper block contains the protein solution (67 µl or 188 µl), the lower block, the salt solution. A cylindrical quartz glass plug containing also the salt solution separates the salt and buffer chamber. Upon activation, the glass plug is rotated by 90°C so that all chambers become open and all volumes then come into contact. Likewise, the plug is rotated back during deactivation before returning to earth. Reactors for space and ground controls were prepared in exactly the same manner and had undergone the exact same transport and pre-launch conditions (this included any delay launch time as well). The DIA ground control reactors were activated for the same period of time as the ones that were launched in space in parallel with the time of flight. Two 67 µl reactors were used for the crystallization of ttAspRS and two 188 µl reactors were used for thaumatin. The contents of the reactors and the crystallization conditions are described in Table 1.

The APCF was activated several hours after a microgravity environment was achieved, and deactivated (the stopcocks rotated in reverse) a few hours before reentry. Duration of activation of the crystallization reactors under the microgravity environment was 16 days for this mission. Following the mission the dialysis cells were immediately examined, photographed, and X-ray diffraction analysis initiated.

Crystallographic methods

Three dimensional X-ray data were collected at the EMBL Outstation DESY, Hamburg, Germany on beam line X11 using a MAR Research image plate. Complete data sets of the protein crystals grown on LMS and the corresponding earth controls were obtained using crystals of same size and volume. Data were collected at 20°C with crystal-to-detector distance of 250 mm. Oscillation angles of 0.5° were used with an X-ray wavelength of approximately 0.91Å with exposure time varying from 20 to 30 sec. Data collection was evaluated on line with the programs DENZO and SCALEPACK (Otwinowski & Minor, 1996) at the DESY synchrotron station. Both earth and microgravity grown crystals were collected to 2.0 Å with $R_{sym's}$ ranging from 0.023 to 0.435 for ttAspRS. Similarly, earth and microgravity grown crystals of thaumatin were collected to 1.6 Å with $R_{sym's}$ ranging from 0.021 to 0.175 for reflections having an I/σ greater than 3.

The mosaicities of ttAspRS and the thaumatin crystals, obtained under both ground and space growth conditions, were evaluated by measuring the rocking widths for selected reflections presented as the full width at half maxima (FWHM) (Helliwell, 1988). Crystal mosaicity yields the angular dispersion of the crystal blocks characterizing the crystals and in turn reflects the intrinsic crystal order (Weisgerber & Helliwell, 1993). Space and earth grown crystals of the same volumes were mounted in standard glass capillaries. Data for mosaicity measurements were recorded by using a CCD detector on beamline CRG BM2 (D2AM) at ESRF, Grenoble, France. This particular synchrotron beamline produces a highly collimated, intense radiation of very low divergence and minimal $\delta\lambda/\lambda$. The critical energy was 19.5 keV with a focused beam of 0.3 mm diameter at the sample with a maximum vertical divergence of 0.15 mrad and a maximum horizontal divergence of 9.0 mrad (Ferrer et al., 1996; personal communication). The intensity of the full beam was about 10^{11} ph/sec at 0.98 Å wavelength with an energy resolution, $\delta\lambda/\lambda$, of approximately 10^{-4}. Direct monochromatic measurements were obtained by recording data over oscillation ranges of 0.5 degree for indexing of reflections and subsequently an oscillation angle of 0.003 degrees with 0.2 degrees of crystal rotation at 10 seconds exposure per frame. The data for mosaicity analysis were processed with XDS and images of the intensities visually observed and quantitated with MARVIEW (Kabsch, 1988a, 1988b).

Reflections were measured in the vertical plane with respect to the direct beam so that a fully recorded reflection can be expressed as:

$$\varphi_r = \gamma + \eta + (\delta\lambda/\lambda)\tan\theta$$

where φ is the reflecting range, γ is the mean divergence in the plane defined by the direct and the diffracted beams, η is the crystal sample mosaicity, λ is the average wavelength of the X-ray beam and θ is the Bragg angle of the reflection (Snell et al., 1995; Ferrer et al., 1996). The values of γ and $\delta\lambda/\lambda$ were minimized in this study by considering only reflections located in the vertical plane including the incident beam and those at low resolution. The measured FWHM value has the instrument resolution function value IRF (0.15 mrad or 0.009°) deconvoluted out. The profiles presented here were not corrected for Lorentz broadening.

Results and Discussion

Visual and microscopic observations

Crystals were observed in the two dialysis reactors containing thaumatin and only in one reactor containing the ttAspRS for microgravity. All of the corresponding dialysis reactors activated as ground controls for both proteins contained crystals . There was a clear increase in average and largest sizes of crystals grown by dialysis in microgravity compared with ground controls. For thaumatin the number and sizes of crystals from the dialysis reactors were assessed with an optical microscope and are summarized in Table 2. Each of the space flight reactors contained more than 1000 crystals having an average size range of 0.4 (Fig 1) The corresponding ground control reactors contained about twice the number of crystals having an average size range of 0.3 mm.

In the space reactor containing ttAspRS, three huge crystals were found in the protein chamber in the midst of precipitation measuring over 3 mm in its longest dimensions in size accompanied with some very small crystals. However, the corresponding ground controls contained only very few crystals also with no more than

two to three in each reactor having the largest size of about 2mm in length. Even though ttAspRS crystals obtained from both space and earth grown environments were relatively large, the crystals grown in microgravity were exceptionally large (Fig 2).

Visually, the quality of the crystals of both proteins obtained from space, particularly those growing free of any surfaces, and including the largest, was very high. They appeared virtually flawless, with no observable imperfections, striations, or habit anomalies. Crystals attached to the cell walls (and which presumably nucleated there) did show defects near the sites of growth initiation but became flawless as growth proceeded into the bulk solution.

X-ray intensity measurements

X-ray diffraction data were collected from a total of three thaumatin crystals grown in microgravity. The data were merged to form a single data set. We have compared individual crystals grown in space and on earth in similar APCF cells. In all measurements, the amount of data greater than 3σ (the average I/σ in all resolution ranges) was better for the microgravity crystals than for the earth controls. Both earth and space crystals diffract easily beyond 1.6 Å with the inclination of the space grown crystal to extend to higher resolution. A quantitative comparison in the high resolution range 2.1-1.6 Å of a representative crystal from space and earth having the same size and volume is shown in Fig. 3. The data show reproducibly a significant increase of the I/σ ratio for the space grown crystals over all the resolution range investigated (Ng, *et al.*, 1997).

In the same manner three-dimensional intensity data were collected from two ttAspRS crystals grown in space (one of these is shown in figure 2). Figure 4 shows the distribution of observable data, I/σ greater than 3 compared to its corresponding earth-grown crystals. For the resolution range studied, space grown crystals yield as much as 93% more diffraction intensities than the control crystals grown on earth. However, at the resolution limits, the diffraction intensities of the earth and space grown crystals were only marginally different.

Mosaicity measurements

Fig. 5 and 6 presents typical mosaicity profiles of representative reflections from both space and earth grown crystals of thaumatin and ttAspRS respectively. The reflection profiles lie in the vertical plane of diffraction at approximately 4 Å resolution and their intensities were normalized for direct comparison. In the case of thaumatin, the curves appear coarse, displaying numerous shoulders, particularly in the latter portions of the profiles (Fig. 5). For all reflections, such irregularities were present, suggesting that the local features of the profile could be reflective of intrinsic properties of the crystal.

Each set of reflection profiles of the space and earth grown crystals were averaged and Gaussian fits of the sets of profiles were calculated (solid lines). Full widths at half maxima (FWHM) of the Gaussian curves were measured and in the case of thaumatin, the FWHM was 47 millidegrees (0.047 deg) for a crystal grown on earth (panel A) compared to 18 millidegrees for the space crystal (panel B). The difference in mosaicity between space and earth grown ttAspRS were much more dramatic showing the ttAspRS crystal from space to be about 8 times less mosaic than its corresponding earth control (Fig 6).

Notably, in all the reflections of all the space thaumatin grown crystal mosaicity profiles analyzed, a principle shoulder is observed in the beginning of the profiles while the end of the profiles remain very smooth and the curve diminishes sharply. We have no clear explanation for this observation. It may be possible that

these shoulders are indicative of some degree of twinning in the crystal or due to other defects not detected by low-magnification visual microscopy produced during storage or transport on the ground. This phenomenon contributes to the non-symmetrical fit of the Gaussian curves. In our measurements, the Gaussian plots are fitted to the principle peaks in which the FWHMs were evaluated. We have only considered the principle peak at this instant to represent the actual mosaicity profile for the space grown crystals. Even if the shoulder widths were included in the measurement of the FWHM, the value would still be significantly less than that of the earth grown crystals.

Consistently, reflections from crystals grown in microgravity from both space missions displayed narrower peaks of greater amplitude. This is likely a consequence of reduced discrete defects and dislocations compared to crystals grown on earth. The relative intensity and peak width differences of averaged profiles measured from reflections derived from space and earth grown crystals presented in Fig. 5 and 6 typify the mosaicity of thaumatin and ttAspRS crystals obtained on earth and in space. Tables 3 and 4 summarize the mosaicity evaluations of the space and earth grown crystals.

Conclusion

The results presented here for thaumatin and ttAspRS crystals grown in microgravity reinforce the conclusions of other reports based on different macromolecules that a microgravity environment can provide unique advantages (Giegé *et al.*, 1995). In these experiments the microgravity grown crystals were consistently and significantly larger, and substantially more defect free as judged by direct visual inspection. The resolution limit of the diffraction pattern, the I/σ ratio as a function of the Bragg angle, and the mosaic spread of crystals are generally agreed to reflect both the degree of internal order and the long range defect structure and its distribution within the crystal. That is, they serve as measures of the average statistical disorder of the molecules about the lattice points, as well as the extent of local but severe disorder introduced by defects such as dislocations, stacking faults, point defects or incorporated foreign material (Malkin *et al.*, 1996a). All of the data presented here, both intensity distributions and mosaic spread measurements, imply a higher degree of internal order, a lower defect density, and a reduction of severe faults for crystals grown in the absence of gravity.

Similar results, based on intensity data for microgravity grown crystals of several proteins, have been reported previously (DeLucas *et al.*, 1989; Day & McPherson, 1992; Koszelak *et al.*,1996), and comparable results based on mosaicity measurements have been presented for others (Snell, Weisgerber & Helliwell, 1996). Our conclusion is that they are mutually supportive and complementary, and both suggest the same conclusion, that crystals grown in microgravity can be significantly improved in their diffraction properties when compared with those grown on earth.

Acknowlegement

References

1   Bosch, R., Lautenschlager, P., Potthast, L. and Stapelmann, J. (1992) *J. Cryst. Growth* **122**, 310-316

2   Day, J. and McPherson, A. (1992). *Protein Science* 1, 1254-1268.

3   Delarue, M., Poterszman, A., Nikonov, S., Garver, M., Moras, D. and Thierry, J. C. (1994) *EMBO J.* **13**, 3219-3229

4   DeLucas, L. J., Suddath, F. L., Snyder, R., Naumann, R., Broom, M. B., Pusey, M., Yost, V., Herren, B., Carter, D., Nelson, B., Meehan, E. J., McPherson, A. and Bugg, C. E. (1986) *J. Crystal Growth* **76**, 681-693

5   DeLucas, L. J. and Bugg, C. E. (1987) *Trends in Biotech.* **5**, 188-192

6   DeLucas, L. J., Smith, C. D., Smith, C. D., Smith, H. W., Senadhi, V. K., Senadhi, S. E., Ealick, S. E., Bugg, C. E., Carter, D. C., Snyder, R. S., Weber, P. C., Salemme, F. R., Ohlendorf, D. H., Einspahr, H. J., Clancy, L., Navia, M. A., McKeever, B. M., Hagabhushan, T. L., Nelson, G., Babu, Y. S., McPherson, A., Koszelak, S., Stammers, D., Powell, K. and Darby, G. (1989) *Science* **246**, 651-654

7   DeLucas, L. J., Smith, C. D., Smith, W., Senadhi, V.-K., Senadhi, S. E., Ealick, S. E., Carter, D. C., Snyder, R. S., Weber, P. D., Salemme, R. R., Ohlendor, D. H., Einsphar, H. M., Clancey, L. L., Navia, M. A., McKeever, B. M., Nagabhushan, T. L., Nelson, G. and Bugg, C. E. (1991) *J. Crystal Growth* **110**, 302-311

8   Erdmann, V. A., Lippmann, C., Betzel, C., Dauter, Z., Wilson, K., Hilgenfeld, R., Hoven, J., Liesum, A., Sainger, W., Muller-Fahrnow, A., Weber, G., Stegen, K. and Plaas-Link, A. (1989) *FEBS Lett.* **259**, 194-198

9   Eriani, G., Delarue, M., Poch, O., Gangloff, J. and Moras, D. (1990) *Nature* **347**, 203-206

10   Ferrer, J.-L., Hirschler, J., Roth, J. and Fontecilla-Camps, J. C. *ESRF Synchrotron Report* (1996), 27-28

11   Fraser, T. H. and Rich, A. (1975) *Proc. Natl. Acad. Sci. USA* **72**, 3044-3048

12   Giegé, R., Puglisi, J. D. and Florentz, C. (1993) *Progr. Nucleic Acid Res. Mol. Biol.* **15**, 129-206

13   Giegé, R., Drenth, J., Ducruix, A., McPherson, A. and Saenger, W. (1995) *Prog. Crystal Growth and Charact.* **30**, 237-281.

14   Helliwell, J. R. (1988) *J. Cryst. Growth* **90**, 259-272

15   Kabsch, W. (1988a) *J. Applied Crystallography* **21**, 67-71

16   Kabsch, W. (1988b) *J. Applied Crystallography* **21**, 916-924

17   Ko, T.-P., Day, J., Greenwood, A. and McPherson, A. (1994) *Acta Cryst. D* **50**, 813-825

18   Koszelak, S., Leja, C. and McPherson, A. (1996) *Biotech. And Bioengin.* 52, 449-458.

19   Malkin, A. J., Kuznetsov, Y. G., Glantz, W. and McPherson, A. (1996a) *J. Struct. Biol.* **117**, 124-137

20   Malkin, A. J., Kuznetsov, Y. G., Glantz, W. and McPherson, A. (1996b) *J. Phys. Chem.* **100**, 11736-11743

21   McPherson, A. (1976) *Crystallography Reviews* **6**, 157-308.

22   Moras, D. (1992) *Current Opinion Struct. Biol.* **2**, 138-142

23   Ng, J. D., Lorber, B., Witz, J., Théobald-Dietrich, A., Kern, D. and Giegé, R. (1996) *J. Crystal Growth* **168**, 50-62

24   Ng, J. D., Lorber, B., Giegé, R., Koszelak, S., Day, J., Greenwood, A. and McPherson, A. (1997) *Acta Cryst. D*, In press

25   Ogata, C. M., Gordon, P. F., de Vos, A. M. and Kim, S. H. (1992) *J. Mol. Biol.* **3**, 893-908

26   Otwinowski, Z. and Minor, W. (1996) *Meth. in Enzymology* **276**, 307-326

27   Poterszman, A., Plateau, P., Moras, D., Blanquet, S., Mazauric, M.-H., Kreuzer, R. and Kern, D. (1993) *FEBS Lett.* **325**, 183-186

28   Ruff, M., Krishnaswarny, S., Boeglin, M., Poterszman, A., Mitschler, A., Podjarny, A., Rees, B., Thierry, J.-C. and Moras, D. (1991) *Science* **252**, 1682-1689
29   Schimmel, P. R. and Söll, D. (1979) *Annu. Rev. Biochem* **48**, 601-648
30   Schimmel, P. (1987) *Annu Rev. Biochem* **56**, 125-158
31   Snell, E. H., Weisgerber, S., Helliwell, J. R., Wechert, E., Hölzer, K. and Schroer, K. (1995) *Acta Cryst. D* **51**, 1099-1102
32   Snyder, R. S., Fuhrmann, K. and Walter, H. U. (1991) *J. Cryst. Growth* **110**, 333-338
33   Sprinzl, M. and Cramer, F. (1975) *Proc. Natl. Acad. Sci. USA* **72**, 3049-3053
34   Weisgerber, S. and Helliwell, J. R. (1993) Joint CCP4 & ESF-EACBM newsletter on Protein Crystallography **29**, 10-13

FIGURE LEGENDS

Figure 1.   Crystals of thaumatin grown in microgravity.   The average size of the crystals were approximately 0.4 mm in the longest direction seen directly in the protein chamber of the APCF reactor

Figure 2. Crystals of the ttDRS grown in microgravity (upper panel, A) and on earth (lower panel, B). a) d) A) The biggest crystal measured to be 3.3 mm x 2.5 . This crystal was carefully removed from the APCF reactor chamber, washed with a sodium formate wash buffer and placed on a glass cover slip for visual evaluation before the x-ray analysis. B) The control crystals grown on earth measured up to 2.0 mm x 1.1 mm.   One of the crystals was transferred into a glass cover slip and carefully rinsed with a sodium formate wash buffer to remove the precipitated debris for observation before mounting into a capillary glass tube for x-ray analysis.

Figure 3. Graphs of the intensity (I) *versus* estimated error (σ) ratio as a function of resolution ($\sin^2\theta/\lambda^2$) for thaumatin earth and space grown crystals analyzed by synchrotron sources. The graphs are presented as modified I/σ over resolution where the value of I/σ 's are the effective "signal-to-noise" for the diffraction pattern at the resolution corresponding to the respective ($\sin^2\theta/\lambda^2$) values.

Figure 4. Graph of the intensity (I) versus estimated error (σ) ratio as a function of as a function of resolution ($4\sin^2\theta/\lambda^2$) for ttDRS earth and space grown crystals analyzed by synchrotron source. For the resolution range shown, space grown crystals yield as much as 93% more diffraction intensities ($>3\sigma$) than the control crystals grown on earth. However, at the maximum resolution limit, the diffraction intensities of the earth and space grown crystals were only marginally different.

Figure 5. Profiles of three representative reflections (17 -1 23), (-2 12 12), and (16 -10 5) at 4 Å were each evaluated from an earth (A) and space grown thaumatin crystal (B) studied for LMS. Reflections were obtained in the vertical diffraction plane such that the rotation axis was horizontal and perpendicular to the X-ray beam. Each set of reflection profiles for space and earth grown crystals were averaged and Gaussian fits of the sets of profiles were calculated (solid lines). The Gaussian plots were fitted to the principle peaks in which the FWHMs were evaluated. Only the principle peak is considered to represent the actual mosaicity profile for the space grown crystals. The full width at half maximum (FWHM) of a Gaussian fit for each profile was measured and its value deconvoluted out by the instrument resolution function value, IRF (0.15 mrad or 0.009°). FWHM values are indicated by short horizontal lines in the profiles and they show that the space grown crystal are about 2.5 times less mosaic than that of the earth grown. The intensities shown are normalized and the actual peak intensities measured to 250,000 counts per 0.1 seconds for the space crystal. In contrary, the spot intensities corresponding to the same reflections for the earth crystal were approximately two times less. Panel C shows a relative comparison of the averaged mosaicity profiles from an earth to a space grown crystal for the same reflections.

Figure 6. Profiles of three representative reflections (14 8 9), (4 33 -13), and (-14 5 -7) at 4 Å were each evaluated from an earth (left panel) and space grown ttDRS crystal (right panel). Reflections were obtained in the vertical diffraction plane such that the rotation axis was horizontal and perpendicular to the X-ray beam. Each set of reflection profiles for space and earth grown crystals were averaged and Gaussian fits of the sets of profiles were calculated (solid lines). Only the principle peak is considered to represent the actual mosaicity profile for the space groan crystals. The full width at half maximum (FWHM) of a Gaussian fit for each profile was measured and its value deconvoluted out by the instruments resolution function value, IRF (0.15 mrad or 0.009°). The intensities shown are normalized and the actual peak intensities measured to 570,000 counts per 0.1 seconds for the space crystal. In contrast, the spot intensities corresponding to the same reflections for the earth crystal were approximately 19 times less.

TABLES

Table. 1. Content of APCF Reactors

Table 2. Number and Size of Space and Earth Grown Crystals in APCF Dialysis Reactors

Table 3. Mosaicity Characteristic of Ground and Space Grown Thaumatin Crystals

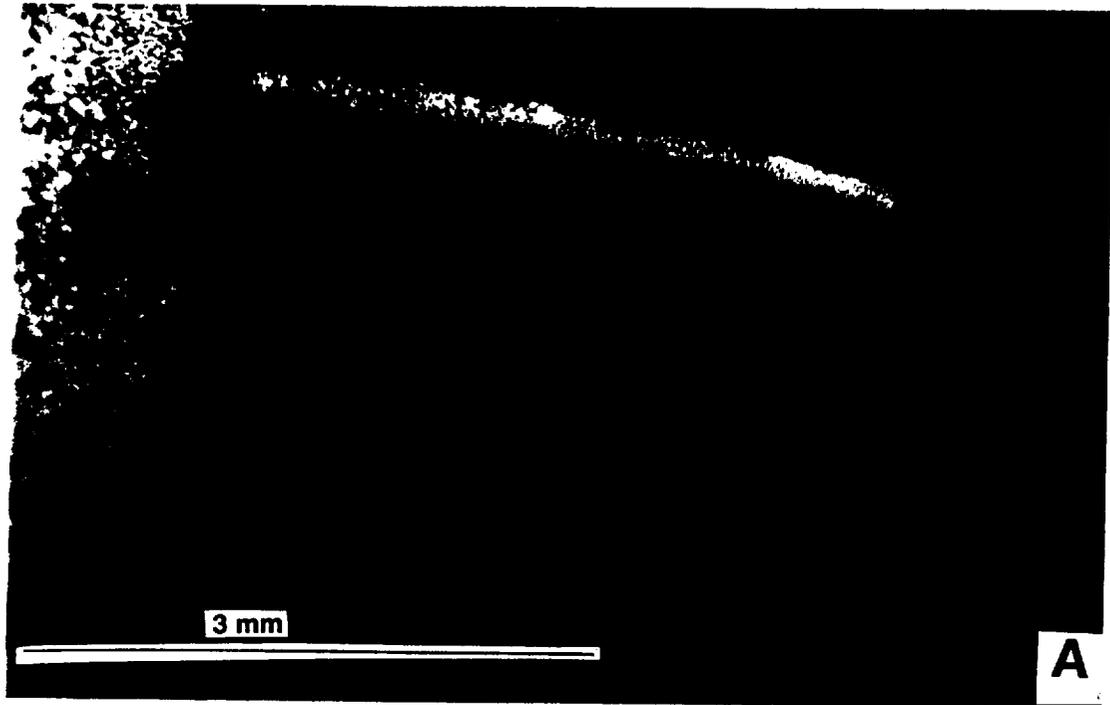**Table 4.** Mosaicity Characteristic of Ground and Space Grown ttAspRS Crystals

1 mm

Figure 1

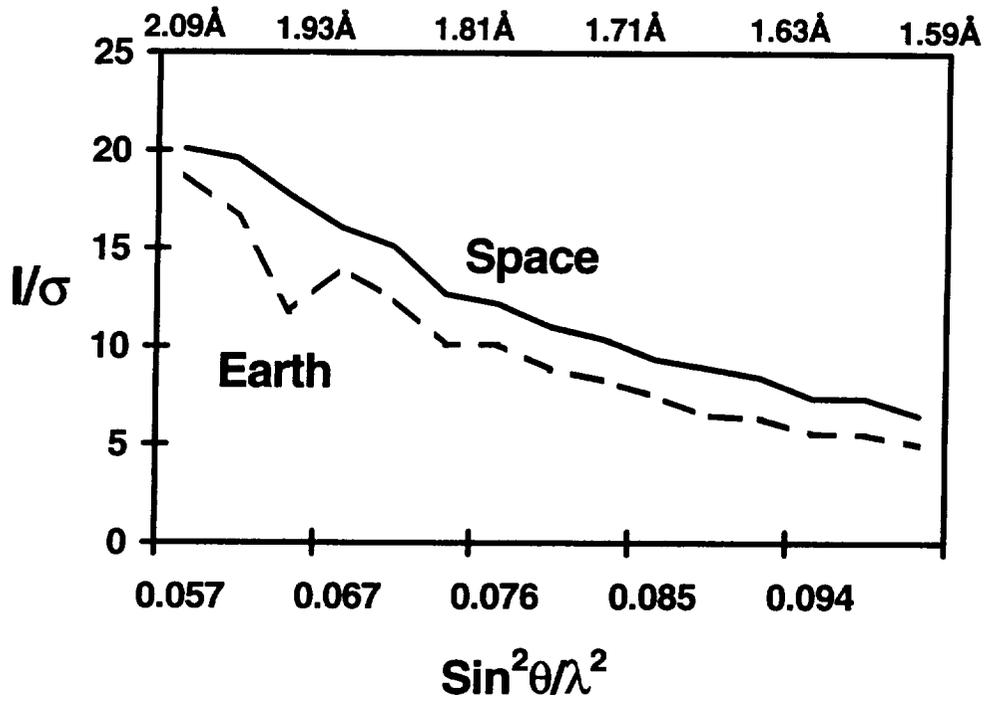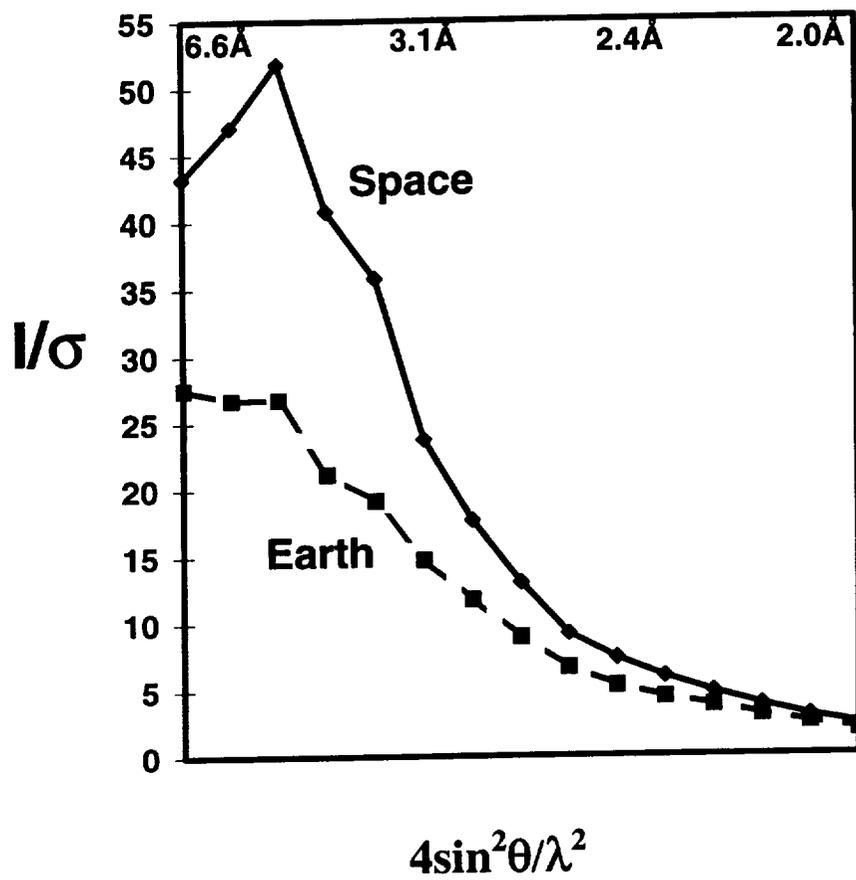3 mm

A

B

Figure 2

Figure 3

Figure 4

Figure 5

Earth

Space

FWHM = 64mdeg

FWHM = 8mdeg

Normalized Intensity
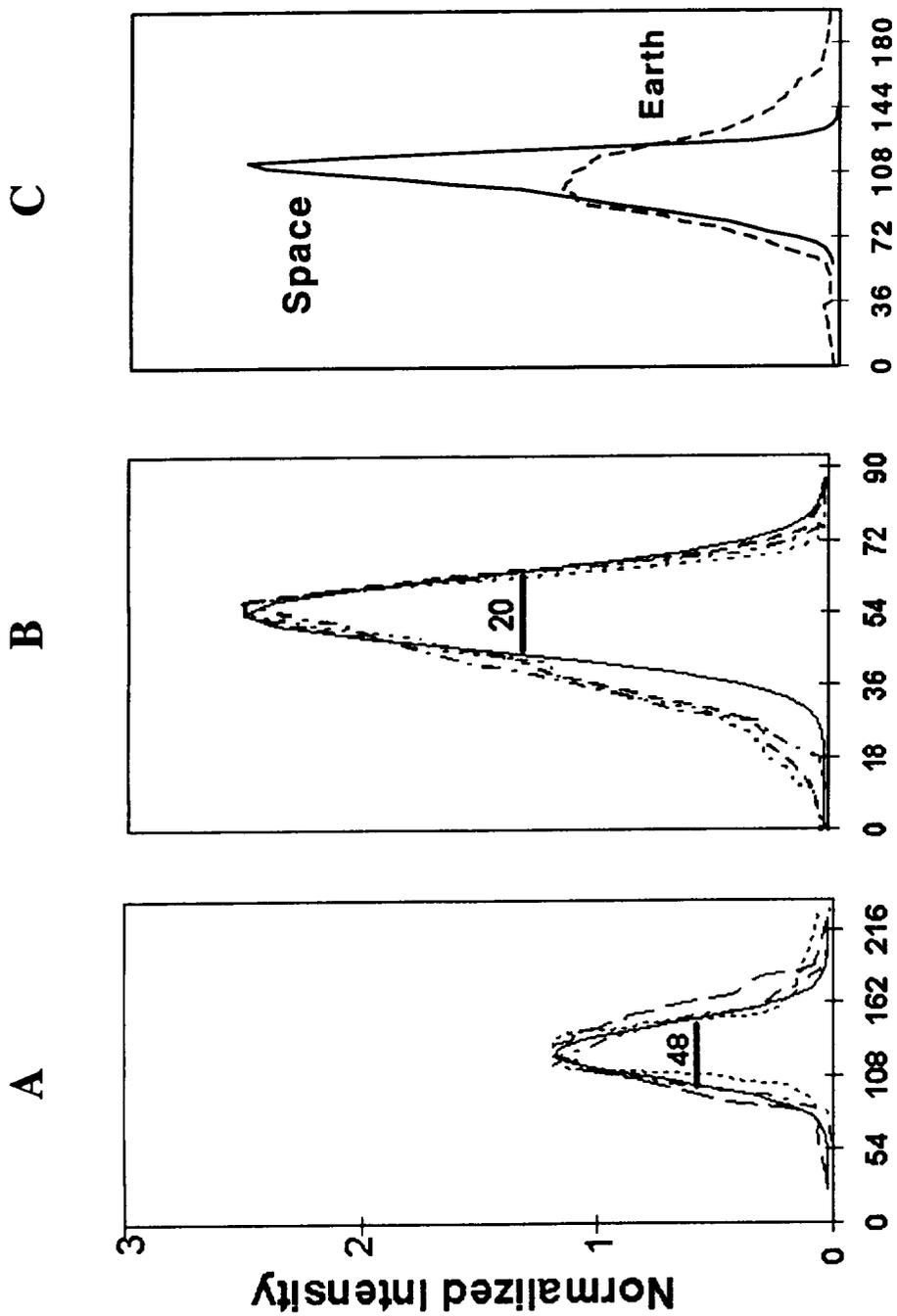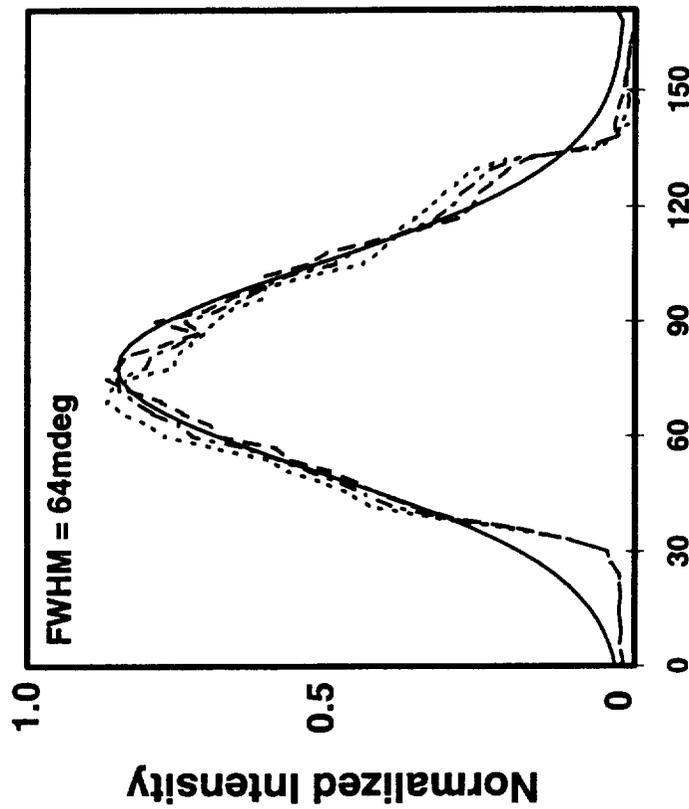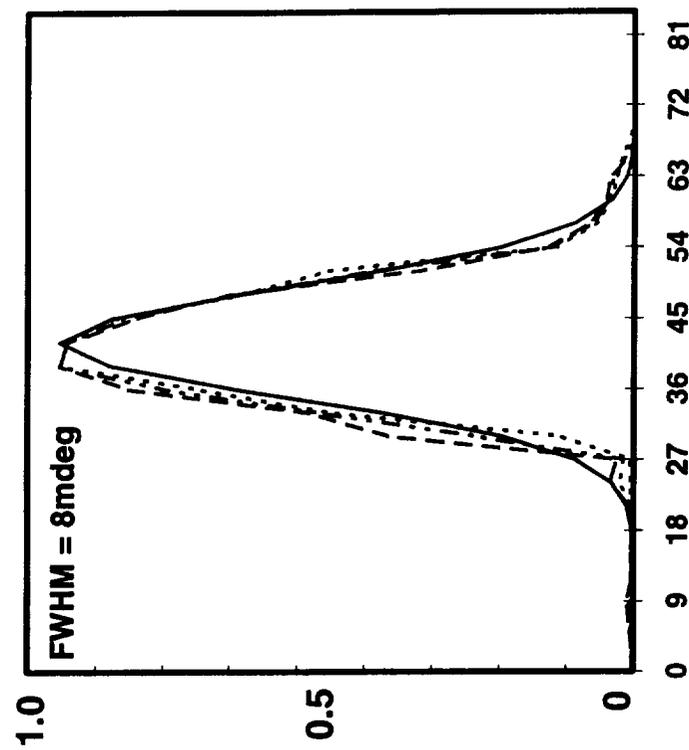
Scan in mdeg

Figure 6

146

Table 1. Content of APCF Reactors

Reactor no.	Protein	Protein			Buffer		Piston		Salt	
		Protein conc. (mg/ml)	Buffer	Volume (µl)	Buffer	Volume (µl)	Buffer	Volume (µl)	Buffer	Volume (µl)
1	Thaumatin	20	A	188	B	59	B	246	B	295
2	Thaumatin	20	A	188	B	59	B	246	B	295
3	ttAspRS	20	C	67	D	59	D	246	D	295
4	ttAspRS	20	C	67	E	59	E	246	E	295

Solution A: 0.1 M ADA buffer and 0.20 M sodium tartrate pH 6.5.
Solution B: 0.1 M ADA buffer and 0.95 M sodium tartrate pH 6.5.
Solution C: 25 mM Tris-HCL buffer, 1 mM $MgCl_2$, 1 mM DTT pH 7.5.
Solution D: 40% saturated ammonium sulfate in 25 mM Tris-HCL buffer, 1 mM $MgCl_2$, 1 mM DTT pH 7.5.
Solution E: 50% saturated ammonium sulfate in 25 mM Tris-HCL buffer, 1 mM $MgCl_2$, 1 mM DTT pH 7.5.

Table 2. Number and Size of Space and Earth Grown Crystals in APCF Dialysis Reactors

Space

Reactor	No. of crystals	Average Size(mm) (longest dimensions)
(Protein chamber size)		
1 (188µl)	1250	0.4
2 (188µl)	1150	0.4

Corresponding Earth Controls

No. of crystals	Average Size(mm) (longest dimensions)
2000 +	0.3
2000 +	0.3

Reactors containing more than 2000 crystals are noted as 2000+. (Number of crystals exceeding 2000 could not be counted with high accuracy; therefore, a more precise number was not indicated in these reactors).

*Even though reactors flown on LMS contained many crystals from space as well as on the ground, it was qualitatively observed that there were less and bigger crystals grown in the space reactors than those that grew on earth.

Table 3. Mosaicity Characteristic of Ground and Space Grown Thaumatin Crystals.

Crystal	Earth 1	Earth 2	Space 1	Space 2
FWHM (mdeg)	54	47	21	18
Deviation (mdeg)	5	5	3	5
Number of spots	5	3	5	3

The presented FWHM values have the instrument resolution function value deconvoluted out.

Table 4. Mosaicity Characteristic of Ground and Space Grown ttAspRS Crystals.

Crystal	Earth 1	Earth 2	Space 1	Space 2
FWHM (mdeg)	68	64	12	8
Deviation (mdeg)	5	5	3	2
Number of spots	5	3	4	3

The presented FWHM values have the instrument resolution function value deconvoluted out.

Lysosome Crystal Growth in the Advanced Protein Crystallization Facility Monitored via Mach-Zehnder Interferometry and CCD Video

Principal Investigator:

Dr. John Helliwell
University of Manchester
Manchester, England

Final Written Report

Prof. John R. Helliwell[1] (P.I.) and Titus J. Boggon[1]

Co-workers:
Interferometry : Peter Lautenschlager[2], Lothar Potthast[2]
X-ray Evaluation : Edward H. Snell[3], D. Peter Siddons[4], Vivian Stojanoff[5]

Lysozyme Crystal Growth In The Advanced Protein Crystallization Facility Monitored Via Mach-Zehnder Interferometry And CCD Video

1. Structural Chemistry Section, Department of Chemistry, University of Manchester, Oxford Road, Manchester, M13 9PL UK.
    E-mails: John.Helliwell@man.ac.uk and titus@spec.ch.man.ac.uk

2. Dornier GmbH, Raumfahrt-Infrastructruktur, 88039 Friedrichshafen, Germany

3. NASA, Laboratory for Structural Biology, Code ES76, Bldg 4464, MSFC, Huntsville, Al 35812. USA

4. NSLS, Brookhaven National Laboratory, Upton, NY 11973, USA

5. ESRF, Ave. des Martyrs - B.P. 220, 38043 Grenoble Cedex, France

Aims of the Experiment

The complex system of crystallisation is the major bottle-neck to obtaining high quality X-ray diffracting protein crystals. It is hypothesised that by reducing the number of parameters which influence the crystal growth system it would be easier to understand, and therefore adapt and control the system to produce better quality crystals. In particular that microgravity might well reduce mosaicity indicative of a longer range 'coherence length' or domain size, over earth grown counterparts, thus realising the perfect protein crystal limit[1]. Microgravity protein crystal growth negates the buoyancy effects of convection and sedimentation, leaving undisturbed diffusion kinetics to dominate solutal fluid flows. Microgravity protein crystal growth is therefore a method of reducing the number of parameters which can adversely influence the growth of highly perfect protein crystals. With this in mind, the two main aims of the experiments we performed on the LMS mission were to conduct analyses of both the protein crystal growth medium in microgravity and of the quality of the resulting crystals.

It has been shown that in the near ideal crystal growth environment of microgravity, lysozyme crystals grow to give the most perfect internal order yet observed in a protein crystal[2,3], whereby the microgravity crystals were significantly better than earth grown controls. This result has been confirmed with other proteins, although not to such a degree of perfection[4]. The aim then of this work is to understand to a better degree the crystallisation process in microgravity and in future to apply the lessons learnt, about e.g. crystallisation geometry, g-jitter stability[5] or crystallisation conditions, to future missions.

Our investigation firstly centred on crystallisation solutal kinetics, using Mach-Zehnder interferometry. The aim of which was to monitor the solutal movements via correlation with changes in the gradient of refractive index in the observed area. Charge Coupled Device (CCD) video was also used to verify the positional stability of the crystals during growth, whereby a comparison of the growth rates and movements of crystals could be made with previous microgravity experiments[5-8].

Secondly, an X-ray analysis investigating mosaicity (rocking curve), reciprocal space mapping, and topography of the resulting crystals was undertaken. The perfection of the crystals is being compared between microgravity grown, and earth grown, and also with crystals obtained from previous missions[2,3,6,9].

Ground trials and preparation experiments

Ground control experiments were conducted during the mission. The crystallisations were set up at the same time, and using the same solutions, as those of the mission. All parameters were kept as identical as possible to the microgravity case, although a temperature stability during growth of 20 ± 0.1 °C was not possible, and ±1 °C was used.

Interferometric ground control crystallisations were carried out at Dornier GmbH using the APCF-Engineering Model. These experiments were prepared using exactly the same protocol as the microgravity mission.

The mission

Four lysozyme crystallisations were carried out in microgravity, and four identical experiments were conducted as ground controls during the period of the mission. Two crystallisation conditions were used, one with a higher precipitant concentration, and one with a 7 % lower precipitant concentration. The crystallisations used dialysis geometry, containing 541 μl of precipitant, 59 μl of buffer and 188 μl of protein solutions. Two microgravity reactors (reactors 7 and 9) were monitored using Mach-Zehnder interferometry and CCD video, the

other two microgravity reactors were not visually monitored during the mission. All reactors produced crystals, some of which were subsequently analysed using various X-ray sources.

Evaluation of Mach-Zehnder Interferometer images

Of the two reactors monitored using Mach-Zehnder interferometry, one (reactor 7) contained the slightly higher precipitant concentration so it was monitored at a slightly faster rate. Due to time constraints on digitally recording the images (about 4 minutes per whole image), whole interferograms were not able to be collected for the first 15 hours after APCF activation. Instead 2 windows were defined (w1 and w2 in figure 1), which monitored the average grey value at 4 and 6 minute intervals for reactors 7 and 9 respectively. After 15 hours, interferograms recording the whole reactor were collected at 11 minute intervals for both reactors (figure 1).

Unfortunately the laser was unsteady, and a combination of mode switching and loss of intensity occurred throughout the mission. This was problematic, especially in the first 15 hours, when average grey values were the only method of analysis. Consequently, fringes were probably missed in that period. However, a more complete analysis is possible with the whole interferograms collected after the 15 hour point, although, these also have been affected by the problematic laser (figure 2).

There was, however, enough data to suggest some very interesting results. Firstly, the direction of fringe movement reversed at about the 8 hour point in both reactors, and then again at the point that crystals become visible in the CCD video monitoring, between 25 and 31 hours (depending on the position within the protein chamber)(figure 2). Compared to the solitary reversal in fringe movement direction present in the ground control experiments[10], this is a surprising result which should be looked at more closely. It suggests that a different pre- and post- nucleation process occurs in microgravity compared to the earth grown case. We are at present also modelling the effects of a diffusion dominated crystallisation experiment.

Finally, the whole protein chamber interferograms demonstrated the stability of fluid within microgravity crystallisation by showing an effect that is rarely seen using Mach-Zehnder interferometry on earth. Depletion zones are visible around growing crystals (figure 3).

Evaluation of CCD video images

The two reactors that were monitored using interferometry were also monitored using CCD video. Images of the whole protein chamber were taken at one focal length position every 2 hours beginning 15 hours after activation of the APCF (MET 0/21:17) for reactor 7. In reactor 9 the first image was taken after 90 hours of APCF activation. In our two previous missions, we had not yet had such a chance before to analyse such a high frequency of CCD video images, and covering the whole protein chamber. This is a major step forward in capability and was important (see below).

Previously, in our CCD video monitored experiment on Spacehab-1 a bulk movement of crystals was noted at the time that the EURECA satellite was retrieved (unpublished results). In the IML-2 mission, we tracked 3 crystals moving over 40 minute periods[5], but due to the narrow field of view, and 8 hour time delay between groups of images, our analysis of these crystal movements was restricted.

It was exciting therefore to analyse images from LMS that viewed the whole protein chamber and at a much higher frequency. Crystals became visible at varying times throughout the reactor, with the first crystals visible 25 hours 37 minutes after APCF activation. We noted significant crystal movements (figures 4 and 5) throughout the mission, whereby nucleation events occurred throughout the chamber but were very quickly followed by a global sedimentation drift towards the top of the reactor. The only crystals that remained in their

154

nucleation positions were those that grew on the chamber walls. By following 20 different crystals for the periods that they could be accurately tracked (figure 5), sudden global movements could be seen, in addition to the steady drift, at the 76, 102 and 145 hour points, as well as many other times. The total drift distance, for all 20 crystals analysed, over time periods ranging from 24 to 260 hours, ranged between 0.42 and 3.38 mm with an average speed of ~0.004 microns / second (i.e., 40 Å / second). The sudden movements were much larger; total distances travelled being ~0.2 mm in ~2 hours, i.e., ~0.03 microns / second, 300 Å / second).

We have also previously described the monitoring of crystal growth rates[5,6] and correlation of spurts and lulls in these growth rates with astronaut exercise periods. It is possible to perform this analysis from the images we have, and we will do this in the future.

Relation to earlier work and the aims

CCD video of 3 previous protein crystal growth microgravity missions, Spacehab-1, IML-2 and the EURECA satellite, clearly shows that crystal movements are affected by the geometry of crystal growth apparatus, and the quality of the microgravity. Dr N.E. Chayen[i] grew Apocrustacyanin C_1 crystals on the IML-2 (STS-65) Shuttle mission using a vapour diffusion geometry. The crystals clearly showed cyclic motion at a speed of 2 microns / second throughout their growth, akin to that expected from Marangoni convection[8]. This work, agreeing with the theory[11], highlighted major anxieties with protein crystal growth in microgravity using the 'hanging drop' technique (which incorporates a liquid - vapour phase boundary). Lysozyme crystal growth using the dialysis membrane technique onboard the Spacehab-1 (STS-57) and IML-2 Shuttle missions showed relatively small, but significant, crystal movements as described above. However, these results clearly show that the dialysis technique (which has no liquid - vapour phase boundary) produces a much more stable environment for protein crystal growth than the vapour diffusion technique. We have also analysed protein crystal growth onboard an unmanned platform. α-Crustacyanin was grown on the ESA's EURECA satellite using a liquid-liquid free interface diffusion geometry (again incorporating no liquid - vapour phase boundary) by Dr P.F. Zagalsky[ii]. We noted that for long periods of time the free floating crystals grew without moving[7], and were only disturbed by failures of the temperature control system. The results obtained from the LMS mission reinforce, and expand upon, the results obtained previously. We are attempting, at present, to link crystal movements observed during the LMS mission to gravitational accelerations affecting the mission. This is overall within the context of trying to consistently achieve protein crystal quality improvements through the harnessing of microgravity[9].

X-ray analysis of crystal perfection

Synchrotron X-ray analyses were carried out at the NSLS using beamline X26C. A variety of methods were used to analyse a number of crystals. Crystal mosaic spread measurements by use of rocking curves is an indicator of the internal physical perfection present[1]. The addition of an analyser crystal between the sample and detector enables reciprocal space mapping of ω, the sample axis, and ω', the analyser axis[12]. Reciprocal space maps in one axis provide a measure of pure mosaicity effects (volume and orientation), and in the other axis strain effects. In combination with the technique of X-ray topography[13], a very finely detailed picture of a single reflection can be obtained to produce an in-depth knowledge of the overall internal order of the crystal. We conducted such data collections on a number of crystals at the NSLS, the analysis of which is still in progress, although two examples are shown here (figure 6).

[i] Biophysics Section, Blackett laboratory, Imperial College of Science, Technology and Medicine, London. SW7 2BZ UK
[ii] Royal Holloway, University of London, Egham, Surrey TW20 0EX UK.

Using the Manchester X-ray source, R-AXIS area detector and a variety of processing packages, two similar crystals, one grown on the LMS mission, and one using the same conditions, but on earth, were analysed. The data merging statistics are shown in Table 1. Under these experimental conditions, it is clear that when the crystal perfection is not harnessed (e.g., via an ultra-fine step scan technique ~0.0001°, see refs 3 and 4) there is no signal to noise optimisation especially figures 3c and 4) and hence, the data quality (R_{merge}, I/σ) are essentially identical. For the LMS microgravity grown lysozyme crystal the data collection protocol was as follows: 60° of 0.75° oscillations at a distance of 250 mm using 30 minute exposures, followed by 60° of 0.50° oscillations at a distance of 300 mm using 20 minute exposures. For the earth grown crystal the data collection protocol was identical, and then in addition 60° of 1.5° oscillations at a distance of 450 mm using 4 minute exposures were recorded. The LMS crystal was 0.50 x 0.50 x 0.35 mm (0.0875 mm^3) and the earth control crystal was 0.70 x 0.50 x 0.45 mm (0.1575 mm^3).

	LMS		LMS Ground	Control
Resolution	Rmerge	Completeness %	R merge	Completeness %
99.00 - 4.19	0.054	95.1	0.056	98.8
4.19 - 3.33	0.064	98.8	0.064	99.2
3.33 - 2.91	0.075	99.2	0.07	97.1
2.91 - 2.64	0.085	99.6	0.08	97.5
2.64 - 2.45	0.093	99.9	0.09	96.6
2.45 - 2.31	0.093	99.6	0.09	97.7
2.31 - 2.19	0.099	99.3	0.097	96.9
2.19 - 2.10	0.105	98.1	0.105	96.1
2.10 - 2.02	0.12	94.3	0.116	94.9
2.02 - 1.95	0.135	88.8	0.139	92.1
1.95 - 1.89	0.165	77.3	0.163	88.7
1.89 - 1.83	0.186	66.5	0.187	81.4
1.83 - 1.78	0.239	62.1	0.249	70.9
1.78 - 1.74	0.271	54.5	0.255	64.3
1.74 - 1.70	0.393	45.1	0.344	56.1
Overall	0.072	85.5	0.069	88.8

Table 1. X-ray data sets collected on LMS and LMS ground control lysozyme crystals on the Manchester R-AXIS area detector using a MoKα anode (λ = 0.71 Å wavelength). Overall I/σ for the LMS crystal = 15.7 and for the ground control crystal = 16.5. Identical X-ray generator (RU 200 rotating anode) power settings were used).

Lessons for future missions from LMS

There were problems experienced with the interferometry side of the experiment and which fell under two categories. Firstly, an unstable laser overheated many times whereby wavelength shifts (and changes in the interferometric pattern) and intensity losses were experienced. The grey-scale data collection (before 15 hours) and many of the whole interferograms were rendered much more complicated for analysis. Secondly, the lack of whole interferograms collecting data over the important, and unusual, period before 15 hours should be addressed in a future mission.

The CCD video analysis of the LMS crystallisations show a significant crystal drift within the Shuttle (also seen on the IML-2 mission[5]). This is in contrast with protein crystal growth experiments that took place onboard the EURECA satellite where completely stationary crystal growth was observed for long periods of time[7]. The comparison of these sets of CCD video results points towards protein crystallisations conducted onboard

unmanned platforms as a more stable environment. Nevertheless the overall drift speed of 40 Å / second presumably is tolerable but will be of interest to those investigators modelling the physical chemistry of protein crystal growth. However, the sudden jumps of ~0.2 mm over 2 hour periods (i.e., 0.03 microns / second, 300 Å / second) due presumably to sudden g-jitter disturbances, is a more serious anxiety for realising the best quality protein crystals.

Overal conclusions

As well as the dynamics of the fringe reversal, more microgravity crystals were made available and allowed the X-ray analyses, thus considerably extending our earlier work.

References

1. J.R. Helliwell, 1988, *J. Cryst. Growth*, 90, 259-272.

2. J.R. Helliwell, E.H. Snell and S. Weisgerber, 1996, *Proceedings of the 1995 Berlin Microgravity Conference* edited by L. Ratke, H. Walter and B. Feuerbacher, *Springer Verlag*, 155-170.

3. E.H. Snell, S. Weisgerber, and J.R. Helliwell, E. Weckert, K. Hölzer and K. Schroer, 1995, *Acta Cryst. D* 51, 1099-1102.

4. J. Ng and R. Giegé, *To be published*.

5. E.H. Snell, T.J. Boggon, J.R. Helliwell, M.E. Moskowitz and A. Nadarajah, *Acta Cryst. D, in press*.

6. N.E. Chayen, T.J. Boggon, A. Cassetta, A. Deacon, T. Gleichmann, J. Habash, S.J. Harrop, J.R. Helliwell, Y.P. Nieh, M.R. Peterson, J. Raftery, E.H. Snell, A. Hädener, A.C. Niemann, D.P. Siddons, V. Stojanoff, A.W. Thompson, T. Ursby and M. Wulff, 1996, *Quarterly Rev. Biophysics*. 29, 227-278.

7. T.J. Boggon, N.E. Chayen, P.F. Zagalsky, E.H. Snell and J.R. Helliwell, *Faraday Transactions*, submitted.

8. N.E. Chayen, E.H. Snell, J.R. Helliwell and P.F. Zagalsky, 1997, *J. Cryst. Growth*, 171, 219-225.

9. E.H. Snell, A. Cassetta, J.R. Helliwell, T.J. Boggon, N.E. Chayen, E. Weckert, K. Hölzer, K. Schroer, E.J. Gordon, and P.F. Zagalsky, 1997, *Acta Cryst D* 53, 231-239.

10. E.H. Snell, J.R. Helliwell, T.J. Boggon, P. Lautenschlager, and L. Potthast, 1996, *Acta Cryst. D* 52, 529-533.

11. R. Savino and R. Monti, 1996, *J. Cryst. Growth*, 165, 308-318.

12. E.H. Snell, 1997, *Canadian Space Agency, In press*.

13. V. Stojanoff, D.P. Siddons, E.H. Snell and J.R. Helliwell, 1996, *Synchrotron Radiation News*, 9, 25-26.

Figure captions

Figure 1 : An example of a whole interferogram with interference fringes clearly visible. The two grey value measuring windows are marked as w1 and w2, and the white strip indicates the area analysed in figure 2.

Figure 2 : Analysis of the movement of fringes within the white strip shown in figure 1. The average grey value of pixels in x within the white strip has been obtained and shown here as a single pixel. The height (y) is unchanged for both sets of pixels. This figure shows an overview of the movements of fringes within the white strip over 34 hours. Direction of fringe movement reversal occurs between 25 (R) and 31 (R') hours (depending on latitude within the chamber) correlating with the first crystals becoming visible (at which time there is a loss of definition in the fringe pattern experienced). The effect of laser instability is clearly seen as large jumps in the fringe pattern, and also as pale strips.

Figure 3 : Shows the merging of an interferogram and a CCD video image taken with a 3½ minute interval between the images. A protein depleted zone is visible.

Figure 4 : Sequence of 4 CCD video images taken at a) 1d 18h 32m, b) 2d 18h 4m, c) 4d 8h 25m and d) 15d 15h 32m (these timings are MET). The images show the movement of crystals over the whole LMS mission. It is significant to note that while many crystals nucleate throughout the protein chamber, all sediment to the top of the reactor (right hand side of the pictures). Crystals that do not move throughout the whole mission have grown attached to the chamber wall.

Figure 5 : Three graphs showing the movements of 20 crystals. Graph a) shows X versus Y, b) X versus Time and c) Y versus Time. The units are pixels and hours (MET). Sudden crystal movements are visible at 76, 102 and 145 hours, especially in figure 5b, in addition to the gradual global drift.

Figure 6 : Example of a reciprocal space map a) and an X-ray topograph b) of microgravity grown LMS lysozyme crystals. The reciprocal space map shows ω versus ω', with intensity on the z axis.
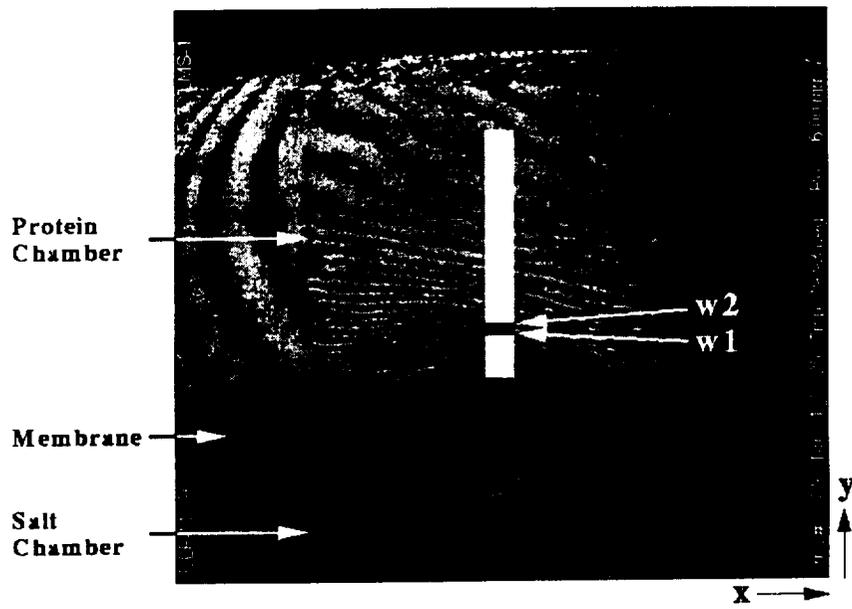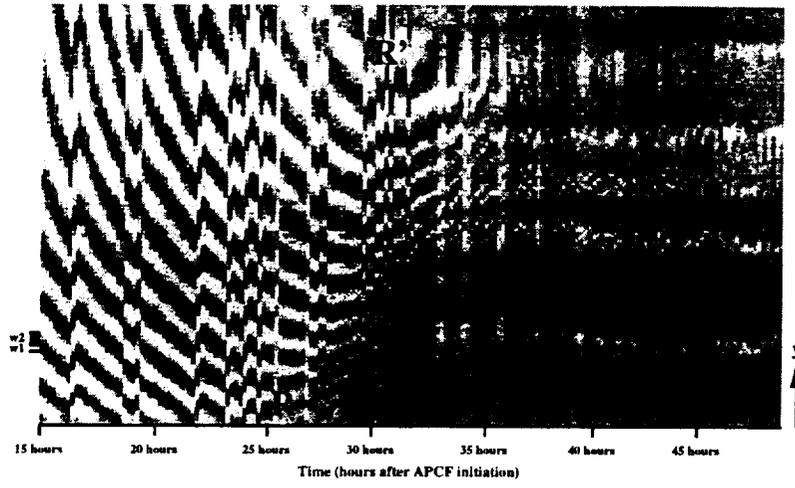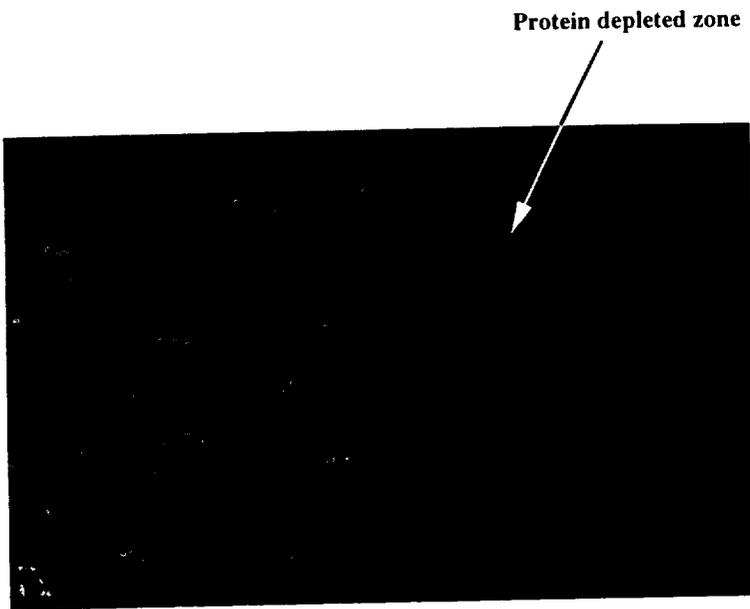
Figure 1

Figure 2

Figure 3

(a) MET
01/18:32

(b) MET
02/18:04
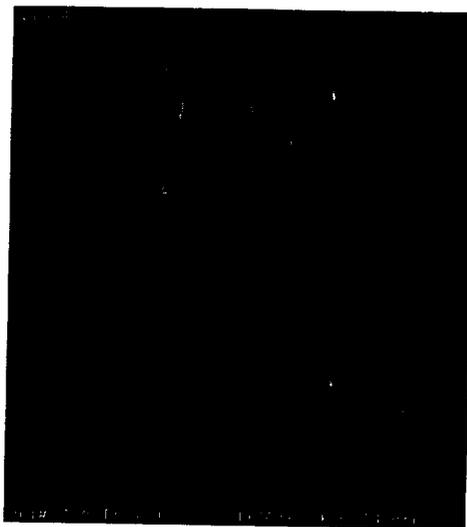
(c) MET
04/08:25
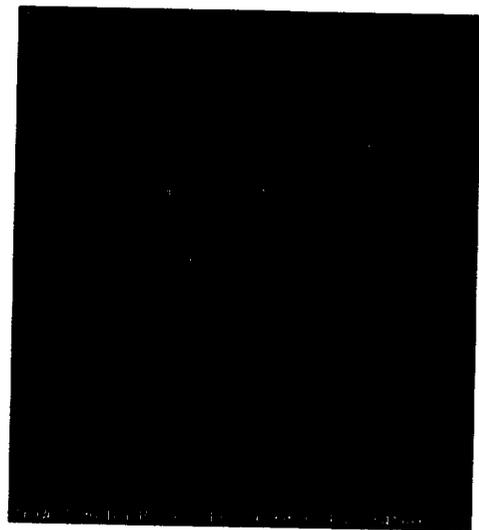
(d) MET
15/15:32

Figure 4
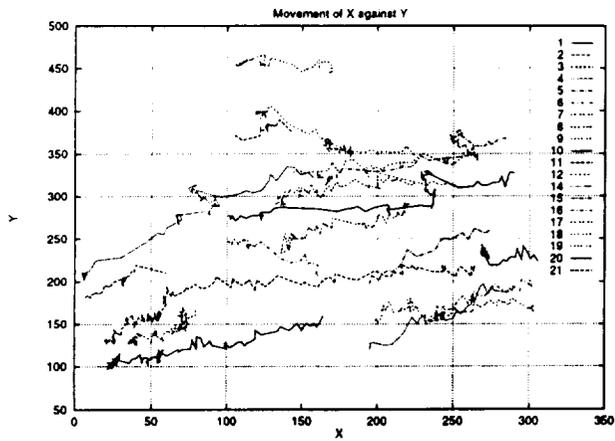
(a)
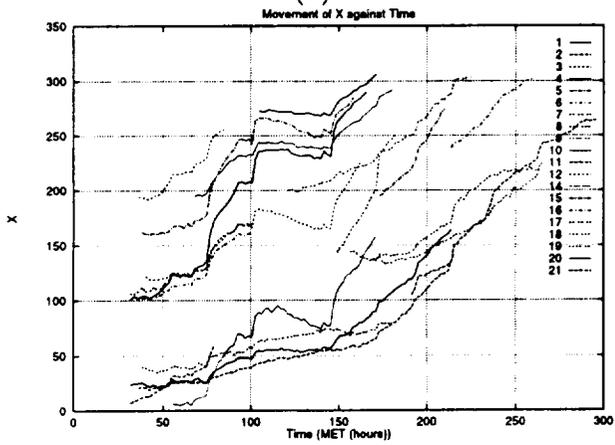
(b)
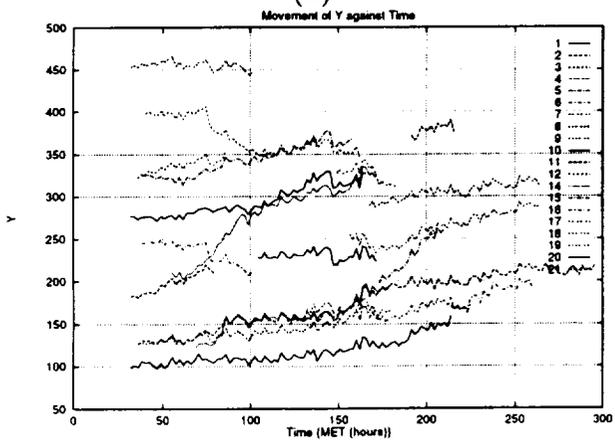
(c)

Figure 5
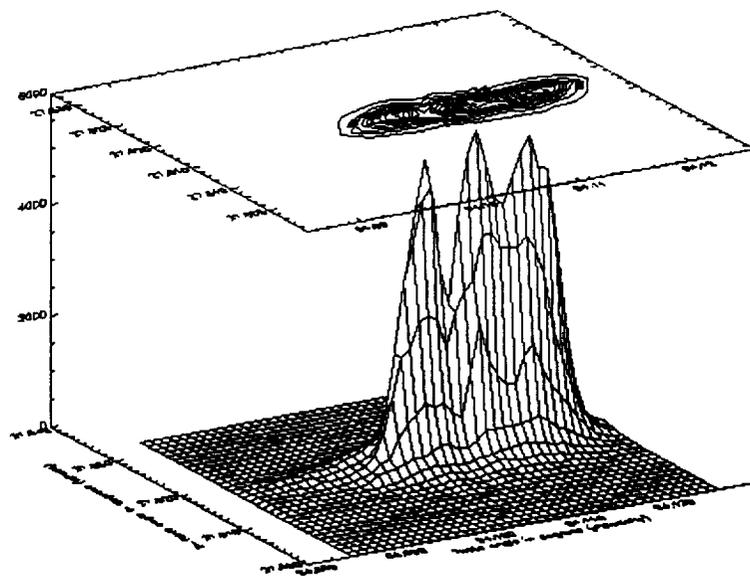
(a)
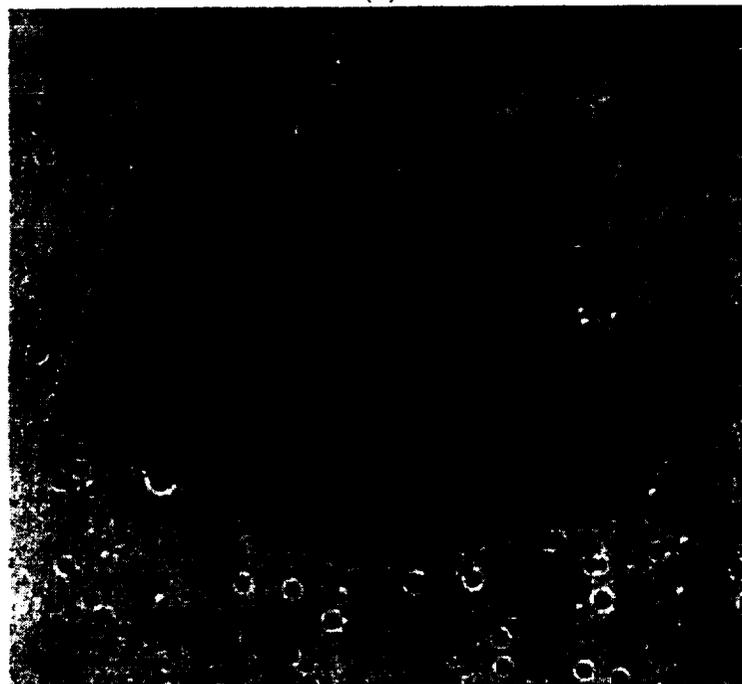
(b)

Figure 6

Advanced Protein Crystallization Facility (APCF)

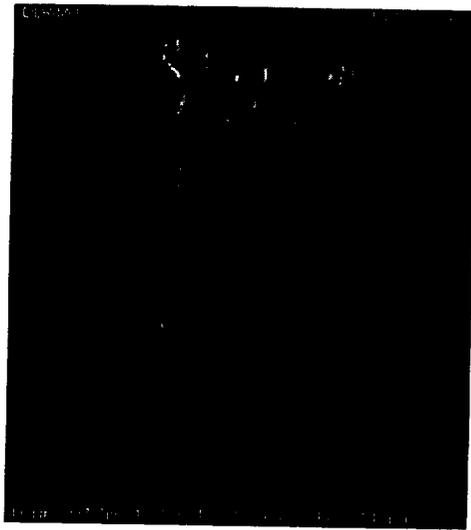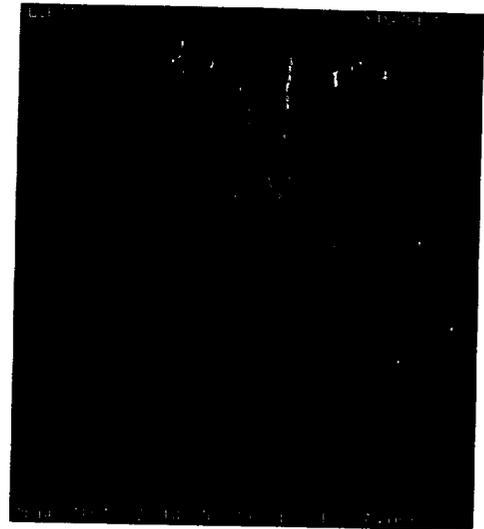# Analysis of Thaumatin Crystals Grown on Earth and in Microgravity

Principal Investigator:

Dr. Alexander McPherson
University of California, Irvine
Irvine, California

Final Report of Advanced Protein Crystallization Facility on LMS:

Analysis of Thaumatin Crystals Grown on Earth and in Microgravity

by

Stanley Koszelak, John Day, Aaron Greenwood and Alexander McPherson

University of California, Irvine, Department of Molecular Biology & Biochemistry
Irvine, CA 92697-3900

Previous experiments have demonstrated that, in at least some cases, macromolecular crystals of improved quality can be grown in a microgravity environment as is obtained, for example, on the U.S. Space Shuttle or the Russian Space Station Mir (DeLucas, *et al.*, 1989; Day & McPherson, 1992; Koszelak, *et al.* 1995; Long, *et al.*, 1996). Presently, the most extensively used facility for such experiments is the European Space Agency (ESA) designed Advanced Protein Crystallization Facility or APCF (Snyder, *et al.* 1991; Bosch, *et al.* 1992). This system allows crystallization to proceed by vapor diffusion, batch, dialysis, and free interface diffusion methods and it provides limited video recording of some experiments as they actually appear in space.

On Space Shuttle missions designated United States Microgravity Laboratory-2 (USML-2, October, 1995) and Life and Microgravity Sciences (LMS, June, 1996), joint experiments were carried out by our French (Strasbourg) and American (Riverside) groups based on the crystallization of the protein thaumatin. Using common protein, buffer, and precipitant solutions, thaumatin was crystallized at a variety of protein concentrations using two different approaches, dialysis and liquid-liquid diffusion. Following retrieval of the samples, post flight microscopy and X-ray analyses were carried out on the crystals grown in microgravity. Of particular interest to us were (1) relevance of the choice of methodology, (2) the influence of protein concentration on crystal size, and (3) quantitative comparison of the microgravity grown crystals with those produced on earth.

Materials and Methods

Thaumatin was purchased from Sigma Biochemicals, St. Louis, Mo. and dissolved in 0.1 M ADA buffer at pH 6.5. The precipitant solution was 1.6 M sodium tartrate in 0.1 M ADA at

pH 6.5 All solutions were sterilized by microfiltration before loading of flight samples. Solution used by both laboratories were made in Strasbourg and divided between investigators.

Thaumatin is a monomeric protein from the African Serendipity Berry valued for its intensely sweet taste and its use as a non caloric sweetener. It has a molecular weight of 21,500 contains four disulfide bridges, and possesses a high degree of stability. It consists primarily of beta structure organized in two associated domains. The structure was first determined in an orthorhombic crystal at 1.7 Å resolution (Ogata, *et al.* 1992), and later in a second orthorhombic, a monoclinic, and a tetragonal crystal form (Ko, *et al.* 1994). The tetragonal crystal form, grown from tartrate, was also refined to 1.7 Å resolution, and was that studied in these experiments. Tetragonal thaumatin crystals can be grown in a conventional laboratory in 12 to 48 hours at room temperature by a variety of methods. The crystals are of space group $P4_12_12$ with a=b=59Å and c=158Å having a single molecule as the asymmetric unit. The habit is that of a tetragonal bipyramid, often reaching linear dimensions greater than 1mm. The crystals, which contain about 45% solvent, are mechanically robust. Their growth has been studied by a variety of physical techniques including interferometry (Kuznetsov, *et al.* 1995) and atomic force microscopy (Malkin, *et al.* 1996a and b).

The APCF has been previously described (Giegé, *et al.* 1995) and, indeed, successful experiments with other proteins and viruses have been reported (McPherson, 1996; Koszelak, *et al.* 1995). An APCF unit provides for a total of 48 individual crystallization cells maintained at constant temperature (22°C ≠ 0.1° in this case) from the time of loading, the duration of the mission, to analysis. Both dialysis and free interface diffusion cell types are activated by 90° rotation of a stopcock valve that establishes continuity between protein and precipitant chambers.

For dialysis, a semi permeable membrane separates the two chambers. In experiments conducted on USML-2 the Strasbourg group used five dialysis crystallization reactors and the Riverside group three free interface diffusion reactors. For LMS, the Strasbourg group used two reactors of the dialysis type and the Riverside group eight of the liquid-liquid diffusion type.

The APCF was activated on both missions several hours after a microgravity environment was achieved, and deactivated (the stopcocks rotated in reverse) a few hours before reentry. Several cells were observed during the mission at fixed intervals and recorded by video microscopy. In the case of the dialysis cells, parallel experiments were carried out in Strasbourg, France in identical cells during the periods of both missions. No parallel ground controls were carried out for the free interface diffusion cells since the method functions quite differently in a one g environment. Following the missions the dialysis cells were returned to Strasbourg for analysis and the free interface diffusion cells to Riverside. They were, in both cases, immediately examined, photographed, and X-ray diffraction analysis initiated.

At the University of California at Riverside, complete three dimensional X-ray diffraction data were collected at 17°C on the crystals grown on USML-2 by free interface diffusion as described previously (Ko, *et al.*, 1993a, b; Larson *et al.*, 1993) from capillary-mounted crystals using a San Diego Multiwire Systems (SDMS) double multiwire detector system (Xuong *et al.*, 1985) with crystal-to-detector distances of 535 mm. Frame sizes were 0.14° with 2-3 min/frame. The x-rays were generated by a Rigaku RU-200 rotating anode generator operated at 45 kV and 145 mA with a Supper monochromator to give 1.54Å radiation. Crystals were exposed for 24-48 h. Data collection procedures and experimental parameters were identical for both earth and space grown crystals. Redundancy of recordings ranged from four to eight. Data correction,

reduction, merging, and statistical analysis used the programs supplied by SDMS. For both earth and microgravity grown crystals the $R_{sym's}$ varied from 0.035 to 0.06 to the limits of resolution of the data sets.

Results

Visual and Microscopic Observations: For both missions crystals were observed in all of the cells, both dialysis and free interface diffusion, for microgravity and for ground controls. There was a clear increase in average and largest sizes of crystals grown by the French group by dialysis in μg compared with ground controls, an example, that of lysozyme is shown in Figure 1. In the best of the three free interface diffusion cells, the largest crystals were three to five times the volume of the best crystals produced in either laboratory on earth. In both types of cells some of the largest thaumatin crystals measured more than 2 mm from apex to apex of the tetragonal bipyramids.

The number and sizes of crystals from the dialysis reactors were assessed under an optical microscope. Each of the flight reactors contained 30 to 250 crystals having a size range of 0.4 mm to 1.8 mm. The corresponding ground control reactors contained approximately 550 to 30,000 crystals having a size range of 0.100 mm to 0.9 mm (see report by Ng, *et al.* for details).

A notable observation originating independently from both the Strasbourg group (using dialysis) and the Riverside group (using free interface diffusion) was the dependence of average and largest size on protein concentration, a major experimental variable. Independent of approach, the largest crystals clearly grew at highest protein concentration and the smallest crystals at lowest protein concentration. This is shown in Figure 2 for crystals grown at three

different protein concentrations (35, 17 and 7 mg/ml) by free interface diffusion under otherwise identical conditions.

Visually, the quality of the crystals, particularly those growing free of any surfaces, and including the largest, was very high. They appeared virtually flawless, with no observable imperfections, striations, or habit anomalies. Those attached to the cell walls (which presumably nucleated there) did show defects near the sites of growth initiation but became flawless as growth proceeded into the bulk solution.

X-ray Intensity Measurements: X-ray diffraction data were collected from a total of four thaumatin crystals grown in microgravity by free interface diffusion in microgravity. All were from a cell which was under video observation. The data were merged to form a single data set. This microgravity set was then compared with the best data ever previously obtained from crystals grown in a conventional laboratory, data which was, in fact, used to solve and refine the reported structure of the tetragonal thaumatin crystals (Ko, *et al.*, 1993a). This comparison is shown as a modified Wilson plot (Wilson, 1949 and 1970) in Figure 3 in which the average intensity divided by its estimated error is plotted as a function of $\sin^2\theta/\lambda^2$.

As with several previously reported investigations of macromolecular crystal growth in microgravity, two features of the comparison emerged. First, the I/σ ratio of reflections obtained for crystals grown in microgravity was substantially higher (approximately double) that for ground grown crystals, and over the entire resolution range analyzed. Second, the limit of resolution of the diffraction pattern was somewhat higher for microgravity grown crystals compared to those grown on earth, 1.5 Å vs. 1.7 Å resolution respectively. While 0.2 Å may appear only a marginal increase, in this portion of the resolution range it is significant and,

171

combined with the improved I/σ over the entire resolution range, yields nearly 30% more diffraction intensities (> 3σ) for the microgravity grown crystals. We would like to point out that the true limit of resolution for the microgravity crystals was never measured in this analysis because technical constraints prevented collection of data beyond 1.5 Å. The continued strength of the diffraction pattern at the 1.5 Å mark suggested to us that the actual resolution limit of the microgravity grown crystals was beyond this point.

Conclusions

The results presented here for thaumatin crystals grown in microgravity in the APCF by two different techniques are consistent. They reinforce the conclusions of other reports based on different macromolecules that a microgravity environment provides distinct advantages. In the best of only a few thaumatin crystals grown in microgravity, compared with several orders of magnitude more trials conducted on earth, the microgravity grown crystals were consistently and significantly larger, and substantially more defect free as judged by direct visual inspection. In this investigation this appears to be independent of the choice of crystallization method and the loading and handling of the APCF cells.

An interesting observation was that there was a clear correlation between ultimate crystal size and protein concentration. This suggests that in future experiments, the optimal results may be obtained by even further increasing macromolecule concentration over that utilized in the conventional laboratory. This is contrary to what one would do generally in the conventional laboratory where the best results are usually achieved at the lowest levels of supersaturation.

The resolution limit of the diffraction pattern, the I/σ ratio as a function of the Bragg angle, and the mosaic spread of crystals are generally agreed to reflect both the degree of internal

order and the long range defect structure and its distribution within the crystal. That is, they serve as measures of the average statistical disorder of the molecules about the lattice points, as well as the extent of local but severe disorder introduced by defects such as dislocations, stacking faults, point defects or incorporated foreign material (Malkin, *et al.* 1996). All of the data presented here, both intensity distributions and mosaic spread measurements imply a higher degree of internal order, a lower defect density, and a reduction of severe faults for crystals grown in the absence of gravity.

While similar results, based on intensity data for microgravity grown crystals of several proteins, have been reported previously (McPherson, 1997; Koszelak, 1995, 1996, DeLucas, *et al.* 1989), and comparable results based on mosaicity measurements have been presented for others (Helliwell, *et al.* 1996; Ferrer, *et al.* 1996; Snell, *et al.* 1995), this is the first experiment to produce crystals grown by multiple methods and analyzed by both approaches. Indeed, our conclusion is that they are mutually supportive and complementary, and both suggest the same conclusion, that crystals grown in microgravity can be significantly improved in their diffraction properties when compared with those grown on earth.

Apart from lysozyme, no other protein crystal has been used to investigate mosaicity differences between earth-grown and space-grown crystals. The data presented here indicates that the mosaic spread of reflections from microgravity grown thaumatin are reduced by more than a factor of two over earth grown crystals. This is comparable to what was observed for tetragonal lysozyme where space-grown crystals were observed to be improved by a factor of three over corresponding earth controls (Helliwell, *et al.* 1996; Ferrer, *et al.* 1996; Snell, *et al.* 1995).

References

Day, J. and McPherson, A. Macromolecular crystal growth experiments on International Microgravity Laboratory-1. *Protein Science* 1, 1254-1268, (1992).

DeLucas, L. J., C. D. Smith, H. W. Smith, V. K. Senagdi, S. E. Senadhi, S. E. Ealick, C. E. Bugg, D. C. Carter, R. S. Snyder, P. C. Weber, F. R. Salemme, D. H. Ohlendorf, H. M. Einspahr, L. Clancy, M. A. Navia, B. M. Mckeever, T. L. Nagabhushan, G. Nelson, Y. S. Babu, McPherson, A., S. Koszelak, D. Stammers, K. Powell and G. Darby. Protein Crystal Growth in Microgravity. *Science* 246, 651-654 (1989).

Ferrer, L. J., Hirschler, J., Roth, M. and Fontecilla-Camps, J. C. (1996) ESRF Experiments Reports. Pg. 27-28.

Giegé, R., Drenth, J., Ducruix, A., McPherson, A. and Saenger, W. (1995) Prog. Cryst. Growth and Charact. 30, 237-281.

Helliwell, J. R., Snell, E. and Weisgerber, S. (1996) In Materials and Fluids Under Low Gravity, Lecture Notes in Physics (L. Ratke, H. Walter and Feuerbacher B., eds.), pp. 155-170, Springer.

Ko, T.-P., Ng, J. D., Day, J, Greenwood, A. and McPherson, A. X-ray structure determination of three crystal forms of canavalin by molecular replacement. *Acta. Cryst.* D49, 478-489 (1993).

Ko, T.-P., Day, J., Greenwood, A. and McPherson, A. The Structures of Three Crystal Forms of the Sweet Protein Thaumatin. *Acta Cryst.*, D50, 813-825, (1994).

Koszelak, S., Day, J., Leja, C., Cudney, R. And McPherson, A. Protein and Virus Crystal Growth on International Microgravity Laboratory-2. *Biophysical Journal* 69, 13-19 (1995).

Larson, S. B., Koszelak, S., Day, J., Greenwood, A., Dodds, J. A. and McPherson, A. The three dimensional structure of satellite tobacco mosaic virus at 2.9 Å resolution. *J. Mol. Biol.*, 231, 375-391 (1993).

Long, M. M., Bishop, J. B., Nagabhushan, T. L., Reichert, P., Smith, G. D. and DeLucas, L. J. (1996) *J. Cryst. Growth* 168, 233-243.

Malkin, A. J., Kuznetsov, Y. G., Glantz, W. and McPherson. Atomic force microscopy studies of surface morphology and growth kinetics in thaumatin crystallization. *J. Phys. Chem.* 100, 11736-11743 (1996).

Malkin, A. J., Kuznetsov, Y. G. and McPherson, A. Defect Structure of Macromolecular Crystals. *J. Struc. Biol.* 117, 124-137 (1996).

McPherson, A. Macromolecular crystal growth in microgravity. *Crystallography Reviews*, 6(2) 157-308 (1996).

174

Ogata, C.M., Gordon, P.F., de Vos AM, and Kim, S.H. (1992). *J. Mol. Biol.* <u>3</u>, 893-908.

Snell, E. H., Weisgerber, S., Helliwell, J. R., Weckert, E., Hölzer, K. and Schroer, K. (1995) *Acta Cryst.* <u>D51</u>, 1099-1102.

Snyder, R. S., Fuhrmann, K. and Walter, H. U. (1991) *J. Cryst. Growth* <u>110</u>, 333-338.

Xuong, N.-H., Nielson, C., Hamlin, R. and Anderson, D. (1985) *J. Appl. Cryst.* <u>18</u>, 342-360.
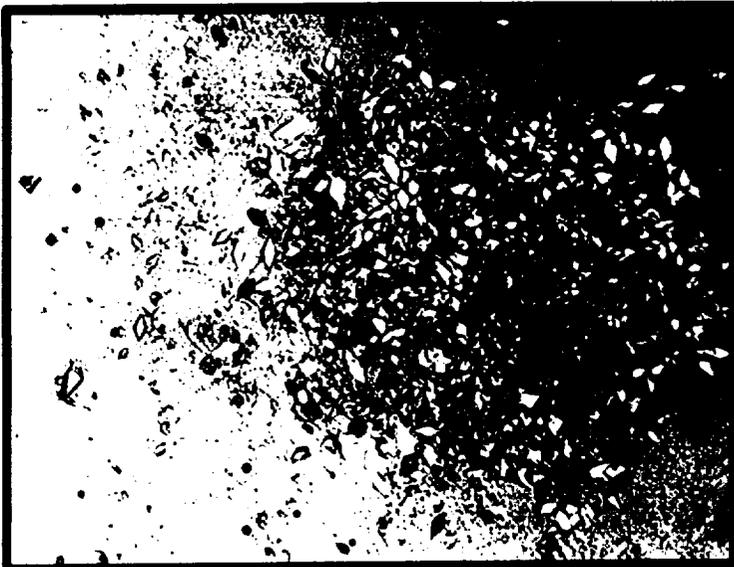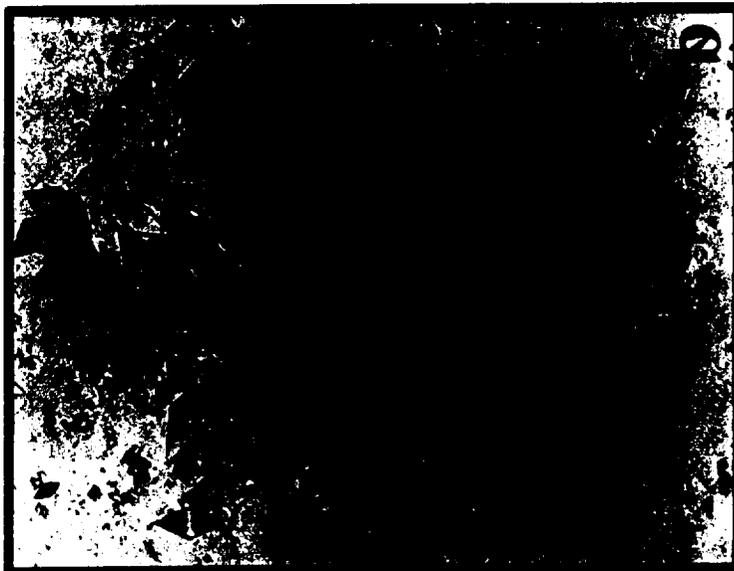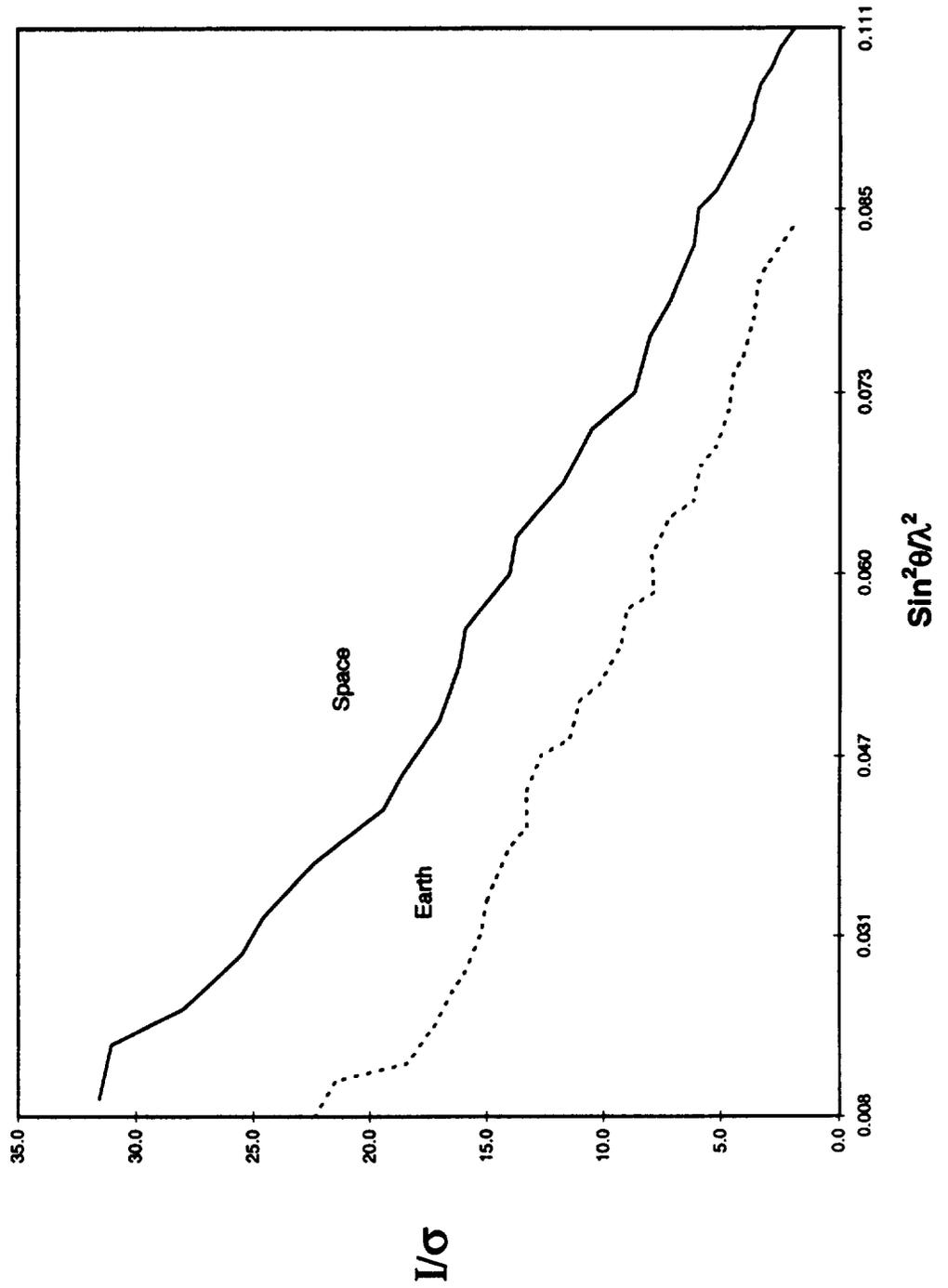
Figure 1

Figure 2

Figure 3

178

Advanced Protein Crystallization Facility (APCF)

Crystallization of the Nucleosome Core Particle

Principal Investigator:

Dr. Timothy Richmond
ETH Zürich
Zürich, Switzerland

Report on Crystallization of the Nucleosome Core Particle during Space Shuttle mission STS-78 using APCF

Armin Mäder and Timothy J. Richmond
Institut für Molekularbiologie und Biophysik
ETH Zürich

7 August, 1997

Reference: APCF/LMS-95-11

Objectives

We asked for participation in the microgravity crystallization program with the aim of improving the X-ray data quality in the resolution range of 1.8-2.8 Å for our crystals of the nucleosome core particle. Specifically, we attempted to obtain crystals with reduced mosaic spread.

Background

The DNA in chromatin of all eukaryotic organisms is organized in arrays of nucleosomes. Two copies of each histone protein, H2A, H2B, H3, and H4 assemble in an octamer that wraps 147 base pairs of DNA around it to form a 206 kD nucleosome core. With the addition of linker DNA and histone H1, the nucleosome is formed. This highly conserved nucleoprotein complex occurs essentially every 200±40 bp throughout all eukaryotic genomes. The repeating nucleosomes further assemble into higher order helices. The nucleosome shapes the DNA molecule both at the atomic level by bending and twisting it, and on the much larger scale of genes by forming a higher order structure.

We have recently determined the atomic structure of the nucleosome core particle containing a defined sequence DNA by X-ray crystallography at 2.8 Å resolution (*Nature* in press). The structure was solved by multiple isomorphous replacement (MIR) using three heavy atom derivatives based on recombinant histone proteins and data collected at the European Synchrotron Radiation Facility (ESRF). This protein/DNA complex, the largest solved to date, shows how four pairs of histone fold domains are responsible for organizing 121 bp of DNA while extensions of the histone fold bind the termini of the DNA superhelix and help stabilize the overall structure. The remainder of the histone molecules, the histone tails, are arranged to contribute the formation of the higher order helix.

The limit of X-ray diffraction data from the nucleosome core particle crystals extends anisotropically to 1.8-2.2 Å and would a permit a molecular structure to be built with greater accuracy than that based on the data to 2.8 Å. This represents an increase of 2.7-fold in the quantity of data available at the higher resolution. At 2.0 Å resolution, even the ordered solvent molecules could be included in the structure. However, the crystal mounting method that is most convenient and that was used for the 2.8 Å data collection puts the long axis of the rod-shaped crystals roughly parallel to rotation axis used to sample diffraction space. This orientation is not ideal because the orthorhombic crystals have cell dimensions of approximately 110 x 200 x 110 Å where the c-axis is along the long axis of the rod. Therefore, the separation of diffraction intensities center to center with respect to the crystal rotation in the vicinity of the h0l projection is only 0.6° for the diffraction intensities at 2 Å resolution. Since the crystals have high mosaic spread, approximately 0.9-1.5° depending on the particular crystal, complete measurement of the high resolution data would not be possible because of overlapping diffraction intensities. The growth of crystals under microgravity conditions was attempted to eliminate this problem stemming from imperfect crystals.

Methods of Data Acquisition and Analysis

X-ray diffraction patterns from crystals grown in space and on the ground were obtained using the Swiss/Norwegian beam line (SNBL) facility at the European Synchrotron Radiation Facility, Grenoble (ESRF). The SNBL optics included a focusing monochromator and mirror. The goniometer and detector consisted of a 30 cm MAR image plate device. The exposures were made using a film to crystal distance to optimize the signal to noise ratio. Exposures were made for 30 to 60 min, allowing us to observe crystal sampled intensities to the diffraction limit of approximately 2.0 Å observed previously on undulator beam lines (ID9 and ID13 lines at ESRF) in 0.5 to 3 minutes. The wavelength used was 0.873 Å with the synchrotron operating at 200 mA in 2/3 fill mode. The beam size at the crystal was nominally 0.3x0.3 mm.

Flight versus Ground Results

We used four 88 ml hanging drop reactors at 20° C during the spacelab flight on Space Shuttle mission STS-78 in June/July 1996. The hanging drop reactors were originally designed to accommodate a protein volume decreasing in the course of the experiment. However, our crystallization conditions are higher in salt concentration at the beginning of the experiment compared to the final equilibrated solution. The HD reactors were modified to allow for the increase in volume. None of the crystallization drops were lost and all were qualitatively recovered at the end of the experiment.

The morphology and size of the space grown crystals did not differ from the ground control crystallization experiments significantly (Table 1).

Reactor	Reservoir buffer mM MnCl$_2$/ KCl	Crystal characteristics
1S	43/48	Many small rods: 100-200 x 100-200 x 500-1000 m Often hexagonal; few holes.
1G	43/48	Many small crystals.
2S	35/40	As for 1S
2G	35/40	Large and small crystals
3S	30/35	Several big crystals: 300-400 x 300-400 x 1000-1500 m Hollow funnels: typical of big crystals.
3G	30/35	Large and small crystals.
4S	24/29	Several large crystals, hollow funnels.
4G	24/29	Large and small crystals.

Table 1. APCF crystal growth experiments.

S - space experiments, G - ground experiments. All initial volumes were 50 ml and increased 1.5-1.8-fold on equilibration. A reservoir volume of 700 ml was dispensed in two 350 ml absorbers. The starting protein concentration was at 8 mg/ml in 84 mM MnCl$_2$, 60 mM KCl and 20 mM Potassium/Cacodylate pH 6.

There were generally many nucleations in both systems with the consequence of limited crystal size. Most crystals were attached to the Teflon piston of the syringe. All crystals grown in HD reactors whether on ground or in space were inferior in morphology and size to our typical crystals grown under very slow vapor diffusion conditions in our laboratory.

Analysis of crystals grown either on the ground or in space showed no discernible differences in the limits of diffraction or in mosaicity under the three sample conditions used to record the diffraction patterns (Table 2).

Sample conditions	Diffraction limits - a* / b* / c* axes in Å	
in X-ray beam	Ground grown	Space grown
HL-0, RT	3.8 / 3.8 / 3.0	3.8 / 3.7 / 2.9
HL-24, RT	3.2 / 3.2 / 2.7	3.2 / 3.2 / 2.8
HL-24/2, -180° C	2.2 / 2.2 / 2.0	2.2 / 2.2 / 2.0

Table 2. Diffraction limits of ground and space grown crystals.
The values for the three principle directions of the diffraction pattern are given. HL-0: harvest liquid (37 mM Potassium Chloride, 40 mM Manganese Chloride, 10 mM Potassium Cacodylate, pH 6.0); HL-24: harvest liquid containing 24% 2,4-methyl-pentandiol (MPD); HL-24/2: harvest liquid containing 24% MPD and 2% Trehalose; RT: room temperature, ~24* C.

The diffraction limit values listed in Table 2 are estimated from direct observation of the diffraction patterns. Mosaicity was also evaluated qualitatively by direct observation estimating the number of diffraction spots that obviously occur on successive exposures in a series of five 0.4° rotations of the crystal.

Conclusions

There were no significant differences in the quality of diffraction from crystals grown on the ground or in space using the modified HD reactor. In both cases, the crystals were not as useful for X-ray data measurement as crystals grown under the optimal laboratory conditions. Factors that contributed to this result are possibly: 1) the HD crystallization reactors could not be adapted to match the optimal laboratory setups, and 2) the time available for space crystallization required that the gradient between protein and buffer volumes reach equilibrium 4 to 5-fold faster than in our standard setups. Additionally, other experimental factors such as vibrations or container surface effects may be more important than the presence or absence of gravity.

Another important point should be considered. Nucleosome core particles require that 24% MPD be added not only to prevent ice formation during cryocooling, but to improve the diffraction limit that is initially observed at room temperature. The crystals undergo a repacking with a concomitant reduction by approximately 7% of the b-axis unit cell length. Since the rearrangement of the particle in the crystals may dominate crystal quality and occurs after crystal growth, it was important to compare crystals at room temperature with and without the addition of MPD. We were interested to see if the resolution limits would be improved by space growth. They were not.

In order to observe the highest resolution diffraction intensities, it is necessary to cool the crystals to -180° C before exposure to X-ray radiation because of their high sensitivity to radiation damage. A crystal survives for only one of the 200 exposures required for a 2 Å data set if exposed to X-rays at higher temperatures (i.e. 4° C), and for 16 exposures at -180° C (15-20% general weakening of the overall intensity in the crystal sampled diffraction pattern). As for room temperature exposures, there were no improvements in space versus ground grown crystals when examined at cryotemperature.

Currently, we are refining our 2.8 Å structure of the nucleosome core particle to 2.0 Å resolution using data collected at the ESRF and crystals grown in the laboratory. We were unable to reduce the mosaic spread of the crystals, but we were able to find a method of mounting the crystals so that the short reciprocal b*-axis is along the direction of the rotation axis during data collection. This procedure eliminated the superposition of diffraction intensities sufficiently well to permitted a complete data set to be collected over 24 crystals at -180° C. Accordingly, we have no further requirement to attempt crystal growth in space for this particular project.

Articles / Presentations

I do not foresee publication of our STS-78 results.

Summary

Crystals of the nucleosome core particle of chromatin were grown in space and on the ground using a device especially designed for crystal growth experiments on the space shuttle. The resulting crystals in either case were generally not as large or perfect morphologically as those grown under more optimal experimental conditions in our laboratory. Crystals grown in space and on the ground using the shuttle device showed no significant differences.

Advanced Protein Crystallization Facility (APCF)

Crystallization of Photosystem I

Principal Investigator:

Dr. Wolf Schubert
Free University of Berlin
Berlin, Germany

Crystallisation of Photosystem I
- Results of the LMS Mission

Petra Fromme*, Wolfram Saenger# and Norbert Krauß#

* Max Volmer Institut für Biophysikalische Chemie und Biochemie, TU Berlin, Str. des 17. Juni 135, 10623 Berlin, Germany
# Institut für Kristallographie, FU-Berlin, Takustr. 6, 14195 Berlin, Germany

Background

Plants and cyanobacteria are able to use light for performing oxygenic photosynthesis This is the main biological process on earth where emissive electromagnetic energy from the sun is converted into chemical energy. The first step of the process, the light induced charge separation across the photosynthetic thylakoid membrane, is catalysed by two large membrane intrinsic protein complexes, the photosystems I and II. Photosystem I (PS I) from the thermophilic cyanobacterium *Synechococcus elongatus* is the largest of the 8 membrane proteins, which have been crystallised so far. It occurs in the cyanobacterial thylakoid membrane as a trimer with a molecular weight of 3 x 340 000 Da; The monomer consists of 11 different polypeptides, coordinating ~100 chlorophyll *a* molecules, 25 carotinoids, 3 [4Fe4S] clusters and 2 molecules of vitamin K1. A structural model of this trimeric Photosystem I has been derived from X-ray structure analysis at 4 Å resolution [Krauß N., Schubert W.-D., Klukas O., Fromme P., Witt H.T. and Saenger W. (1996) *Photosystem I at 4 Å resolution: A joint photosynthetic reaction center and core antenna system* Nature Struct. Biol. 3, 365-370]

Objectives

Photosystem I was crystallised under microgravity on USML-2 with very encouraging results. The volume of the obtained crystals was increased by a factor of 10-20 compared to the terrestrial Photosystem I crystals, the largest crystal having a length of 4mm and a diameter of 1.5 mm. The crystals diffract X-rays to a maximal resolution of 3.4 Å and show a mosaic spread of 0.6 $^{\circ}$. A complete native data set was measured from the largest microgravity grown crystal using synchrotron radiation at DESY in Hamburg and evaluated to a resolution of 3.4 Å. This is the best X-ray data set thus far obtained from Photosystem I crystals.

Photosystem I could not be crystallised under optimal conditions during the USML-2 mission. We had to use 20°C for technical reasons; however, the temperature for the best crystallisation of Photosystem I on earth was found to be 4°C. Earth grown crystals of Photosystem I aged at 20 °C for 21 days (which was the flight and transport time during USML-2) do not diffract X-rays to a resolution higher than 5 Å. Crystallisation on LMS was technically feasible at 8°C and performed under this condition in order to further improve the quality of the crystals.

Methods

Two sets of experiments were performed: A) Crystallisation of Photosystem I by dialysis against low salt B) Crystallisation of Photosystem I in the presence of 0.75 M sucrose. The aim of using sucrose in the second set of experiments was to increase the viscosity of the solution, thereby reducing the diffusion rates of salt and protein and to slow down equilibration of the solutions in the reactors. This should lead to a slower growth rate and possibly to a significant reduction of the mosaic spread of the obtained crystals.

For A), small pre-grown crystals of Photosystem I were completely dissolved in buffer A (50 mM $MgSO_4$, 5 mM MES pH = 6.4 and 0.02 % ß-dodecylmaltoside) in order to prepare the protein solution. For B), the crystals were dissolved in buffer B (same as A, but + 1,5 M sucrose). The protein concentration was 80 mg/ml in both cases.

In the APCF microdialysis reactors this solution was dialysed against the same buffers but with reduced salt concentration (equilibration concentration 11 mM $MgSO_4$ for A) and 8 mM for B).

A total of eight APCF reactors were filled according to protocol A, and seven reactors were filled according to protocol B using the same solutions. Of these 15 reactors, 9 were used as ground controls (5 without sucrose, 4 with sucrose,), and 6 were flown in space (3 without sucrose, 3 with sucrose). All ground controls were activated/deactivated at the same time as the flight reactors in space.

Comparison of flight results to ground results

The results are summarised in table 1. In all 9 ground control reactors crystals suitable for X-ray structure analysis were obtained. In contrast, all 6 space reactors contained clear, green solution of Photosystem I, although the control and space chambers were filled under identical conditions.

There are several explanations for this result; the following questions had been addressed:

Have the reactors been activated? --=> yes

• The first possibility for non-crystallisation could be that the space reactors had not been activated. In order to exclude this possibility, the conductivity in the reservoir chamber was measured in all flight and ground control reactors. Without activation of the reactors the conductivity should be as low as conductivity at the beginning of the experiment. This was not the case. All chambers showed conductivities expected for the fully equilibrated chambers with a salt concentration of 11 mM $MgSO_4$.

Is the protein degraded ? => no

• We tested if the protein had degraded in the space reactors (perhaps due to increased temperature during start and landing). This was not the case. The flight protocol shows constant temperature during the whole flight and no degradation bands were visible using SDS gelelectrophoresis.

Is there a nucleation problem? => yes

• Decreased nucleation rate in space was assumed to be the reason for the lack of crystals in the space reactors. In order to test this hypothesis, we added a small crystal to the clear solution (seeding) in one of the space-flown reactors. A shower of small crystals was formed immediately. The same result was observed when a a drop of the clear solution from the space reactors (1 ul) was mixed under a microscope with 1 ul buffer without salt . A large number of small crystal was formed immediately.

These results indicate that the nucleation rate was decreased under microgravity conditions. Figure 1 shows a schematic phase diagram of Photosystem I. The protein solution is undersaturated before activation of the reactors (80mg/ml protein and 50 mM salt). After activation, the salt concentration is first reduced to 30 mM, which on earth is close to the border between metastable zone and the nucleation zone. Finally, the salt concentration is further reduced and the protein concentration in solution decreases due to crystal growth. This crystallisation procedure works perfectly for the ground experiments and was also very successfully used on USML -2 mission (at 20 °C), were we obtained very large crystals in three out of six chambers. We now address the question whether sedimentation of the preformed nuclei accelerates nucleation on earth.

Does the orientation of the (ground control) reactors have an influence on the nucleation

=> yes

• In order to test this possibility we looked for the orientation of the ground control reactors during crystallisation with respect to the number and location of crystals formed in the reactors.

In 5 of the ground controls the reactors were in **vertical orientation** (v in Fig. 2) with the protein reservoirs on top, the salt reservoirs on bottom. In this case the sedimentation of the nuclei would be in direction of the decreasing salt concentration (i.e. nuclei will drift to the dialysis membrane).

4 of the ground controls were in **horizontal orientation** (h in Fig. 2). The reactors were lying on the side during crystallisation (this corresponds to a rotation of 90° relative to the vertical orientation . In this case the sedimentation occurs perpendicular to the decreasing salt gradient.

The observed results were in good agreement with these suggestions: In the 5 ground controls with vertically oriented reactors 15-50 crystals were formed per reactor; in the 4 horizontally oriented reactors only 1-4 crystals were grown. All crystals were grown on the earth directed side, i.e. in the vertical orientation (v) all crystals grew on the membrane and in the horizontal orientation all crystals grew on the bottom side of the reactors.

Does microgravity have an influence on the nucleation rate => yes

• The question arises, why we obtained very large, well ordered crystals at 20°C on the USML-2 mission and no crystals at 8°C on the LMS mission. The results of both missions suggest that microgravity has an influence on the nucleation rate. It appears that due to the lack of sedimentation the nucleation rate is dramatically reduced under microgravity conditions. This led to 0-3 nuclei at 20°C, but at 8°C, where the diffusion rate (and therefore also the nucleation rate) is about a factor of two lower, no nuclei with larger than the critical radius were formed.

Conclusion

The results obtained during LMS mission led to new insights in the first events during Photosystem I crystallisation, which are not only useful for further microgravity experiments, but may improve the crystallisation conditions on earth.

It was found that sedimentation of nuclei is significant under terrestrial conditions and increases the nucleation rate during Photosystem I crystallisation. The optimal conditions for crystallisation under microgravity must therefore be tested directly in space. Systematic investigations should be done to further elucidate the primary events during crystallisation of Photosystem I and to show the direct influence of microgravity on nucleation rate and crystal quality for a membrane protein. A larger number of space experiments has therefore to be performed in the future, including the possibility of seeding. If optimal conditions can be found at 8°C, we expect a significant increase of crystal quality.

Summary

The crystallisation of the large membrane protein Photosystem I was investigated under microgravity on the LMS mission. Comparison of the microgravity to the ground control experiments shows a significant influence of the microgravity on the nucleation rate.

Table 1

Reactor number	Location	presence of sucrose	orientation of the reactor *	number of crystals/reactor
319	ground control	no	v	~ 50
119	ground control	no	v	~ 15
130	ground control	no	v	~ 30
320	ground control	no	h	4
105	ground control	no	h	1
133	ground control	yes	v	~ 20
103	ground control	yes	v	~ 40
321	ground control	yes	h	1
318	ground control	yes	h	3
101	microgravity	no		0
322	microgravity	no		0
317	microgravity	no		0
106	microgravity	yes		0
117	microgravity	yes		0
132	microgravity	yes		0

* v = vertical orientation of the reactor
  h = horizontal orientation of the reactor
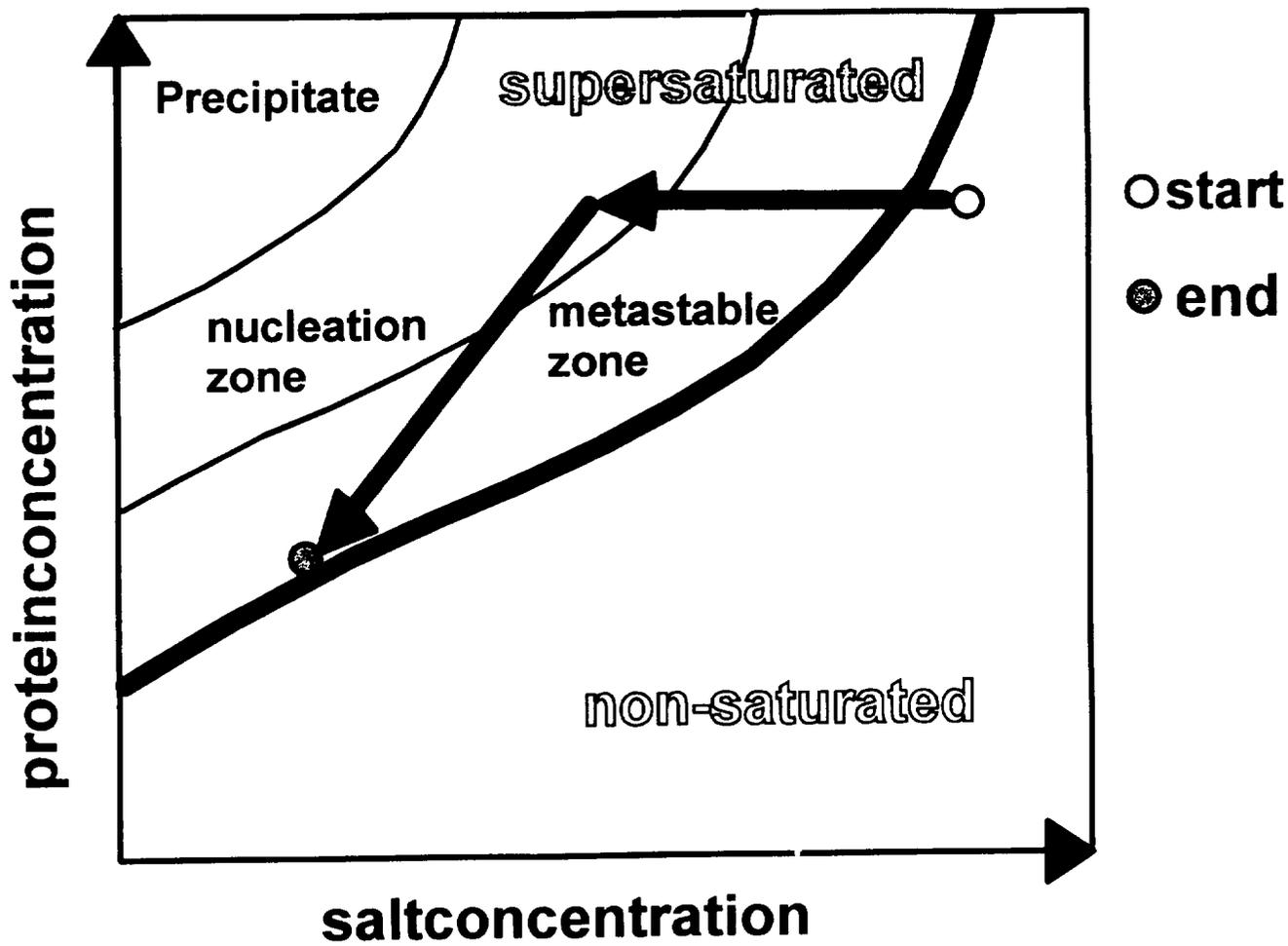
Mechanism of Membrane Protein Crystal Growth: Bacteriorhodopsin-mixed Micelle Packing at the Consolution Boundary, Stabilized in Microgravity

Principal Investigator:

Dr. Gottfried Wagner
Justus-Liebig-Universität
Giessen, Germany

MECHANISM OF MEMBRANE PROTEIN CRYSTAL GROWTH: BACTERIORHODOPSIN-MIXED MICELLE PACKING AT THE CONSOLUTION BOUNDARY, STABILIZED IN MICROGRAVITY

PI:
Torsten Rothärmel
Gottfried Wagner
Justus-Liebig-University
Department of Biology
Senckenbergstrasse 17
35390 Giessen, Germany

Phone: +49-641-99-35140 / 35142
FAX: +49-641-99-35119
e-mail:
Torsten.Rothaermel@bio.uni-giessen.de
Gottfried.Wagner@bio.uni-giessen.de

Co-I:
Christian Betzel
Markus Perbandt
Institut für Physiologische Chemie
c/o DESY; Geb. 22a
Notkestrasse 85
22603 Hamburg, Germany

Phone: +49-40-8998-4744 / 4745
FAX: +49-40-8998-4747
e-mail:
Betzel@EMBL-Hamburg.de
Markus@unisgi1.desy.de

Abstract

The bacteriorhodopsin crystal growth experiment with the Advanced Protein Crystallization Facility (APCF) on the shuttle mission LMS in June 1996 was done to allow crystal growth of bacteriorhodopsin (BR) at the consolution boundary of bacteriorhodopsin-mixed micelle packing, stabilized in microgravity.
The bacteriorhodopsin crystal growth experiments have resulted in crystals of a) needle-shaped, b) cubic-shaped, c) balk-shaped, and d) small cubic-shaped crystals nucleated on the outer end of needles of multicrystalline clusters.
The average edge length of cubic-shaped crystals under microgravity (163.0 μm) and on ground (59.7 μm), and their density (1.125 g/cm^3) were determined.

Introduction:

Membrane proteins catalyze vital reactions such as solute transport, charge separation and conversion of energy, as well as signal transduction. The proton-pumping bacteriorhodopsin (BR) is a small amphiphilic photochromic retinal protein, found in the purple patches of the cell membrane of *Halobacterium halobium*. As a small membrane spanning protein, it does not exceed the lipid bilayer much on either side (1). Detergent-solubilized bacteriorhodopsin is embedded in micelles of different sizes, as a function of the detergent cocktails used (2, 3). The bacteriorhodopsin molecules form filaments which pack together due to weak and easily disturbed hydrophilic interactions between the loop regions of protruding molecules in aligned filaments (4, 5). Three different habits of bacteriorhodopsin crystals, namely a) needle-shaped, b) cubic-shaped, and c) balk-shaped are compatible with three different micelle sizes, received in detergent solutions after bacteriorhodopsin solubilization (2).
Our experience shows that best bacteriorhodopsin crystals grow close to the consolution boundary, where interaction between detergent micelles is enhanced. Reduced gravitational conditions are favourable due to minimal gravity-driven phase separation.

<u>Results:</u>

Consistent with different micelle sizes observed through dynamic light scattering, three different habits of bacteriorhodopsin crystals, namely a) needle-, b) cubic-, and c) balk-shaped crystals could be obtained. The packing of the molecular rods of bacteriorhodopsin was tight and the crystal morphology exhibited smooth surfaces and sharp edges of up to 1 mm in length, and diffractional power with a resolution limit of up to 3.8 Å, as reported before (2, 4).

The LMS-2 (STS-78) microgravity experiment lead to the growth of cubic-shaped bacteriorhodopsin crystals (Fig. 2) with a 20-fold enlarged volume compared to the ground control (Fig. 1).

Vapour diffusion: Laboratory hardware	Liquid-liquid diffusion: APCF 188 µl in Microgravity	Liquid-liquid diffusion: APCF 188 µl on Ground
84.6 ± 6.5 µm (n = 41)	163.0 ± 7.3 µm (n = 13)	59.7 ± 2.3 µm (n = 39)

Fig. 1: Average edge length of cubic-shaped crystals of bacteriorhodopsin, grown under different conditions.

The cubic habit was stabilized under microgravity conditions, while the ground control showed additional multicrystalline needle clusters.
An altered crystal growth protocol produced multicrystalline needle clusters and single needles both on earth and in microgravity.

The density of cubic-shaped crystals was determined by the method of Matthews (6) and Mikol and Giegé (7). Preliminary results of the determination of crystal density with different Ficoll solutions show a density of 1.125 g/cm^3 after 35 min (Fig. 3).
This preliminary density estimation of cubic-shaped bacteriorhodopsin crystals is slightly lower than the density of purple patches in the membrane from *Halobacteria* with 1.18 g/cm^3 (8). The three-dimensional cubic-shaped bacteriorhodopsin crystals would show an slightly increased content of water compared to the two-dimensional crystalline structure in the purple membrane patches.

A new observation was the nucleation of small cubic-shaped bacteriorhodopsin crystals on the end of single needles from multicrystalline bacteriorhodopsin needle clusters (Fig. 4). The multicrystalline needle clusters grown under microgravity showed a slight increase in diameter compared to the multicrystalline needle clusters grown as ground control.
Nucleation of pseudohexagonal needles and orthorhombic bacteriorhodopsin crystals has been described before on benzamidine crystals (9). The observation that pseudohexagonal bacteriorhodopsin crystals could be nucleated on benzamidin-crystals led to the assumption that the activation energy that determines the nucleation probability was lower on the particular benzamidin surface than in solution.

Interestingly, endparts of the surface of the needles of bacteriorhodopsin multicrystalline needle clusters were able to induce a new crystal morphology, since small cubic-shaped bacteriorhodopsin crystals formed at the end of the needles of multicrystalline needle clusters (Fig. 4).
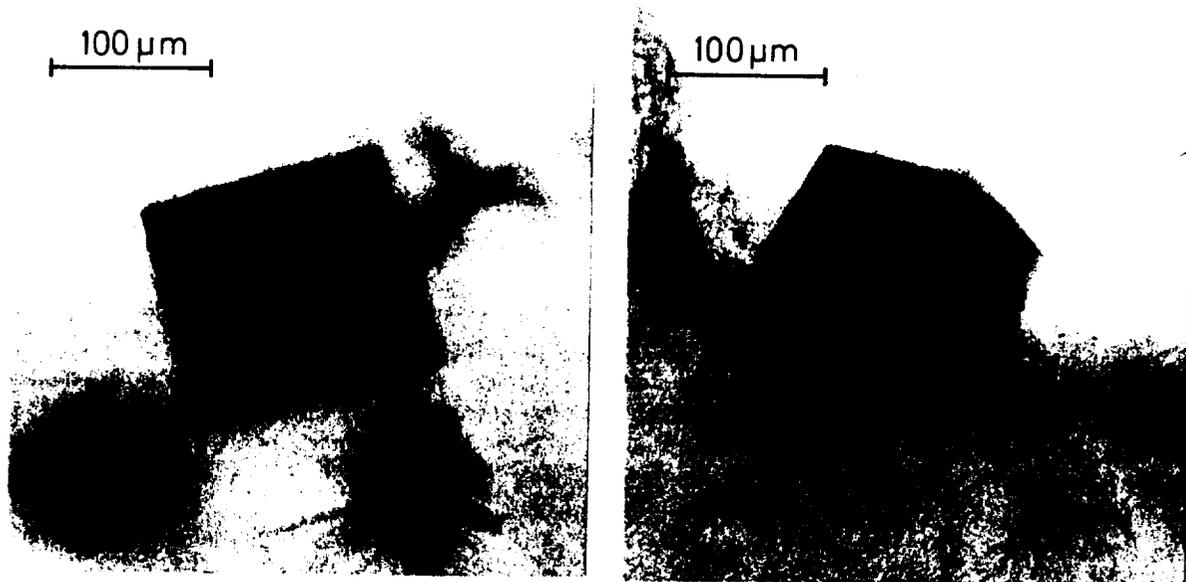

Fig. 2: Cubic-shaped bacteriorhodopsin crystals grown in microgravity with axes of 150 μm in length. The crystal morphology is compact with sharp edges and smooth surfaces.
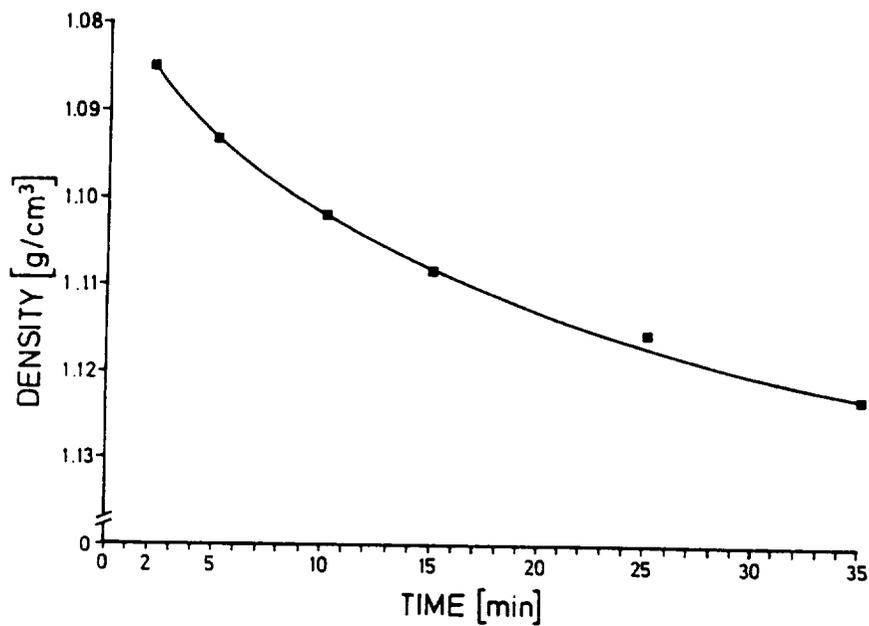

Fig 3: Experimental determination of the density of cubic-shaped bacteriorhodopsin crystals. The density was determined in a step up gradient of Ficoll solutions (from 25-60% w/w) calibrated by estimation with NaH_2PO_4 droplets.
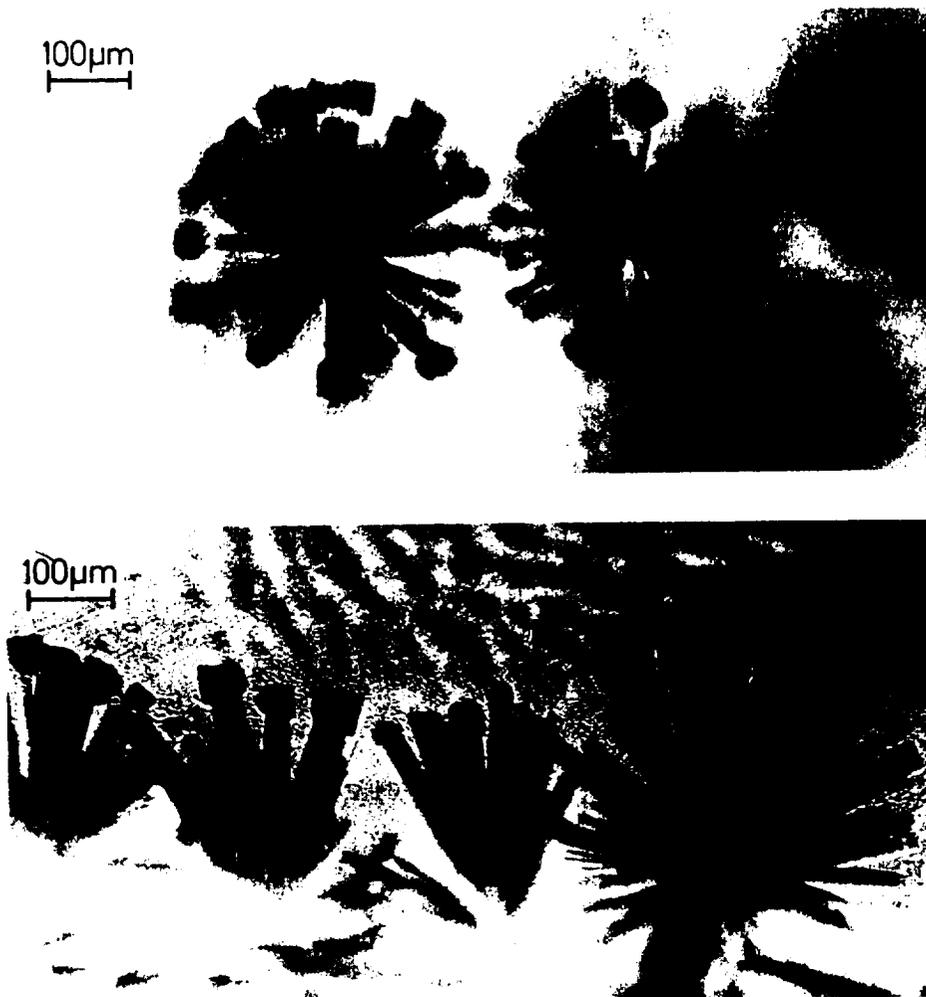
Fig. 4: Multicrystalline bacteriorhodopsin needle clusters with small cubic-shaped crystals on the end of single needles. The multicrystalline needle clusters shown here, are up to 390 μm in diameter; the small cubic-shaped crystals have an edge length up to 45 μm. The clusters fall apart easily.

Another attempt of crystal formation was based on the procedure of seeding. Cubic-shaped and balk-shaped bacteriorhodopsin crystals were transferred in new crystalization set ups of seeding-analogue protocols:

a) The cubic-shaped seeding-crystals dissolved over night after being transferred. The new crystallization set ups led to formation of multicrystalline needle clusters, a few balk-shaped bacteriorhodopsin crystals, and needle-shower (Fig. 5).

b) The balk-shaped seeding-crystallization set ups led to formation of multicrystalline needle clusters and balk-shaped bacteriorhodopsin crystals of increased length and width (Fig. 5).

Electrostatic crosslinkers as additives may have value for optimization of crystallization conditions, since ionic and electrostatic interactions between macromolecules play a role in the crystallization process (10). The linker could act as a multivalent tether, where one end of the linker would interact with a charged surface group of one macromolecule while a second charged group on the same tether could interact with another, and so might influence both pre- and post-nucleation events (10).

Cubic-shaped bacteriorhodopsin crystals formed while the crosslinkers Triglycine, Tetraglycine, and Hexaglycine were added, but did not have an obvious impact on size or appearance of the formed crystals. Gly-Gly free base tended to increase the size of the cubic-shaped crystals on earth, but did not have a clear impact on cubic crystal formation under microgravity.

Seeding-crystals:	New grown crystals:
cubic-shaped crystals edge length: 60-90 μm	multicrystalline needle clusters up to 1.3 mm in diameter balk-shaped crystals up to 840 x 90 μm needle-shower
balk-shaped crystals 300-450 x 30-60 μm	balk-shaped crystals up to 900 x 90 μm multicrystalline needle clusters up to 1.6 mm in diameter

Fig. 5: Bacteriorhodopsin crystal formation in seeding set ups.
Some of the balk-shaped crystals considered new grown in the set up with seeding balk-shaped crystals could be seeding-crystals with increased length, because it was not possible to distinguish between balk-shaped seeding-crystals and new grown crystals of the same habit.

Conclusions:

The chosen crystallization conditions combined with the suppression of gravity-driven convection and sedimentation of bacteriorhodopsin enabled the growth of tightly packed crystals of different habits. Single crystals exhibited a diffractional power with a resolution limit of up to 3.8 Å.
The volume of cubic-shaped bacteriorhodopsin crystalsgrown under microgravity conditions showed a 20-fold enlarged volume compared to the ground control.
A new observation was the nucleation of small cubic-shaped bacteriorhodopsin crystals on the endpart of the surface of needles of multicrystalline needle clusters.
Both effects putatively result from stabilization of the consolution boundary.
Further experiments in microgravity, as a favourable environment of improved crystallo-genesis, provide additional progress in the investigation of difficult membrane proteins such as bacteriorhodopsin.

References
1. D. Oesterhelt, C. Bräuchle, and N. Hampp, Quart. Revs. Biophysics 24:425-478 (1991)
2. T. Rothärmel, G. Wagner, Ch. Betzel, and M. Perbandt, USML-2 report (1997)
3. E. H. L. Tan and R. R. Birge, Biophys. J. 70:2385-2395 (1996)
4. G. Wagner, ESA-Proc. Space Station Utilization, SP-385:235-238 (Dec. 1996)
5. G. Wagner, ESA J. 18:25-32 (1994)

6. B. W. Matthews, J. Mol. Biol. **33**:491-497 (1968)
7. V. Mikol and R. Giegé. In: A. Ducruix and R. Giegé (eds.): Crystallization of Nucleic Acids and Proteins. IRL Press, pp 219-239 (1992)
8. D. Oesterhelt, R. Hartmann, H. Michel, and G. Wagner. In: G. Schäfer and M. Klingenberg (eds.): Energy conservation in biological membranes. Springer-Berlin, pp. 140-151 (1978)
9. G. F. X. Schertler, H. D. Bartunik, H. Michel, and D. Oesterhelt, J. Mol. Biol. **234**:156-164 (1993)
10. B. Cudney, S. Patel, K. Weisgraber, Y. Newhouse, and A. McPherson, Acta Cryst. **D50**:414-423 (1994)

MECHANISM OF MEMBRANE PROTEIN CRYSTAL GROWTH: BACTERIORHODOPSIN-MIXED MICELLE PACKING AT THE CONSOLUTION BOUNDARY, STABILIZED IN MICROGRAVITY

Torsten Rothärmel*, Gottfried Wagner*, Christian Betzel°, and Markus Perbandt°

* Justus-Liebig-University, Department of Biology, Senckenbergstrasse 17, 35390 Giessen, Germany,
  e-mail: Torsten.Rothaermel@bio.uni-giessen.de, Gottfried.Wagner@bio.uni-giessen.de
° Institut für Physiologische Chemie, c/o DESY, Geb. 22a, Notkestrasse 85, 22603 Hamburg, Germany,
  e-mail: Betzel@EMBL-Hamburg.de, Markus@unisgi1.desy.de

The proton-pumping bacteriorhodopsin (BR) is a small amphiphilic photochromic retinal protein, found in the purple patches of the cell membrane of *Halobacterium halobium*.

The experiment was done under microgravity to allow crystal growth of bacteriorhodopsin at the consolution boundary of bacteriorhodopsin-mixed micelle packing and resulted in crystals of a) needle-shaped, b) cubic-shaped (Fig. 1), c) balk-shaped, and d) small cubic-shaped crystals nucleated on the end of needles of multicrystalline clusters (Fig. 2).

The packing of the molecular rods of bacteriorhodopsin was tight and the crystal morphology exhibited smooth surfaces and sharp edges of up to 1 mm in length, and diffractional power with a resolution limit of up to 3.8 Å.

The average edge length of cubic-shaped crystals under microgravity (163.0 µm) and on ground (59.7 µm), and their density (1.125 g/cm^3) were determined. The cubic-shaped bacteriorhodopsin crystals grown in microgravity showed a 20-fold enlarged volume compared to the ground control.

Interestingly, endparts of the surface of the needles of bacteriorhodopsin multicrystalline needle clusters were able to induce a different crystal morphology, since small cubic-shaped bacteriorhodopsin crystals formed at the end of the needles of multicrystalline needle clusters.
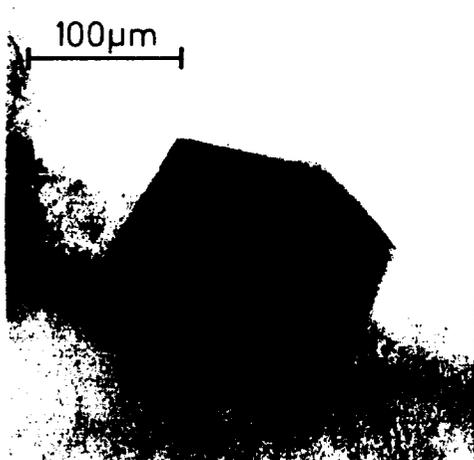

Fig. 1: Cubic-shaped BR crystal grown under microgravity with axes of 150 µm length. The crystal morphology is compact with sharp edges and smooth surfaces.
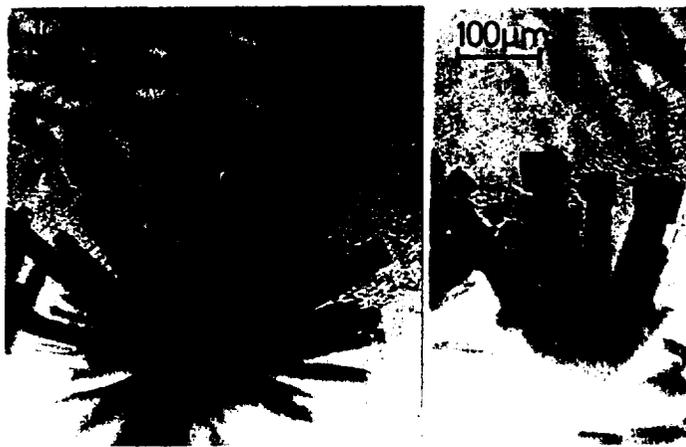
Fig. 2: Multicrystalline BR needle cluster with small cubic-shaped BR crystals on the end of single needles. The multicrystalline needle clusters shown here, are up to 390 µm in diameter; the small cubic-shaped crystals have an edge length of 45 µm.

Advanced Protein Crystallization Facility (APCF)

Crystallization in a Microgravity Environment of CcdB, a Protein Involved in the Control of Cell Death

Principal Investigator:

Dr. Lode Wyns
Free University of Brussels
Brussels, Belgium

CRYSTALLIZATION IN A MICROGRAVITY ENVIRONMENT OF CcdB, A PROTEIN INVOLVED IN THE CONTROL OF CELL DEATH

Prof. Dr. Lode WYNS, Dr. Minh Hoa DAO THI, Dr. Dominique MAES

Department of Ultrastrucutre

Institute of Molecular Biology

Free University of Brussels (VUB)

Belgium

Phone: 32 2 359 02 82

Fax: 32 2 359 02 89

email: ljwyns@vub.ac.be

Introduction

The *E. coli* F-plasmid is very stable inherited in the bacterial population. Plasmid-carrying cells are able to propagate while daughter cells that have not inherited a plasmid copy are selectively killed (Jaffé et al., 1985). The plasmid F-encoded proteins CcdA and CcdB are the key molecules responsible for this postsegregetional killing of bacterial cells. The underlying mechanism is based on a differential decay of the activities of the CcdA and CcdB proteins, the half-life of the cytotoxic CcdB being longer than the half-life of CcdA, that antagonises the CcdB action (Van Melderen, 1994, 1996). When CcdA is absent, CcdB is responsible for cell death, induction of the SOS pathway and inhibition of DNA synthesis (Bex et al., 1983, Karoui et al., 1983; Bailone et al., 1985). CcdA and CcdB are encoded by the *ccd* operon (Miki et al., 1984a,b). They are known to auto-regulate their own expression and it was shown that both proteins acts as a DNA binding repressor, probably after having formed a CcdA/CcdB complex (Tam & Kline, 1989a,b; De

Feyter et al., 1989). Recently it was demonstrated that the CcdB mediated cell-killing involves poisoning of DNA-topoisomerase II complexes (Bernard & Couturier 1992). The Arg462Cys mutation in the DNA gyrase A domain suppresses the lethal character of CcdB. Further experiments showed that, like quinolone antibiotics and a variety of antitumor drugs, CcdB is responsible for gyrase-mediated double-stranded DNA breakage (Bernard *et al.*, 1993). It thus converts the wide-type gyrase in a DNA-damaging agent. This action, which is most likely due to direct binding of CcdB to the DNA gyrase A domain, can be completely reversed by addition of stochiometric amounts of CcdA.

Poisons of eucaryotic topoisomerases are regarded as potent candidates of anti-cancer drugs. Elucidation of the structure and mode of action of the CcdB protein may lead to the design of new antibiotics and anti-tumoral drugs. Effort to crystallise CcdB over the last few years led to the identification of experimental conditions for the growth of several crystal forms. Here we present information concerning the crystallisation behaviour of CcdB and report on a novel crystal form that diffracts to high resolution and is suitable for structure determination. We also report the crystallisation of a mutant that acts as a super killer, probably due to its enhanced affinity for the A subunits of gyrase.

Objectives

- Improvement of crystal quality especially with respect to the systematic twinning problem.
- Crystallization of CcdB mutants using for MIR work.

Materials and Methods

Protein expression and purification of CcdB from Escherichia coli

CcdB was overexpressed in *E. coli* strain MS501 (containing the CcdB permissive mutation R462C in the GyrA gene harbouring plasmid pULB2250). *E. coli* cells were grown at 37°C in LB medium supplemented with 100 mg/l ampicilin and streptomycin. The purification contains the following steps : the ammonium sulphate precipitation using 30-80% cut-off , QEAE column at pH = 8.50 Tris-Hcl buffer ,

gel filtration column.,and finally Mono-S column. using a 0.0 - 1.0 M NaCl gradient. This resulted in a protein showing only a single band on SDS-PAGE and a yield of about 20 mg CcdB per litre of culture. The purified protein was dialysed against water and concentrated to 15.0 mg/ml (assuming a specific absorption coefficient of 16,100 M^{-1} at 280 nm) and subsequently used in crystallisation trials.

Purification of the CcdB Cysteine mutants

The CcdB mutants S70C, S74C, S84C and the double mutant S74C/G77Q were purified by affinity chromatography on activated Thio-Sepharose and washed with buffer containing 50 mM Tris-HCl (pH 7.80) , 1mM EDTA, 0.5M NaCl and 0.1% Triton X-100. and a Mono-Q column using a 0.0 to 1.0 M NaCl gradient. The pure protein was dialysed against water and concentrated before use in crystallisation trials.

Crystallisation

Crystallisation conditions were screened using the hanging drop method and resulted in three crystal forms, the details of which are summarised in Table I. Phase diagrams were also determined by crystallisation using the hanging drop method. For the tetragonal and orthorhombic forms, crystallisations were performed at different pH values, ranging between 6.5 and 9.0, using ammonium sulphate, sodium chloride and sodium acetate as precipitants. For the monoclinic form, the pH was chosen between 4.1 and 4.6 using PEG-6000 or PEG-Me5000 as precipitants. For the double S74C/G77Q, a phase diagram was determined using MPD.

Crystallisation was also attempted in both agarose and silica gels (Robert et al., 1992; Thiessen et al., 1994) for tetragonal and monoclinic forms of CcdB. In agarose gels, the crystallisation have been performed with different concentrations of CcdB ranging from 2.6 - 5.0 mg/ml, using 6%-12% PEG 6000 and 10%-20% PEGMe 5000 as precipitant at pH4.50 for the monoclinic form. For the tetragonal form, the protein concentration was varied between 6.0 and 12.0 mg/ml and the concentration of ammonium sulphate between 0.8 M and 2.0 M. These trials were done both at pH 7.5 and pH 8.5. The agarose concentration was varied from 0 to 2% agarose for all conditions tried. Similarly, the silica gel contents was varied from 2.7 - 5.0 %.

Crystallisation experiments in a microgravity environment of CcdB and its mutants were accepted by ESA for the two missions : USML-2 (1995) and LMS (1996).

Hanging drop (HD) reactors and free interface diffusion (FID) reactors of the *Advanced Protein Crystallisation Facility* (APCF) were used in these experiments. All experiments were duplicated in identical setups on earth, and in the cases where no crystals appeared during the space shuttle mission, the reactors were reactivated on earth after the flight. During the USML-2 mission, one Hanging Drop reactor and one FID reactor were allocated for both the wild type CcdB and for the double mutant S74C/G77Q. During the LMS mission, also a single hanging drop reactor and two FID reactors were available, this time for the wild type protein only.

Data collection and heavy atom screening

Data were collected on an Enraff-Nonius FAST area detector with a rotating anode source operated at 40 kV and 90 mA. Crystals were mounted in capillaries in the usual way and data were collected at 288 K. In the case of monoclinic CcdB, data were also collected at 100 K. These crystals were first transferred to a solution containing of 30% (w/w) PEG 400 and 70% (w/w) of a buffer solution consisting of 100mM sodium acetate buffer pH 4.5, and then shock-frozen in a 100 K nitrogen stream.

Heavy atom derivatives were screened by adding 1 μl of the corresponding compound (dissolved in the mother liquor of the corresponding crystal form) directly to 10 μl hanging drops containing one or more single crystals of monoclinic CcdB. Soaking times and concentrations were varied from 0.1 mM and 1 hour to 25 mM and 5 days, after which they were mounted in glass capillaries and the data collected immediately.

Results and discussion

Tetragonal and orthorhombic crystals

Four years ago, we reported the crystallisation of CcdB in two crystal forms (Steyaert et al., 1993). These were tetragonal and orthorhombic crystals, the details of which are summarised in Table I. Their morphologies are shown in Figure 1. The tetragonal and orthorhombic crystals can be grown using ammonium sulphate, sodium chloride and sodium acetate in the pH range from 6.5 to 9.0. The tetragonal crystals grow most easily, while the orthorhombic form occurs more sporadically,

often together with tetragonal crystals. The asymmetric unit of each of these two crystal forms is rather large, and both crystal forms turned out to be unusable for heavy atom screening.

In the case of the tetragonal form, a 2.7 Å set of data could initially be collected from a crystal grown in ammonium sulphate, but it soon turned out that the crystals often showed no significant diffraction at all. This was especially problematic for crystals grown in sodium acetate, although some of them reached dimensions up to $0.4 \times 0.5 \times 1.5$ mm^3. Also, no suitable heavy atom derivatives could be found.

The orthorhombic crystals allowed for a 2.5 Å native set of data to be collected and consequently, derivative screening was started using these crystals. All prepared potential derivatives were highly non-isomorphous. As apparently all heavy atom compounds tested showed these same results, regardless of concentration and soaking time, a number of native data sets were collected for comparison. Native data from different crystals turned out to be non-isomorphous to each other, the R_{merge}'s being in the range of 30% to 50%.

Monoclinic Crystals

Extensive screening of the crystallisation conditions led to a new, monoclinic, low pH crystal form (Figure 2). These crystals belong to space group C2, with unit cell parameters a = 74.94 Å, b = 36.24 Å, c = 35.77 Å, β = 115.27°. These crystals grow around pH 4.5 using PEG 6000 or PEG-Me 5000 as precipitants. Typically, a drop consisting of 5 μl protein (3 mg/ml in 100 mM MOPS buffer pH =7.0) and 5 μl of 10 -15 % of PEG 6000 or PEG-ME 5000 in 100 mM acetate buffer pH 4.1-4.5. The monoclinic crystal form contains only a single molecule in the asymmetric unit. Therefore, at low pH, CcdB is at most a dimer, the molecular two-fold axis of which coincides with the crystallographic two-fold axis of space group C2..

The zone in which crystallisation occurs is very narrow and the crystals appear only after precipitation has already formed in the drop. Such a narrow crystallisation zone is unusual and makes screening with a wide grid or sparse matrix method difficult. Nevertheless, it is this crystal form that forms the key for obtaining the three-dimensional structure of CcdB, as it is the only one with which we could prepare useful heavy atom derivatives. The crystals that grow spontaneously are highly twinned and are not suitable for data collection. To produce single crystals of

the C2 form, crystallisation was performed by using repeated microseeding in hanging drop and sitting drop setups. The monoclinic CcdB crystals grown in this way turn out to be highly mosaic, and show a large variation in mosaicity from crystal to crystal ($0.5°$ up to $3.0°$ in unfavourable cases). We were, however, unable to fine tune the crystallisation conditions in order to grow crystals with a lower mosaicity reproducibly, despite extensive effort, including attempts with gel growth and crystal growth in microgravity conditions (see below). This is in contrast to the results obtained with other proteins using similar techniques (Sica et al., 1994, Snell et al., 1995). In fact, high and low mosaicity crystals grow together in the same drop, but there is some tendency of the smaller crystals to be less mosaic. Gel growth resulted in crystals essentially similar in size and diffraction quality as those grown in normal hanging and sitting drop experiments.

For crystals with high mosaicity, usable diffraction can be observed up to about 3.0 Å, while the better crystals show diffraction up to 1.6 Å at room temperature. This diffraction limit was observed both for crystals grown by microseeding and crystals grown in gel. Data collection on a flash frozen crystal (refined mosaicity $0.9°$) provided usable data up to at least 1.5 Å (R-merge in the resolution shell from 1.54 to 1.50 Å was 0.146, with a mean I/sigma(I) in this shell of 7.2. Screening for heavy atom derivatives has, until now, resulted in the identification of one single site derivative. This $Hg(Ac)_2$ derivative was prepared by a 20 hours soak in 10 mM mercury acetate. The structure of CcdB will therefore be determined using MIR methods after additional derivatives have been found, or alternatively using MAD on the single site $Hg(Ac)_2$ derivative.

Crystallisation in a microgravity environment

Crystal growth in microgravity conditions was used as a possible solution to overcome the problem of twinning and high mosaicities. The experimental conditions used as well as the outcome of these experiments are summarised in Table II. The number of experiments that could be performed during the two space shuttle missions was limited and the interpretation is complicated by the failure to grow crystals in most of the control experiments on earth. Nevertheless, the fact that crystals could be grown in several reactors during the space shuttle missions, while no crystals appeared in the control experiments on earth do suggest that the

lack of convection and sedimentation has a beneficial effect on protein crystal growth. In the one experiment where both in space and on earth crystals were produced, we did observe a significant decrease of the number of twinned crystals, but no pronounced improvement of the mosaicity was evident.

Crystallisation of cysteine mutants

To look for suitable heavy metal derivatives we decided to make the four following specific serine to cysteine mutants : Ser70Cys, Ser74Cys, Ser84Cys and the double mutant Ser74Cys/Gly77Gln. These mutants were designed for the production of Hg-derivatives in the MIR work and some of them were shown to act as super-killers (Bahassi et al., 1997). No crystals were obtained for the two mutants Ser74Cys and Ser84Cys. The mutant Ser70Cys crystallised in ammonium sulphate as very thin plates, that do not diffract. The double mutant Ser70Cys/Gly77Gln was initially crystallised using MPD as precipitant. The crystals thus formed were thin needles that at most diffract to about 7 Å and do not withstand soaking with mercury salts. Later, well diffracting crystals were formed in the same conditions as where the wild type protein produces the tetragonal form. These crystals are however not isomorphous with the those of the wild type protein. They belong to space group I222 (or $I2_12_12_1$) with unit cell a = 105.58 Å, b = 105.80 Å, c = 91.90 Å and diffract to 2.5 Å resolution (Table I). Although a and b are almost identical and the unit cell constants are very similar to the tetragonal form of the wild type protein, the crystals are not tetragonal. Nevertheless, both crystal forms are probably related, as the tetragonal form of the wild type protein contains a 17 sigma non-origin peak in its Patterson, suggesting a pseudocentering (data not shown).

Conclusions

CcdB is a small dimeric protein that poisons DNA-topoisomerase II complexes. We analysed its crystallisation properties in function of precipitant type, precipitant concentration, pH and protein concentration. This led to a novel crystal form which, in contrast to previously reported crystals, is suitable for structure determination using the MIR method. The space group of this new form is C2, with unit cell parameters a = 74.94 Å, b = 36.24 Å, c = 35.77 Å, β = 115.27°. The asymmetric

unit contains a single monomer. Flash-frozen crystals diffract to at least 1.5 Å resolution, while room temperature diffraction can be observed up to 1.6 Å. The double mutant S74C/G77Q, which acts as a super-killer, crystallises in space group I222 (or $I2_12_12_1$) with unit cell a = 105.58 Å, b = 105.80 Å, c = 91.90 Å. These crystals diffract to 2.5 Å resolution. With the new crystal form we were able to solve the structure of CcdB .as it shown in Figure 3.

Acknowledgements

References

Bahassi, E.M., Jaloveckas, D.R. & Couturier, M. (1997) *In preparation.*

Bailone, A., Sommer, S. & Devoret, R. (1985) *Proc. Natl. Acad. Sci. USA* **82**, 5973-5977.

Bernard P. & Couturier M. (1992) *J. Mol. Biol.* **226**, 735-745.

Bernard, P., Kézdy, K., Van Melderen, L., Steyaert, J., Wyns, L., Pato, M., Higgins P., & Couturier, M. (1993) *J. Mol. Biol.* **234**, 534-541.

Bex F., Karoui H., Rokeach L., Drèze P., Garcia L. & Couturier M. (1983) *EMBO J.* **2**, 1853-1861.

De Feyter, R., Wallace, C. & Lane, D. (1989) *Mol. Gen. Genet.* **218**, 481-486.

Jaffé A., Ogura T.& Hiraga S. (1985) *J. Bacteriol.* **163**, 841-849.

Karoui, H., Bex, F., Drèze, P. & Couturier, M. (1983) *EMBO J.* **2**, 1863-1968.

Miki T., Yashioka K. & Horiuchi T. (1984a) *J. Mol. Biol.* **174**, 605-626.

Miki T., Chang Z.-T. & Horiuchi T. (1984b) *J. Mol. Biol.* **174**, 627-646.

Robert, M. C., Provost, K. and Lefaucheux, F. (1992) In *Crystallisation of Nucleic Acids and Proteins. A Practical Approach*, A.Ducruix and R.Giegé eds. Oxford University Press.

Sica, F., Demasi, D., Mazzarella, A., Zagari, A. and Capasso, S. (1994) Acta Cryst. **D50**, 508-511.

Snell, E.H., Weisgerber, S., Helliwell, J.R., Weckert, E., Hölzer, K. & Schroer, K. (1995) *Acta Cryst.* **D51**, 1099-1102.

Steyaert, J., Van Melderen, L., Bernard, P., Dao-Thi, M.-H., Loris, R., Wyns, L., & Couturier, M. (1993) *J. Mol. Biol.* **231**, 513-515.

Tam., J.E. & Kline, B.C. (1989a) *Mol. Gen. Genet.* **219**, 26-32.

Tam J.E. & Kline B.C. (1989b) *J. Bacteriol.* **171**, 2353-2360.

Thiessen, K. J. (1994) *Acta Cryst.* **D50**, 491-495.

Van Melderen, L., Bernard, P., & Couturier, M. (1994) *Mol. Microbiol.* **11**, 1151-1157.

Van Melderen, L., Dao-Thi, M.-H., Lecchi, P., Gottesman, S., Couturier, M. & Maurizi, M.R. (1996) *J. Biol. Chem.* **271**, 27730-27738.

Figure 1. Photomicrograph of tetragonal and orthohombic CcdB. (a) tetragonal crystals grown from ammonium sulphate, (b) tetragonal crystals grown from ammonium acetate, (c) tetragonal crystals grown from NaCl, (d) orthorhombic crystal grown from ammonium sulphate. All photographs are shown on the same scale. The largest crystal in (d) is about 0.8 mm long.

Figure 2 . Monoclinic CcdB crystals. (a) spontaneously grown, heavily twinned monoclinic crystals, (b) monoclinic crystals grown using microseeding, (c) monoclinic crystals grown in agarose gel, (d) space grown monoclinic crystals. All photographs are shown on the same scale. The largest crystal is about 0.3 mm long.

Figure 3 Ribbon representation of the CcdB dimer.The secondary structure element of one monomer are labelled and colour-coded. While the other monomer is shown in grey. The main five-stranded antiparallel ß-sheet is shown in red, the smaller three-stranded "wing" sheet in purple. The C-terminal α-helix is coloured yellow, and the tree isolated turn of 3-helix ochre. Residues identified by mutagenesis to be involved in the killer function of CcdB are shown as ball-and-stick models. The three C-terminal residues (Trp99 Gly100 and Ile101), mutations of which suppress the killer phenotype , are coloured yellow. The three serines, who's mutation to cysteines enhance the killer phenotype (Ser70, Ser74 and Ser84) ,as well as Leu 83(who's mutation to Ile has a similar effect) are coloured light blue. The LysC cleavage site protected by CcdA is indicated by an arrow on each monomer.

Table I. : Crystals of CcdB.

	wild type			S74C/G77Q
	Form I	Form II	Form III	Form IV
Space group	C2	P4$_2$2$_1$2	P2$_1$2$_1$2$_1$	I222 or I2$_1$2$_1$2$_1$
Unit cell	a = 74.94 Å b = 36.24 Å c = 35.77 Å β = 115.27°	a = b = 104.4 Å c = 88.9 Å	a = 77.62 Å b = 93.28 Å c = 141.44 Å	a = 105.58 Å b = 105.80 Å c = 91.90Å
Resolution	1.6 Å/1.5 Å*	2.7 Å	2.5 Å	2.5 Å
R$_{sym}$	0.061/0.056*	0.092	0.070	0.118
Completeness (%)	90.2/84.9*	95.1	93.1	90.2
Multiplicity	6.87/2.33*	2.93	2.97	3.50
Contents of asymm. unit	1 monomer	2 dimers	4 dimers	2 dimers
Solvent contents (%)	35 %	55 %	55 %	55 %

* after cryocooling

216

Table II : Overview of of the microgravity experiments.

Reactor	Protein drop	Bottom solution/salt chamber	microgravity	earth
USLM-2 HD172	50 µl containing 4.5 mg/ml protein (double mutant) S74C/G77Q) in 100 mM MOPS pH7.0	30 µl containing 30% MPD in 100 mM NaAc pH 4.6	small amount of precipitation and a few needle-shaped crystals	larger needle shaped crystals
USLM-2 HD127	30 µl containing 3.7 mg/ml protein in 100 mM MOPS pH7.0	50 µl containing 10% PEG5000 in 100 mM NaAc pH 4.6	heavy precipitation, a large amount of twinned crystals with an average size of 0.3 × 0.2 × 0.2 mm and a few single crystals with average dimensions 0.1 × 0.05 × 0.02 mm	no crystals
LMS HD 154	40 µl containing 4.5 mg/ml CcdB in 100 mM MOPS pH7.0	40 µl containing of 10% PEG-Me5000 in 100 mM NaAc pH 4.1	slight precipitation and a large amount of crystals, mostly single	small, heavily twinned crystals

217

| ID	Protein solution	Chamber solution	Result 1	Result 2
USLM-2 FID207	115 μl containing 4.5 mg/ml protein (double mutant S74C/G77Q) in 100 mM MOPS pH7.0 mixed with 85 ml salt chamber solution	85 μl containing 2.0 M NaCl and 0.2 M NaAc in 100 mM NaAc pH 4.6	heavy precipitation post-flight re-activation resulted in several needle-shaped crystals	heavy precipitation a large amount of tiny needle-shaped crystals
USLM-2 FID203B	40 μl containing 7.4 mg/ml protein in 100 mM MOPS pH7.0 mixed with 160 ml salt chamber solution	160 μl containing 10% PEG5000 in 100 mM NaAc pH 4.6	slight precipitation One single crystal (0.05 × 0.02 × 0.02 mm) and several larger twinned crystals	heavy precipitation no crystals
LMS FID312B	135 μl containing 4.5 mg/ml CcdB in 100 mM MOPS pH7.0 mixed with 65 ml salt chamber solution	65 μl containing 40% ammonium sulphate in 100 mM HEPES pH 7.5	small amount of precipitation no crystals	heavy precipitation no crystals
LMS FID305B	80 μl containing 4.5 mg/ml CcdB in 100 mM MOPS pH7.0 mixed in 100 mM NaAc pH 4.1	120 μl containing 10% PEG5000	small amount of precipitation no crystals	heavy precipitation no crystals

Figure 1

A

D
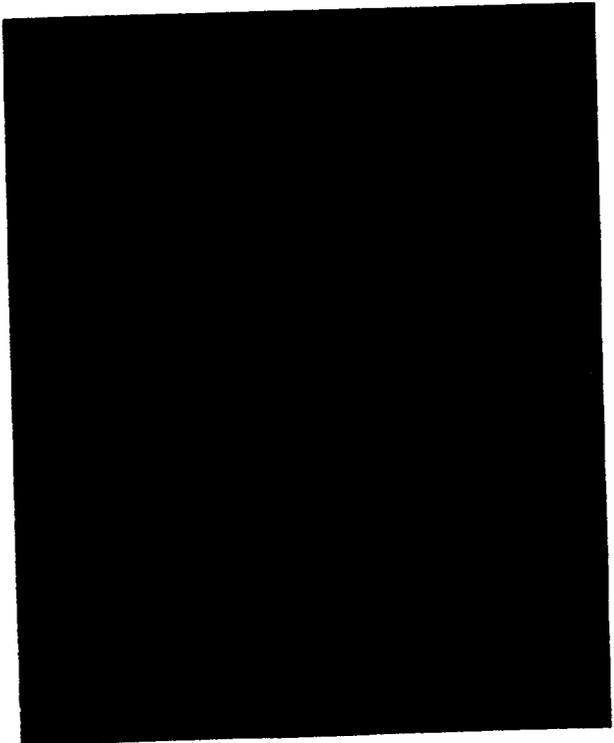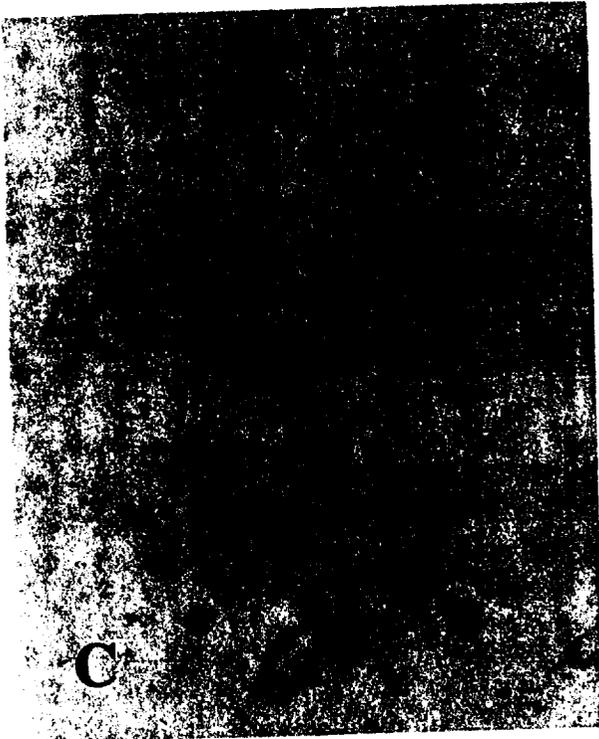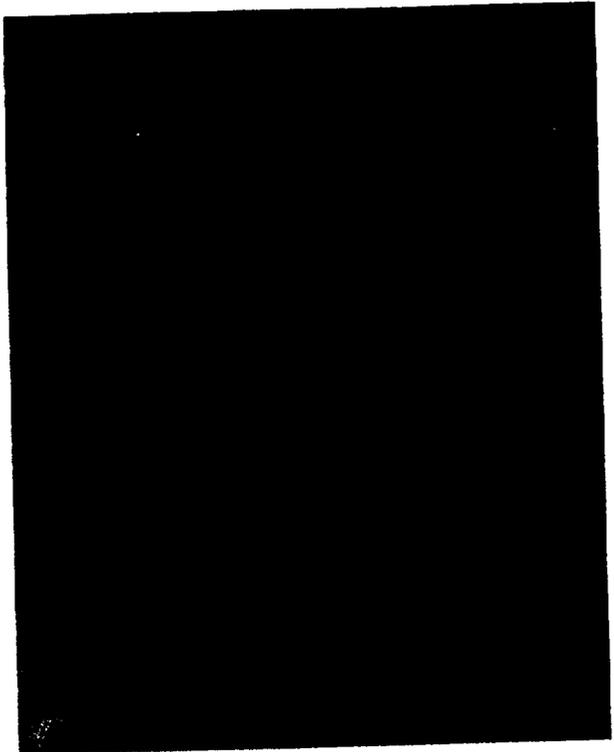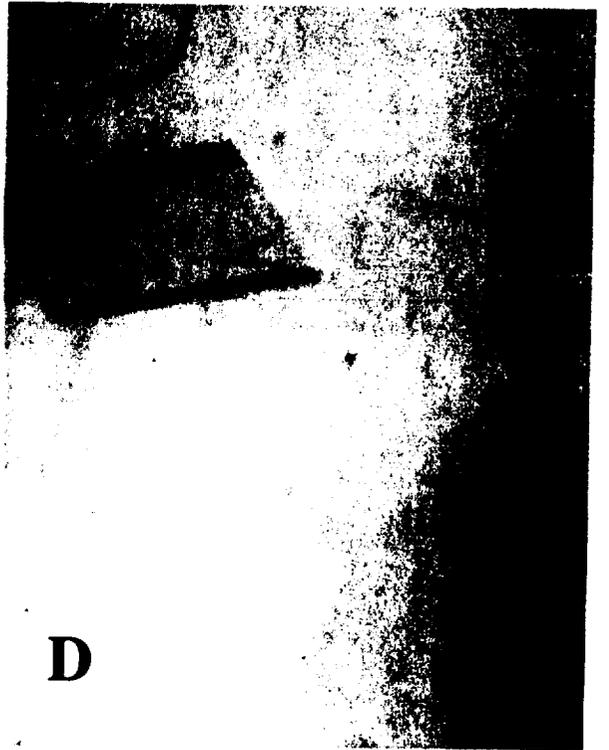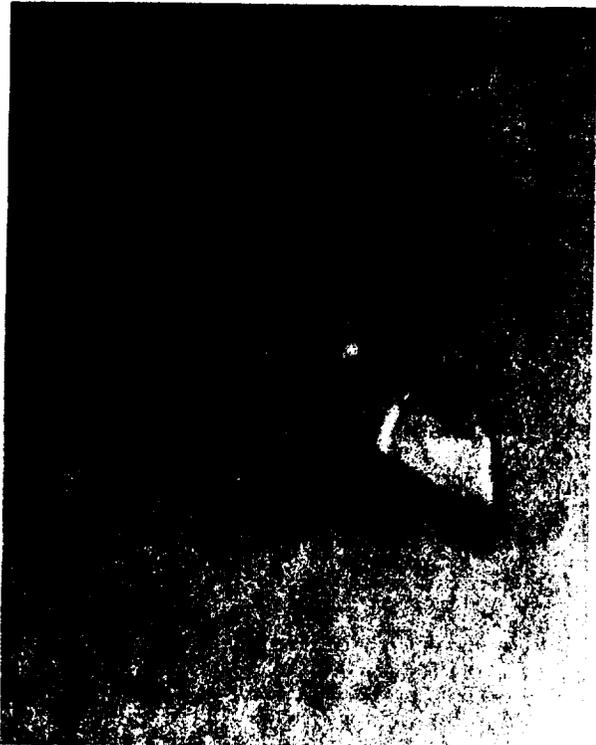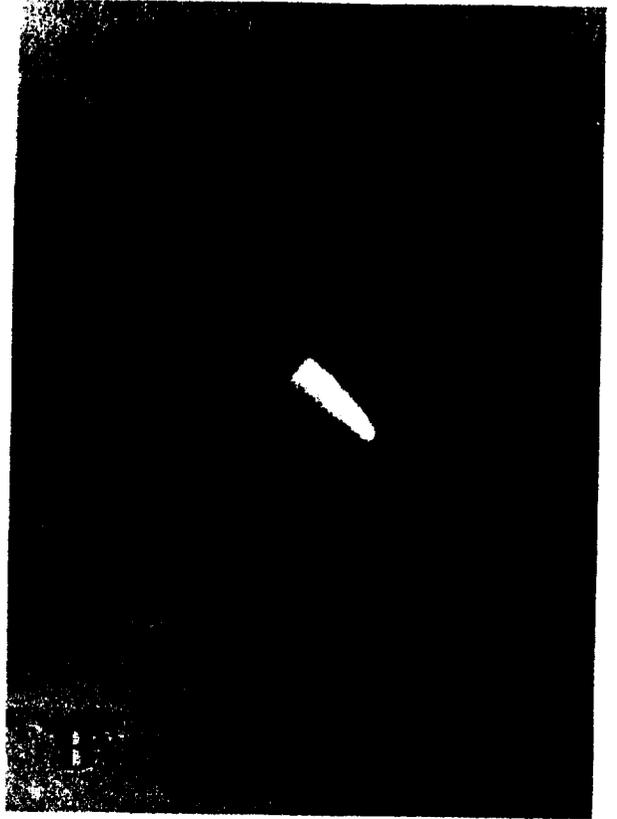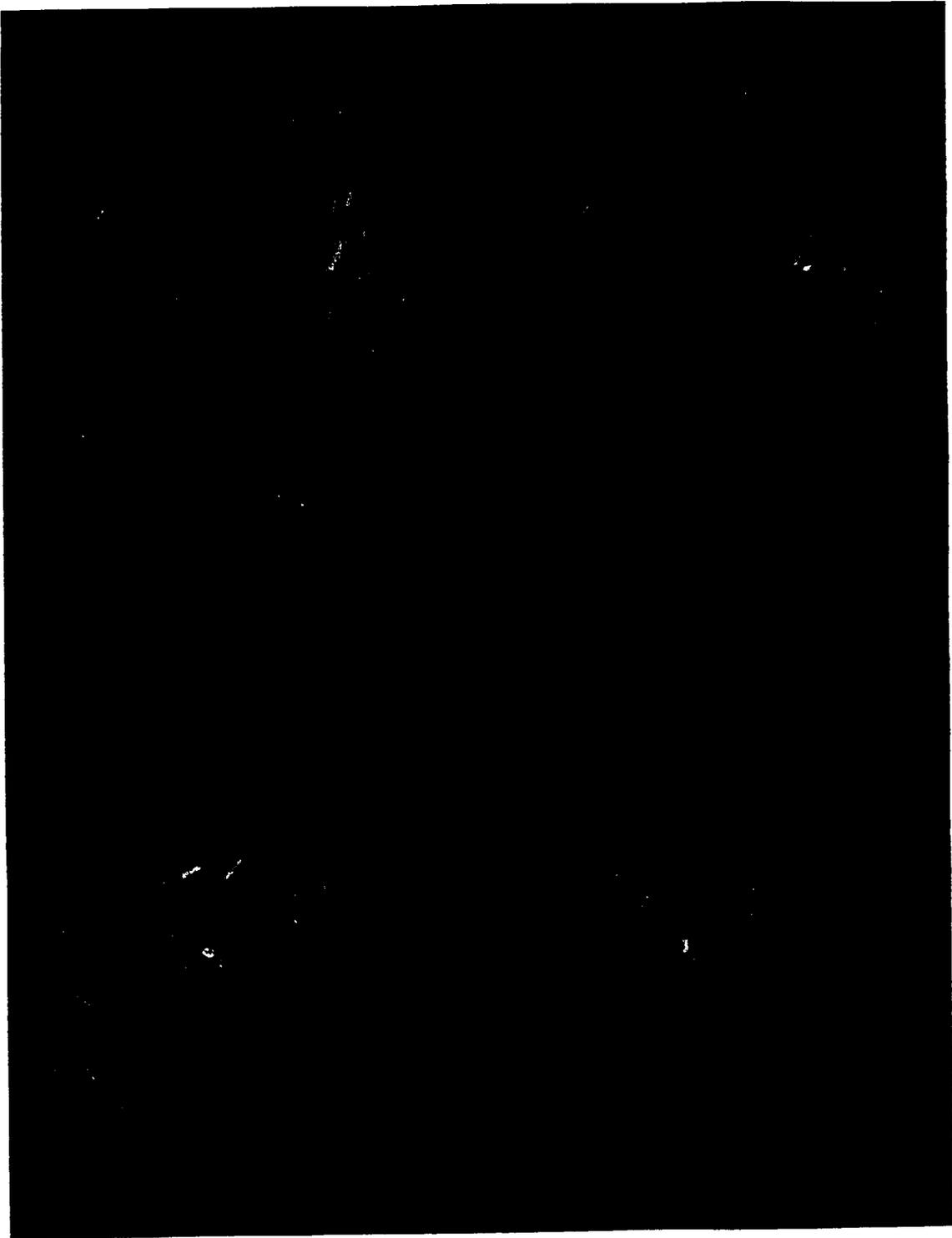
Figure 2

Figure 3

Advanced Protein Crystallization Facility (APCF)

Crystallization of Sulfolobus Solfataricus

Principal Investigator:

Dr. Adriana Zagari
University of Naples
Naples, Italy

A Comparison of Crystals Grown on Earth and in Microgravity in the Advanced Protein Crystallization Facility on the LMS Mission

P.I.   Adriana Zagari[a]
e-mail   *Zagari@chemna.dichi.unina.it*

Co-Investigators : L. Esposito,[a] F. Sica,[a] G. Sorrentino,[a] R. Berisio [a], L. Carotenuto,[b] A. Giordano[c], C.A. Raia[c], M. Rossi,[c] V.S. Lamzin,[d] K.S. Wilson,[d]

[a]*Centro di Studio di Biocristallografia, CNR and Dipartimento di Chimica, Università di Napoli "Federico II", Via Mezzocannone 4, 80134 Naples, Italy,* [b]*Microgravity Advanced Research & Support Center (MARS), Via Comunale Tavernola, 80144 Naples, Italy,* [c]*Istituto di Biochimica delle Proteine ed Enzimologia, CNR, Via Marconi 10 Naples, Italy, and* [d]*European Molecular Biology Laboratory (EMBL) c/o DESY Notkestrasse 85, D-22603 Hamburg, Germany.*

1. Background

Sulfolobus solfataricus is a hyperthermophilic archaeon, which thrives at a temperature of 87 °C and at a pH of 3.5 in the Solfatara volcanic area near Naples, Italy (Raia *et al.*, 1996). The bacterium expresses an NAD^+-dependent alcohol dehydrogenase (SsADH) which has a potential biotechnological application due to its ability to function in these extreme life conditions.

We obtained crystals of SsADH in the apo and holo form complexed with β-Nicotinamide Adenine Dinucleotide Reduced Form (NADH), on Earth. Both forms diffracted to better than 3 Å resolution. Depending on the crystallization conditions, the crystals can assume various morphologies, but commonly exhibit tail coat-shaped ends. Unfortunately, analysis of their diffraction pattern revealed that the crystals were twinned and hence not suitable to X-ray analysis (Pearl *et al.*, 1993; Sica *et al.*., 1994).

An increasing number of reports in the literature describe a remarkable effect of gravity on protein crystal growth. The density gradient on Earth induces convective flows at the crystal interface and,

according to some authors, this can increase the occurrence of defects, dislocations, and other imperfections (DeLucas & Bugg, 1991; Day & McPherson, 1992). In a microgravitational environment, these density-driven flows are removed, retaining an undisturbed depletion zone around the growing crystals and thus favoring more ordered growth (McPherson, 1993; Rosenberg, Muschol, Thomas & Vekilov, 1996). In addition, protein crystals usually sediment and make contacts with foreign surfaces. These surface effects can be avoided in microgravity, favoring high quality crystal growth. For these reasons we carried out SsADH crystallization experiments on the LMS Mission.

2. Objectives

Our goal was to obtain NADH-complexed SsADH crystals of better quality than those grown on Earth. We wanted to compare the characteristics of ground and microgravity-grown crystals, including the occurrence of twinning. Twinning interferes with crystallographic structure determination, and thus we were particularly interested in testing whether microgravity affects twinning. This was the first time such an experiment was carried out.

3. Methods of data acquisition and analysis

Crystallization data

We carried out pre-flight and flight crystallization experiments in 80 µl vapor diffusion (HD) and in 20 µl free-interface diffusion or dialysis (FID/DIA) reactors of the Advanced Protein Crystallization Facility (APCF) (Bosch, Lautenschlager, Potthast & Stapelmann, 1992). Prior to launch, we received one FID/DIA and three HD reactors from Dornier and we optimized the crystallizing conditions in these reactors. The crystal size during these preparatory trials never reached a dimension larger than 0.3 mm, whereas identical reference trials conducted in Limbro plates produced larger crystals (0.5-0.8 mm) with better morphologies.

Initial trials were carried out using either FID or DIA configuration in the FID/DIA reactor. As a

control, equivalent trials were performed in glass capillaries and in dialysis buttons. The best results were obtained using the FID/DIA reactor with the DIA configuration and this method was then adopted for subsequent experiments.

We conducted space and ground reference experiments in eight crystallization reactors (six HD (80 μl) and two FID/DIA (20 μl) reactors according to the specifications listed in Table 1.

The reactors were filled with protein and other reagent solutions in the laboratory of Prof. W. Weber in Hamburg, Germany. The space reactors were mounted in the APCF and taken to the launch site at the Kennedy Space Center (KSC), USA. The ground control reactors were kept at the EMBL c/o DESY, in Hamburg. About eight hours after the launch, both space and ground reactors were activated and were then deactivated one day prior to shuttle re-entry.

X-ray data

Four microgravity-grown crystals and six ground-grown crystals were analyzed using EMBL X11 beam line synchrotron radiation at the DORIS storage ring at DESY in Hamburg. Data were recorded on a Mar Research image plate detector. Additional experiments were conducted at the Biocrystallographic Center in Naples, Italy from one microgravity grown and a few ground-control crystals and were analyzed using a DIP 2030 image plate detector (Nonius) mounted on a rotating anode operating at 40 kV and 90 mA. All data were processed and refined using the HKL package (Otwinowski, 1993). The crystals belong to space group C2 with one dimer in the asymmetric unit, and the cell parameters are, $a = 133.0$, $b = 85.7$, $c = 70.5$ Å, $\beta = 97°$.

3. Flight Results

Crystallization experiments were performed simultaneously on SsADH on Earth and in microgravity. To ensure identical conditions, we used the same reagent solutions, crystallization hardware, and temperatures for both sets of experiments.

Photographs were taken of all APCF reactors one day after landing at KSC. The crystals grown in microgravity inside the DIA reactor are shown in Figure 1a. The space-grown crystals exhibit the

same tail-coat ends as observed in Earth-grown crystals (Fig. 1b). The ground-control DIA reactor contained similar crystals. All the crystals were removed from the DIA reactors, mounted in capillaries and exposed to X-ray radiation. Disappointingly, the large number of the crystals harvested from the HD reactors both in microgravity and on Earth were very small. These crystals diffracted very poorly and could not be used in our analysis. A summary of the space and ground crystallization experiments is reported in Table 1.

Though we started out with identical reagent solutions, we obtained very different results from the HD and DIA reactors. Similar variations have been reported in the literature. For example, during the International Microgravity Laboratory 1 mission, McPherson et al. obtained very different results for the protein canavalin and also for satellite tobacco mosaic virus, (Day & McPherson, 1992). The best canavalin crystals were grown by vapor diffusion, whereas the best tobacco mosaic crystals came from liquid-liquid diffusion. In another instance, Chayen et al. (1997) described a video-camera observation of microgravity protein crystallization in APCF/HD vapor-diffusion reactors; indeed motion was observed in the growing crystals which was attributed to Marangoni effects, due to the presence of free liquid surfaces open to vapor. Considering our results and those cited in the literature, the importance of the method and the experimental apparatus used in protein crystallization seems quite clear.

To assess crystal quality, we used X-ray diffraction analysis. First, we carried out a comparative analysis for microgravity-grown and Earth-control crystals at the EMBL-DESY facility in Hamburg. Initially, crystals grown in microgravity and on Earth diffracted well, up to 1.8 and 2.5 Å resolution, respectively, indicating an improved microgravity-grown crystal quality. Unfortunately, once exposed to the synchrotron beam, the crystals began to decay and this resulted in an incomplete set of maximum resolution data. We collected a complete data set only from one microgravity-grown crystal, though only to 2.3 Å resolution. The ground-control crystals showed a more rapid decay after a few frames, and so only partial data were collected using the best ground-control crystal. Unfortunately,

analysis of the diffraction pattern revealed that microgravity and ground-control crystals were twinned in a similar manner as previously observed on Earth.

We then conducted the same comparative analysis at our own laboratory using one microgravity-grown crystal and a few ground-control crystals. A complete set of data was obtained from the microgravity crystal, though at a lower resolution than in Hamburg, due to the X-ray source lower intensity. Earth-grown crystals again showed greater damage under exposure to conventional source X-rays and thus only partial data sets could be recorded. As a result, we had to merge data from two crystals.

We were able to index spots on the same crystal lattice in all of the samples. A summary of all X-ray data is shown in Table 2.

5. Conclusions

A number of conclusions can be drawn concerning microgravity protein crystallization:

In terms of size, the SsADH microgravity-crystals are larger than ground-control crystals, though still comparable to the best Earth-grown counterpart. This concurs with several but not all cases cited in the literature). As for resolution, SsADH microgravity-grown crystals achieved significantly higher resolution diffraction data, indicating a reduced statistical disorder. Lastly, though severe decay was observed in all SsADH crystals, the microgravity-grown crystals displayed increased stability when exposed to X-rays. The growth method appeared particularly influential for SsADH; a subject currently being examined by a number of laboratories.

Unfortunately, we found that microgravity-crystals of SsADH complexed to NADH were twinned. This was the first time this phenomenon was tested in microgravity. To see whether different results can be obtained under reduced gravity further studies should be planned to examine other factors known to affect twinning, as e.g. stress and secondary nucleation. In conclusion, there are still a number of questions concerning microgravity protein crystallization which warrant further investigation.

Acknowledgements

6. References

Bosch, R., Lautenschlager, P., Potthast, L. & Stapelmann, J. (1992) *J Cryst. Growth* **122**, 310-316.

Chayen, N. E., Snell, E.H., Helliwell, J.R. & Zagalsky, P. F. (1997) *J. Cryst. Growth* **171**, 219-225.

Day, J. & McPherson, A. (1992) *Protein Sci.* **1**, 1254-1268.

DeLucas L.J. & Bugg, C.E. (1991) *Advances in Space Biology and Medicine* **1**, 249-278.

McPherson, A. (1993) *J. Phys.D:Appl.Phys.* **26** B104-B112.

Otwinowski, Z. (1993) DENZO, *An Oscillation Data Processing Program for Macromolecular Crystallography.* Yale University, New Haven, CT, USA.

Pearl, L.H., Demasi, D., Hemmings, A. M., Sica F., Mazzarella, L., Raia, C. A., D'Auria, S., & Rossi, M.(1993).*J. Mol. Biol..* **229**, 782-784.

Raia C.A., Caruso, C., Marino, M., Vespa, N. & Rossi, M. (1996) *Biochemistry* **35**, 638-647.

Rosenberg, F., Muschol, M., Thomas, B.R. & Vekilov, P.G. (1996) *J. Cryst. Growth* **168**, 1-27.

Sica, F., Demasi, D., Mazzarella, L., Zagari, A., Capasso, S., Pearl, L. H., D'Auria, S., Raia, C; A. & Rossi, M. (1994) *Acta Crystallogr.* D**50**, 508-511.

Fig.1. a) Photograph of microgravity-grown crystals taken at KSC one day after landing. b)Photograph of a typical NADH-complexed SsADH crystal grown on Earth.

Ground- and microgravity-grown crystals both show typical tail coat-shaped ends.

Table 1. Results of crystallization experiments

Reactor type	No.	Final composition*		Results			
		SsADH mg/mL)	MPD (%v/v)	On Earth		In space	
				N	E	N	E
					(mm)		(mm)
HD	3	11-13	48-50	many	0.10	many	0.10
DIA	1	10	48	10	0.4	5	1.0

* with Tris-HCl buffer, 50mM, pH 8.4, NADH 1mM
N=number of crystals appeared
E=maximum edge

Table 2. Diffraction data of crystals on the ground and in space

Crystal Growth	Diffraction Data							
	Synchrotron Data				Laboratory Data*			
	d1 (Å)	d2 (Å)	C (%)	R_{sym}	d1 (Å)	d2 (Å)	C (%)	R_{sym}
Space	1.8	2.3	89	0.08	2.6	3.0	79	0.12
Ground	2.5	3.2	57	0.17	2.9	3.5	72	0.12

d1 = Resolution limit to which significant data are initially observed

d2 = Resolution to which data have been collected

C = Completeness within d2

$R_{sym} = \Sigma[(I_i - <I>)^2/\Sigma I_i^2$ where I_i is the measured intensity of an individual reflection, and $<I>$ the mean intensity of symmetry-related measurements of this reflection.

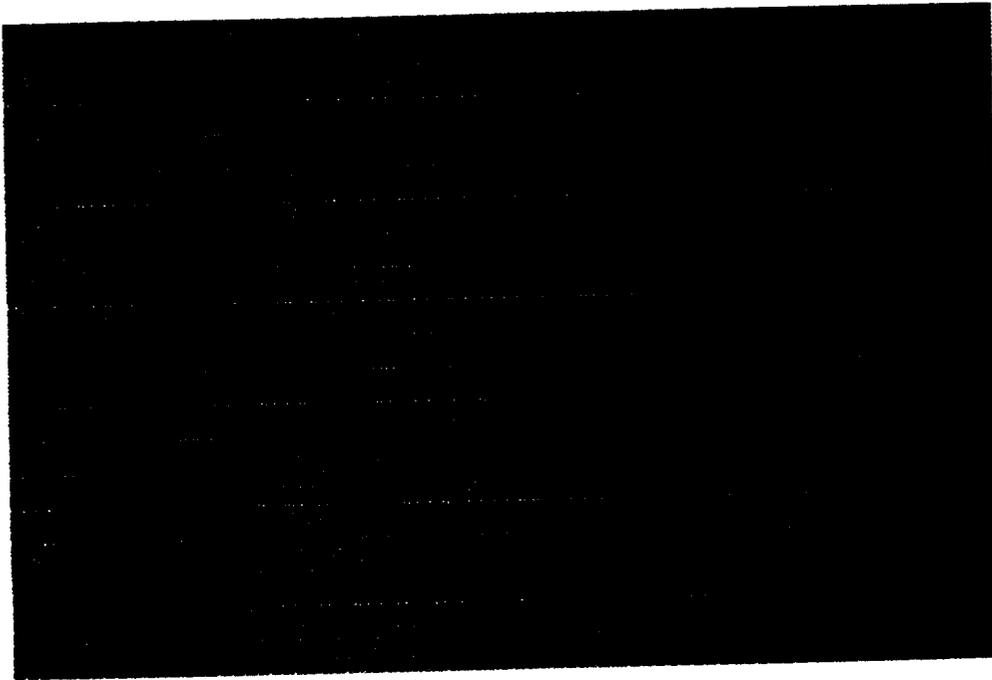*Laboratory data for the ground-grown crystal have been merged from two crystals.

Figure 1A

Figure 1B

Bibliographic citations of articles/presentations resulting from the flight

Research Article:

Esposito, L., Sica, F., Sorrentino, G., Berisio, R., Carotenuto, L., Giordano, A., Raia, C.A., Rossi, M., Lamzin, V.S., Wilson, K.S. & Zagari, A. Protein Crystal Growth in the Advanced Protein Crystallisation Facility on the LMS Mission: a Comparison of *Sulfolobus solfataricus* Alcohol Dehydrogenase Crystals Grown on the Ground and in Space. *Acta Crystallographica D* , accepted.

Invited Lecture:

Sica, F., Esposito, L., Sorrentino, G., Berisio, R., Raia, C.A., Rossi, M., Lamzin, V.S., Wilson, K.S. & Zagari, A. Recent results of protein crystal growth in microgravity Joint Annual Meeting Deutsche Gesellschaft fur Kristalwachstum und Kristallzuchtung and Italian Crystallographic Association - Crystal Growth Section 5-7 March 1997, Fribourg (Germany)

Poster presentation:

Esposito L., Sica F., Sorrentino G., Berisio R., Carotenuto L., Raia C., Rossi M., Lamzin V., Wilson K., and A. Zagari Crystallization of *Sulfolobus solfataricus* Alcohol Dehydrogenase in Microgravity . 17th European Crystallographic Meeting, 24-28 Aug. 1997, Lisbon, Portugal.

Oral Presentation:

Zagari A., Sica F., Mazzarella L. Protein Crystal Growth: a Case Study in Microgravity. 27th National Meeting of the Italian Crystallographic Association, 12-14 September Perugia, Italy.

234

Summary

Alcohol dehydrogenase crystals from *Sulfolobus solfataricus* were grown in the Advanced Protein Crystallization Facility during the U.S. space shuttle's Life and Microgravity Sciences Spacelab mission. Large diffracting crystals were obtained by dialysis and poor quality crystals were obtained by vapor diffusion. The quality of both the space and ground-based crystal was analysed by X-ray diffraction. The space crystals showed improved size and diffraction resolution limit. The phenomenon of twinning, however, which was observed in the Earth-grown crystals, was also present in those grown in space.